Electrospun Nanocellulose: A New Biomaterial

Katia A. Rodriguez Rivera

Thesis submitted to the faculty of the Virginia Polytechnic Institute and State University
in partial fulfillment of the requirements for the degree of

Doctor of Philosophy

In

Materials Science and Engineering

Scott H. Renneckar, Chairman

Paul Gatenholm

Abby R. Whittington

Alexander O. Aning

September 23, 2011

Blacksburg, VA

Keywords: Cellulose, Electrospinning, Architectural Guidance, Surface Guidance, Tissue Engineering

Electrospun Nanocellulose: A New Biomaterial

Katia A. Rodriguez Rivera

ABSTRACT

Science and engineering studies on biocompatible implantable materials for tissue and organ repair have recently focused on polymeric materials to serve as scaffolds for cellular integration. Cellulose in many forms has been demonstrated as potential biopolymer for tissue engineering; however, it has not been previously electrospun into a scaffold for tissue engineering applications. The overall goal of this research project was to produce electrospun cellulose acetate (CA) nanofibers with specific architectures and surface chemistries to be evaluated as scaffolds for tissue regeneration. The size and morphology of electrospun CA was impacted by polymer concentration, solvent system, and solution flow rate. The conversion of CA electrospun scaffolds into regenerated cellulose by exposure to NaOH ethanol solution was successful for scaffolds produced at polymer solution flow rate of at least 1 mL/h. The regeneration process resulted in minimal degradation of the cellulose while retaining the original fiber structure of the scaffold. *In vitro* cytotoxicity evaluation of the fibrous cellulose scaffolds on a culture of mouse fibroblast (L-929) cells indicated that this material posed no threat to mammalian cells.

Electrospun cellulose scaffolds with different architectures and surface chemistries were designed and evaluated to enhance scaffold properties and cell adhesion. The morphology of the partially regenerated cellulose revealed only a broad diffraction peak for the scaffold material, while the fully regenerated cellulose showed a characteristic semi-crystalline cellulose II diffraction pattern. Fiber orientation and porosity of the scaffolds were controlled by electrospining CA solution onto the edge of a rotator wheel and laser microablation, respectively. Bioactivity of the scaffolds was shown to be enhanced via scaffold surface modification with either anionic or cationic functional groups. Biomimetic Ca-P crystal mineralization on electrospun cellulose fibers was produced by means of carboxymethyl cellulose (CMC) adsorption and treatments with simulated body fluid (SBF) or phosphate buffer saline (PBS) solutions. Porosity and Ca-P crystals enhanced osteoprogenitor cell adhesion on the electrospun cellulose scaffolds. Cationic modification by trimethyl ammonium betahydroxy propyl (THAMP) derivation and adsorption of extracellular matrix proteins on cellulose fibers promoted adhesion and proliferation of neural-like (PC12) and myoblast (C2C12) cells. Differentiation of myoblast cells (C2C12) towards myotubes on electrospun cellulose scaffolds was controlled by surface chemistry and mechanical properties. Together these studies showed great potential for cellulose acetate to be electrospun and converted into a viable biocompatible tissue engineering scaffolds.

I would like to dedicate this work to my grandmother, Refugio, and my parents Esperanza and Elias.

Acknowledgements

This research project was supported by the USDA NIFA AFRI Grant 2010-65504-20429, USDA CSREES, Special Research Grant 2008-34489-19377, Institute of Critical Technology and Applied Science of Virginia Tech, and the Wallenberg Wood Science Center of Sweden. This work would not have been accomplished without the assistance from several persons at Virginia Tech and Chalmers Technology universities. I am grateful to my advisers, Dr. Scott Renneckar and Dr. Paul Gatenholm, for their support and guidance throughout my graduate career. I would like to thank to Dr. Abby Whittington, Dr. Joseph Freeman, and Dr. Alex Aning for serving on my graduate committee. The author acknowledges the Sustainable Engineered Materials Institute of Virginia Tech and the Biosynthetic Blood Vessel (BBV) laboratory of Chalmers for providing materials and access to equipment used in this research. My gratitude to Dr. Audrey Zink-Sharp from Wood Science and Forest Products Department for kindly teach me and allow me to use light and scanning electron microscopes. I express my sincere appreciation to Rick Caudill for his invaluable help in XRD characterization. I would like to thank to fellow graduate students and labmates, from the Self-Assembled Wood Macromolecule Interface Lab (SAWMIL), Travis Church, Dr. Zhiyuan Lin, Qingqing Li, and Wei Zhang for their support and assistance inside the lab. I am thankful to Stephen McCartney from Nanoscale Characterization and Fabrication Laboratory at Virginia Tech for his assistance with scanning electron microscopy. I wish to thank to Dr. Niven Monsegue of Materials Science and Engineering Department at Virginia Tech for his support and advice throughout the development of this thesis project. In addition, the author wishes to thank Dr. Anne Wendel and Dr. Anders Mårtensson, from Department of Chemical and Biological Engineering of Chalmers, for their significant assist in XPS, SEM, TGA, and BET characterization. I would like to express my special gratitude to Esa Väänänen, from Chemistry Department of Chalmers, for his invaluable work fabricating devices used in the electrospinning process. I wish to thank fellow graduate students and labmates, from BBV laboratory of Chalmers, Hector Martinez, Johan Sundberg, Carin Hagsten, Alexandra Glantz, and Nikolaj Vest for their support in the lab. I am especially grateful to Hector Martinez for his support in the design of electronic devices employed in the electrospinning process. I want to thank Nikolaj Vest for helping me to perform tensile testing measurements. I am also grateful to Magdalena Zaborowska, Dr. Aase Bodin, Dr. Olga Naboka, and Dr. Sara Johannesson, from Chalmers University, for their support inside lab and out. The author recognizes Swerea IVF AB from Sweden for allowing access to equipment to fabricate nano-micro scaffolds, in particular to Anna Thorvaldsson for teaching me the technique. Finally, I would like to thank my family and friends for their endless love, support, and encouragement.

Attribution

Scott Renneckar - Ph.D. (Department of Wood Science and Forest Products, Virginia Tech) is the primary Advisor and Committee Chair. He provided extensive guidance for the research as well as comments and guidance on the writing.

Paul Gatenholm - Ph.D. (Department School of Biomedical Engineering and Sciences, Virginia Tech and Wallenberg Wood Science Center Biopolymer Technology, Department of Chemical and Biological Engineering, Chalmers University of Technology) is Advisor and Committee member. He also provided extensive guidance for the research performed in this thesis.

Chapter 4: Novel architectures of cellulose: aligned, microporous, and scale integrated.

Travis Church - M.S. (Department of Macromolecular Science and Engineering, Virginia Tech) created the AutoCAD files and provided training for the laser operation in the fabrication of the microporous electrospun cellulose scaffolds.

Chapter 5: Electrospun Cellulose a New Member of Nanocellulose Family

Wei Zhang - Ph.D. student (Department of Wood Science and Forest Products, Virginia Tech) performed additional contact angle measurements.

Chapter 7: Evaluation of Cell Response on Electrospun Cellulose Scaffolds

Nelson Laboratories - (Salt Lake City, UT, USA) performed the cytotoxicity evaluation of the electrospun fibers.

Johan Sundberg - M.S. (Department of Biopolymer Technology, Department of Chemical and Biological Engineering, Chalmers University of Technology) performed the MC3T3-E1 cell study.

Alexandra Glantz - M.S. (Department of Biopolymer Technology, Department of Chemical and Biological Engineering, Chalmers University of Technology) was a master student supervised by the author. She fabricated the nano fibers coated lyocell microfibers scaffolds and performed the PC12 cell study.

Hector Martinez – Ph.D. student (Department of Biopolymer Technology, Department of Chemical and Biological Engineering, Chalmers University of Technology) supervised together with the author a senior designer group from Tissue Engineering class at Chalmers. The senior designer group was integrated by: Andreas Carlsson, Md. Khairul Hoque, Maryam Karimi, and Therese Klang. In the senior designer project the C2C12 cell study was carried out.

Table of Contents

List of Figures

Chapter 1

Chapter 2

Chapter 3

Chapter 4

Chapter 5

Chapter 6

Chapter 7

Appendix A

Appendix B

List of Tables

Chapter 2

Chapter 3

Chapter 4

Chapter 5

Chapter 6

Chapter 7

Appendix A

List of Equations

Chapter 3

Chapter 5

Chapter 1. Introduction

Tissue engineering is a transdisciplinary field that seeks the development of scaffold materials to maintain, repair, or enhance tissue and organ function. A scaffold is a support that mimics the extracellular matrix and plays the function of a temporary skeleton for cell growth to allow tissue regeneration [1]. An ideal scaffold material needs to be biocompatible, have mechanical properties similar to those of the tissue being repaired, and include specific biological signals. The biological recognition of the scaffold will express and promote tissue formation through cell attachment, proliferation, and differentiation. Nanofibrous scaffolds are widely studied, due to their extracellular matrix-like structure [2, 3]. Various methods for preparing nanofibrous scaffolds have been explored. These methods include electrospinning, phase separation, and self-assembly. Of these, electrospinning has shown to be a promising technique suitable for producing interconnected and highly porous fibrous scaffolds [2, 4]. Until now, numerous synthetic (polylactide-co-glycolide and polyε-caprolactone) and natural (chitosan, collagen and gelatin) polymers have been successfully electrospun into non-woven porous matrices [2, 5]. Cellulose is an abundant natural occurring polysaccharide that has exhibited good biocompatibility, but not previously tested in its electrospun nano-fiberous form for tissue engineering studies.

Cellulose derivatives such as cellulose acetate (CA) and hydroxypropyl cellulose can be effectively electrospun [6-8]. Several studies have reported the applicability of cellulose-based materials for culturing cells and for implantation [9-12]. Most of the biomedical application of cellulose-based materials have been used as bacterial produced cellulose [12-18], regenerated cellulose sponges [10, 11], and solution spun cellulose cloth (lyocell) [19-21]. These materials do not offer the ability to control the scale of the fibers in the nano to micro diameter regions. The goal of this work is to further the understanding of nanofibrous cellulose-based scaffolds and to overcome their dimension limitation by electrospinning into nanoscale fibers.

1.1 Background

1.1.1 Extracellular Matrix

The native extracellular matrix (ECM) is a three-dimensional network of biomacromolecules, and acts not only as a structural scaffold but also as an environment directing the actions of tissues and cells [22]. The basic structure of ECM consists of nanofibrous collagen scaffolds and glycoproteins (fibronectin, laminin, and elastin) that help adhere cells to the collagen fibers. In addition, growth factors (GFs) and hydrophilic proteoglycans with large glycosaminoglycans are present in the ECM. These macromolecules interact with the cells in or adjacent to the matrix [4]. Designing ECM-mimicking artificial matrices (scaffolds) is an important subject in the tissue engineering field [4, 22].

1.1.2 Scaffold Design

It is critical for the scaffold to mimic the structure and properties of ECM to direct the macroscopic process of tissue formation [4, 22]. Therefore, the scaffold design should consider the biocompatibility of the material and the ability for cells to attach and proliferate (bioactivity). The proposed structure should have an appropriate mechanical strength and biodegradation profile. It should include features such as pores and channels to promote cell migration and diffusion of oxygen and nutrients through the scaffold [4, 22].

1.1.3 Biomaterials

Medical biomaterials are defined as biocompatible materials planned for being in contact with living tissue and biological fluids. These materials are used to diagnose, treat or replace a particular tissue, organ or function in the body [23]. Biomaterials are classified into metals, polymers, ceramics, and composites. In order for a material to be classified as a biomaterial, this needs to fulfill some requirements. These requirements are biocompatibility, ability to be sterilized, functionality, and manufacturability [24].

1.1.3.1 Polymers

The fact that polymers can be engineered with a variety of properties such elasticity, stiffness, hydrophilicity, and hydrophobicity, to mention some, have made them very attractive to use in the fabrication of scaffolds and implants [24]. Polymers are usually divided into synthetic and naturally derived. Within the synthetic polymers, polylactic acid, polyglycolic acid, polyethylene glycol, and polyurethane are the most commonly used in the biomedical field [4]. Collagen, chitosan, alginate, and gelatin are some of the most important natural polymers used in this field [2].

1.1.4 Biocompatibility

Biocompatibility is known as "the ability of a material to perform with an appropriate host response in a specific application" [23]. It is well established that materials employed for medical diagnostic and therapeutic purposes require biocompatibility testing before human use. A biocompatibility assessment is "a measurement of the magnitude and duration of the adverse alterations in homeostatic mechanism that determine the host response" [23, 25]. There is a complete and general regulation to carry out in vivo biocompatibility testing published by U.S. Food and Drug Administration, ASTM, and ISO [25]. In the International Standard ISO, the in vivo biocompatibility test of implant devices and scaffolds is denominated implantation-ISO 10993-6.

1.1.5 Polymers Biodegradation

Since polymers are widely used in biological environments, the subject of polymer degradation in such environments has become an important subject. When choosing polymers as potential biomaterials the consideration of biodegradation is a main concern on the list of safety standards. There is an obvious difference between the kinds of degradation than *in situ* animal environment will be able to cause compare to external environments. This main dissimilarity is that materials are exposed to the active tissue of the body, which is highly sensitive and intolerant to the intrusion of foreign bodies. This hostile environment has a tendency to eliminate any unknown material placed into it. The concern is whether any material can function within the tissue of the body for the required period without suffering undesired degradation, and most importantly without inducing any undesirable tissue response [23].

Polymeric biomaterials undergo degradation in the body due to interaction with surrounding fluids and tissues. Discoloration of the implant or scaffold, appearance of crazes, or significant change in mechanical properties are indications that degradation is taking place. Polymers normally degrade by two main mechanisms: swelling-dissolution or chain scission. Other means of polymer degradation in the presence of physiological environment are enzyme-catalyzed degradation and environmental stress cracking. The factors that can influence the degradation rate are chemical susceptibility of the material, degree of crystallinity, amount of available water, and material surface area to volume ratio [25].

1.1.5.1 Swelling-Dissolution Mechanism

Hydrophilic polymers will swell in physiological environment. The water molecules adsorbed into the polymer will make the material more ductile by reducing secondary bonding between chains. Swelling could also affect crystallinity, mechanical and thermal properties of the polymer. In extreme cases, the polymer could dissolve entirely if the chain is solublized and without the presence of cross links between chains [25].

1.1.5.2 Chain Scission Mechanism

In contrast, chain scission involves breaking primary bonds instead of secondary interactions. This mechanism implicates the separation of chain segments at the point of rupture of bonds that leads to an overall decrease of molecular weight. Molecular weight has an important impact in mechanical and thermal properties of the polymer. Chain scission can occur via hydrolysis or oxidation reactions [25].

1.1.5.3 Enzyme-Catalyzed Degradation

A diversity of enzymes is used in the body to achieve synthesis and cleavage of natural polymers. Enzymes have particular attraction for certain chemical groups present in polymers. In some cases enzymes can cause hydrolytic or oxidative degradation of polymers, if the polymers possess chemical functional groups similar to their target moieties. However, each person produces different amounts of enzymes and hence is difficult to predict to what degree enzyme-catalyzed degradation may affect polymeric materials [25].

1.1.5.4 Environmental Stress Cracking

When a polymer is exposed to enough stress in the biological environment, the exterior of the implant develops deep cracks vertical to the loading axis. Even though, the exact mechanism of this degradation type is not well understood, it is known that inflammatory cells are required before environmental stress cracking will arise [25].

1.1.6 Bioactivity

Synthetic scaffolds apart from mimicking the ECM structure should be integrated with macromolecular bioactive agents in order to modulate cell matrix interactions [4]. Surface engineering of bio-inert polymers is often required to introduce bioactive species that can promote cell adhesion, proliferation, and differentiation [4, 22, 26]. Up to present, there is a large amount surface engineering techniques to enhance biocompatibility. This work usually relies on surface modification of the polymeric material, chemical and physical characterizations, and biocompatibility assessment through cell culture [22, 26]. Adsorption of ECM proteins (containing cell surface receptors such as laminin, fibronectin, and vitronectin) on biomaterial surfaces and the biological recognition between the cells and adsorbed proteins is well documented [26, 27]. Another approach is the immobilization of RGD (Arg-Gly-Asp) amino acid sequence, which is the minimal fragment of the active site of adhesive proteins such as fibrinogen, fibronectin, and the von Willbrand factor [26, 27]. Additionally, polymer surface modification approaches to prepare very hydrophilic or super hydrophobic biomaterial surfaces have been explored. It has been inferred that the hydrophilicity/hydrophobicity of biomaterial surface influences its biocompatibility from a perspective of water molecular structure proximity to the surfaces [26]. A strategy to enhance osteintegration and bioactivity, in bone regeneration, is surface coating the scaffold with hydroxyapatite-like minerals [16, 20]. Hydroxiapatite (HA) is a natural component of bone. Model studies have shown that a hydroxyapatite layer increases the expression of mRNA encoding the bone matrix proteins osteocalcin, osteopontin, and bone sialoprotein [28]. Several techniques to coat calcium phosphate (Ca-P) onto an implant material are available. Simulated body fluid (SBF) treatment is a usual procedure to create a surface apatite layer on biomaterials [13, 16, 20, 29]. SBF is an electrolyte solution that mimics the inorganic composition of the blood human plasma [20]. Simulated body fluid (1.0 SBF) was initially designed to test the bioactivity of artificial bone material in vitro because its composition is very close to human blood plasma. SBF solutions of different concentrations (1.5 and 5 times SBF

concentration) have also been used for coating of hydroxyapatite (HA) on the surface of bioinert materials with artificially introduced surface functional groups that have an ability of inducing the HA nucleation in SBF solutions [19, 20].

1.1.7 Scaffold Interconnectivity

It is thought that for successful tissue regeneration a scaffold with topographic features and geometry on the macro, micro and nano scale levels needs to be created. Since cells live in a complex mixture of pores, ridges, and fibers within the ECM; an important feature for a promising biomaterial is its porosity [30]. Macroscopic pores (>100 μm) in a nanostructured scaffold play an important role in cell seeding distribution, cell migration throughout the 3D space, cell signaling, and mass transport [31].

1.1.8 Fabrication of Scaffolds by Electrospinning

In the field of tissue engineering, electrospun fibers are used as scaffolds for tissue growth [2, 32]. This is due to the small fiber size, high surface area, potential to form three-dimensional (3D) structures, and the ability to mimic ECM [32]. There are many different polymers that can be electrospun. Biodegradable and natural polymers are two common groups that are used for this purpose [2]. Some of the benefits of electrospinning in contrast to other methods (phase separation, self-assembly, template synthesis and drawing) are its simplicity, high productivity, high controllability, cost-effectiveness and the ability to provide fibers from many different types of polymers [2, 33]. Essentially, electrospinning consist of a pipette to hold a polymer solution, a pump to control the solution flow rate, two electrodes to generate an electrical potential difference, a direct current voltage supply (in the range of kV), and a collector [32, 34]. To electrospin a polymeric solution, it is important to use volatile solvent or mixture of solvents, because solvent evaporation is indispensable in order to have pure and dried nanofibers [2]. For this reason in some cases a heater is used on the collector. The electrospinning method creates an electrical gradient by applying a charge on the solution and grounding the collector, which is placed at a certain distance from the capillary (or needle) in order to pull the polymers through the capillary (Fig. 1) [2, 32, 35]. This action will create a jet of solution from the capillary to the collector. The method relies on the evaporation of the solvent to form solid polymer fibers. The fibers made by electrospinning have a diameter in the sub-micron range [35].

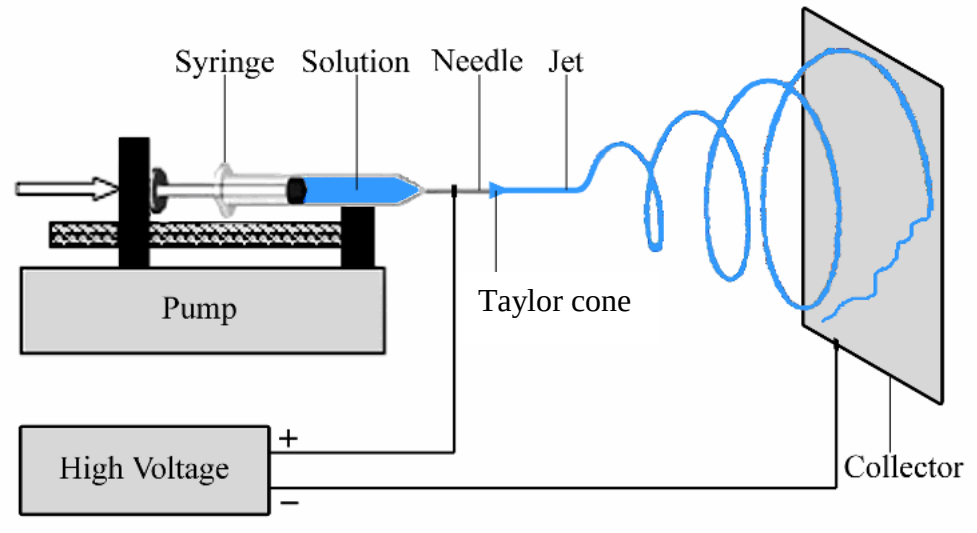

Figure 1. 1 Conventional electrospinning setup [36].

Either natural or synthetic polymers can be electrospun and the resulting solution has different behavior. Examples of natural polymers that have been processed by this technique are cellulose and its derivatives, collagen, chitosan, hyaluronic acid, DNA and RNA [2, 32]. In the synthetic category are polyurethane, polylactic acid, polycaprolactone and polygicolic acid. It is also possible to electrospin a mixture of both kinds of polymers to improve or change properties in the final product and these are called nanocomposites fibers [4]. The electrospinning technique has three kinds of parameters to control. The first type is system parameters, which include the polymer molecular weight and its distribution, the architecture of the polymer such as branched or linear polymers and the solution properties, such as viscosity, conductivity and surface tension. The second type of parameter is related to the process. In this category the factors to be considered are electrical potential, flow rate, concentration, distance between capillary or pipette tip and collector, motion of the collector. Finally, the third type includes environmental parameters such as temperature, humidity percentage and air velocity are relevant [34, 35]. It is well known that through parameter control, nanofiber diameter, porosity, assembly and morphology can be changed to design and fabricate a desired type of nanofiber to specific application [35]. Electrical properties, surface tension, and viscosity of the solution will affect jet formation, how the solution will be stretched out from the tip of the capillary, during electrospinning. It has been shown that the viscosity of the solution affects the diameter of the fibers, the shape of initiating droplets and the jet trajectory [35]. A larger size of the fiber diameters has been related to an

increasing viscosity of the solution and also by increasing the flow rate [35, 36]. Morphology of the electrospun material is also a function of the molecular weight, viscosity and in some cases of the solution preparation time, known as the aging process [36]. For example, with higher viscosity solutions smooth fibers and few beads are formed [35, 36]. The electrospinning process varies greatly depending on the set-up of the equipment. Hence, it is important to establish appropriate conditions and parameters in order to control and optimize the electrospinning system to obtain the target product [35, 36].

1.1.8.1 Control of Fiber Orientation

For many applications, it is necessary to control the spatial orientation of the electrospun fibers. In tissue engineering, fiber alignment is of special interest, due to the fact that several native tissue structures are formed of aligned fibers. However, due to the bending instability associated with the spinning jet, the electrospun fibers are normally deposited on the surface of collector as random non-oriented, nonwoven mats [37]. A number of approaches, mainly relying on modifying the jet movement by controlling the electric field, have been demonstrated to directly collect electrospun nanofibers as uniaxially aligned arrays. Two of these approaches involve the use of a rotating drum or a pair of split electrodes as the collector [37, 38]. Alignment of fibers has been observed when a cylinder with high rotating speed was used as a collector. However, the degree of oriented nanofibers produced by this technique is far from perfect [37]. This design has been modified by using a wheel-like disc as a collector [39]. The fibers collected in the edge of the wheel were oriented parallel to each other along the edge. It was found that the electrostatic field strength dramatically increase near to the edge of the disk. Because of the strong electrostatic attraction, the charged fibers were constantly wound on the edge when the disk was rotating at a relatively at high speed [37, 39].

1.1.9 Cellulose

Cellulose is a linear homopolysaccharide composed of β (1→4) linked D-glucose monomers and is the most prevalent biopolymer produced on earth [9, 40]. This polysaccharide is produced by plants, alga, and bacteria [41]. Cellulose has been utilized in applications from paper and textiles to materials in wound healing [41]. Cellulose is not soluble in water and other common organic solvents due to its rigid

chain and strong inter- and intra-molecular hydrogen bounded structure. There are several solvent systems able to dissolve cellulose, e.g., N-methylmorpholine-N-Oxide (NMMO), ionic liquids, NaOH/urea solution, cuen, cuoxam, cadoxen, as well as Lithium Chloride/N,N-dimethylacetamide (LiCl/DMAc). As a result, cellulose can be processed into a range of forms such as membrane sponges, microspheres, non-woven, and knitted textiles [41, 42].

1.1.9.1 Biomedical Applications of Cellulose

Biomaterials based on cellulose and its derivatives have been used as membranes for hemodialysis, diffusion controlling, and carriers for enzyme immobilization, as matrices for pharmaceuticals and drug-releasing scaffolds [42-45]. Their mechanical properties can match with those of hard and soft tissue [42]. Hence, examples include bone regeneration [11, 13, 21, 46], tissue engineering in post-injury brain [42], connective tissue formation, scaffolds for growing functional cardiac cell constructs in vitro [9], blood vessels [12, 17, 18], for artificial livers [47], expansion of progenitor hematopoietic cells in culture [48], and suppression of matrix metalloproteases action in wound healing [49, 50]. In all those studies relevant results have been obtained.

1.1.9.2 Biocompatibility

Cellulose *in vivo* biocompatibility is well demonstrated [11, 40, 51, 52]. Bacterial cellulose (BC), which is synthesized by Gluconacetobacter xylinum, displays unique physical, chemical, and mechanical properties including high crystallinity, cellulose Iα (70–90%), high water holding capacity (up to 200 times of its dry mass), a well developed surface area comprised of nanofibers, elasticity, and mechanical strength [40, 41, 53]. BC has shown outstanding in vivo behavior during implantation, as demonstrated by Helenius and co-workers [40]. BC did not cause any chronic inflammatory response or foreign body reaction. Furthermore, BC was well integrated to the host tissue that was difficult to distinguish a distinct interface between the implanted material and the surrounding tissue [40]. Biocompatibility studies performed on cellulose-based materials (cellulose sponge, cellulose acetate, cellulose phosphate, and other cellulose derivatives) have shown negligible foreign body and inflammatory responses [11, 46, 51, 52, 54]. Consequently, they are also considered biocompatible [10, 11, 52]. Unlike BC, cellulose extracted and regenerated from plants has lower crystallinity with an alternate crystalline

structure, lower molecular weight, and much lower water retention capability [40, 53]. It has been shown that cellulose-based material biocompatibility can be further improved by functionalization with small amount of cations [20, 52].

1.1.9.3 Biodegradation

In nature cellulose is degraded by microbial and fungal enzymes. Cellulose biodegradation in animal or human tissues is believed to be limited. This process is not only due to the fact of absence of cellulases that attack the β (1-4) linkage of cellulose but also to the high crystalline structure of cellulose that limits it accessibility [11, 52, 55]. However, there are oxidative and hydrolytic enzymes in the body that could potentially break cellulose down by acid hydrolysis. Miyamoto *et al*.[52] studied the in vivo biocompatibility and re-sorption of cellulose and some cellulose derivatives. The absorption and compatibility of regenerated cellulose (produced from CA) samples with different degree of crystallinity were analyzed. An important difference in absorption of cellulose due to crystalline structure was found. Singh *et al*. studied the degradation of periodate oxidized cellulose under physiological conditions. It is known that periodate oxidized cellulose degrades into small molecules such as glycolic and 2,4-dihydroxybutyric acid. *In vitro* and *in vivo* in rats model results showed a faster degradation in the first few days and a steady state is reached about a month of exposure [55]. By itself, the β (1-4) linkage between the glucose units in cellulose is relatively stable. However, it has been reported that cellulose can be made susceptible to hydrolysis by introducing chemical modifications [9, 52, 55, 56]. This chemical modification of cellulose has the potential to increase degradability by disrupting its highly ordered structure [40, 57]. Therefore, increasing the amount of amorphous regions and augmenting hydrophilicity of cellulose-based materials have been reported as approaches to improve their biodegradability *in vivo* [9, 52, 55, 56]. Märtson *et al*. evaluated the long term behavior of cellulose sponges (mixture rayon-cotton) implants in rat model. It was concluded, after 60 weeks of implantation follow up, that cellulose sponge is a slowly-degradable implantation material and that the total subcutaneous disappearance of cellulose needed more the 60 weeks [11]. They have suggested that cellulose in vivo degradation is a function of mechanical, biological, and chemical factors [11]. Entcheva *et al*. developed an interesting methodology to grow cardiac cells in cellulose-base scaffolds *in vitro*. They used cellulose acetate as molded material, following by post regeneration to cellulose. This study provided data on cellulose scaffold biodegradability *in vitro* by enzymatic hydrolysis. They proved that celluloses are cytocompatible in mammals. The final product of the degradation process was glucose,

which a natural nutrient for cells [9]. Consequently, the rate of cellulose degradation will depend on several factors, including availability of enzymes to degrade cellulose, cellulose crystallinity, chemical composition of the main chain and side groups of cellulose, the hydrophilic–hydrophobic balance, surface area, aggregation state and the shape and morphology of the cellulosic material [57].

1.1.9.4 Cellulose Bioactivity

Cellulose by itself is a neutral polysaccharide with no charged groups to be used in molecular recognition [57]. This facilitates biocompatibility, however limits cell adhesion and migration [27, 57]. Therefore, surface modification strategies have been designed to facilitate cell attachment. To this end, Bodin et al has develop a novel technique to modify nanocellulose in wet state with RGD-conjugated xyloglycan, and has reported enhanced endothelial cell adhesion [27]. Furthermore, ECM proteins typically do not readily adsorb on cellulose surface. Watanabe et al develop a strategy to overcome this issue, which consisted in the formation of trimethyl ammonium betahydroxy propyl (TMAHP) cellulose. They proved that the modification of the ionic charge of cellulose increased adsorption of collagen and promoted cellular adhesion to the cellulose surface [58]. In addition, the deposition of calcium phosphate mineral onto cellulose substrates has improved bone formation [59]. The formation of HA like crystals on cellulose has been successfully carried out in several studies [13, 15, 16, 19, 20]. Many studies have reported that a pretreatment of the substrate with Ca+2 containing solution is necessary to catalyze the calcium phosphate mineralization on the scaffold during subsequent exposure to SBF solution [20]. These studies investigated techniques to nucleate and grow calcium phosphate crystals on cellulose surfaces by modification via phosphorylation and chemical oxidation. Furthermore, functionalization with carboxyl groups in cellulose can be carried out by different means, chemically by selective oxidation reactions, exposure to plasma of oxidative gases, or physically by adsorption of citric acid [19]. Irreversible adsorption of polymers containing carboxylic acid groups is another technique to enhance the number of carboxylate groups on surfaces of cellulose substrates. The irreversible adsorption of carboxymethyl cellulose (CMC) is a well described procedure in paper making [60, 61]. The attachment of CMC onto the cellulose surface is thought to be a co-crystallization process; however, the mechanism of this procedure remains conjectural [61].

1.2 Experimental Plan

The overall goal of this dissertation project is to evaluate the potential of electrospun nanocellulose fibers as biomaterial in terms of capability to engineer scaffolding properties and biological performance. With this in mind, five complementary tasks were performed: (1) fabrication of nanocellulose scaffolds by electrospinning technique, (2) engineering scaffolding properties, (3) evaluating physical, chemical, and mechanical properties, (4) introducing bioactive molecules that stimulate cell adhesion and proliferation, and (5) evaluating the cytotoxic, adhesion, and proliferation responses of mammalian cells to the designed materials.

The first task was determining parameters to electrospin cellulose acetate nanofibers with adequate morphology and fiber size that preserved their structure when converted into cellulose nanofibers (Chapter 3). Engineering scaffold properties centered on the fabrication of microporosity, fiber alignment, and hierarchical structures based on electrospun nanocellulose fibrous membranes (Chapter 4).

The next task was to determine the conversion of cellulose acetate into cellulose nanofibers together with the evaluation of changes in wettability, crystalline structure, and surface morphology (Chapter 5). The mechanical properties and surface area were determined as a function of fiber orientation (Chapter 5).

The third task was to surface modify electrospun cellulose fibers by introduction of negative (CMC) and positive (THAMP) charges to attach biological active molecules (hydroxyapatite-like minerals, laminin, RGD-sequence) (Chapter 6). The *in vitro* cytotoxicity of electrospun cellulose fibers was evaluated (Chapter 7). Osteoprogenitor, neural-like, and myoblast cells were seeded onto the electrospun cellulose scaffolds to evaluate the effect of architecture and surface chemical composition on adhesion, proliferation, and differentiation of the cells (Chapter 7).

The conclusions from these studies and their contribution to the tissue engineering field are described at the end of the document in Chapter 8. The results summarized in that chapter demonstrate the feasibility of electrospun nanocellulose as a tissue mimic. Further investigation areas are indicated as well (Chapter 8).

Chapter 2. Materials and Methods

Materials and experimental procedures used in this dissertationresearch are reported in the present Chapter. Section 2.1 describes the electrospinning conditions for Chapter 3. Section 2.2 is related to the fabrication of novel architectures base on cellulose discussed in Chapter 4. The characterization techniques to evaluate physical, chemical, surface, and mechanical properties of electrospun cellulose fibers are described in Section 2.3 and the results discussed in Chapter 5. In section 2.4 the procedures used to improve cellulose bioactivity are described that are addressed in Chapter 6. Finally, section 2.5 contains the cell culture procedures and cell characterization techniques from the results shown in Chapter 7.

2.1 Electrospinning of Cellulose Acetate

2.1.1 Materials. Acetone (99.9%, Sigma Aldrich), isopropanol (99.9%, Burdick & Jackson), dimethylacetamide (DMAc, 99.9%, Sigma Aldrich), and cellulose acetate (Mn = 30,000, 39.8% acetyl groups, Sigma Aldrich), vacuumed-dried, were employed without additional purification.

2.1.2 Electrospinning Process. CA was dissolved in acetone, acetone/isopropanol, and acetone/DMAc, the mixtures had a ratio of 2/1, under constant stirring at room temperature. Each CA solution was placed in a 10 mL disposable syringe and fed by a syringe pump (Harvard Apparatus) through a stainless steel needle with an inner diameter of 0.643mm (Howard Electronic Instruments Inc.). The needle was connected to a high voltage power supply (Spellman's CZE1000R) and positively charged. A voltage of 25 kV was applied between the needle and the grounded collector, in a horizontal collection set-up. The static collector consisted of 10 cm x 10 cm steel mesh covered with aluminum foil. The separation between needle and collector was 25 cm. The experiments were carried out at approximately 20 to 22 °C and relative humidity (RH) of 50 to 60%. The influence of solvent system, concentration, and flow rate on the morphology of CA electrospun fibers was studied. Solutions of CA (17% w/w) in acetone, acetone/isopropanol (2:1), and acetone/DMAc (2:1) were electrospun at flow rate of 1 mL/h. CA concentrations of 10, 13, 15, 17, 18, and 19 % (w/w) were tested for acetone/DMAC (2:1) solvent system at 1 mL/h. CA solution of 17% in acetone/DMAc (2:1) at flow rates of 0.025, 0.1, 0.25, 0.5, 1, and 3 mL/h were electrospun. The conditions tested in the electrospining experiments are

summarized in Table 2.1. Morphological and microstructural features of the samples were investigated by scanning electron microscopy (SEM), LEO (Zeiss) 1550 field-emission and Neoscope from Nikon Instruments. The analysis was carried out for samples coated in gold-palladium with thickness of 35 to 40 Å. The fiber diameter and size distribution of the samples were evaluated from 200 representative fibers of the samples via image analysis software (NIS-Elements BR 3.1).

Table 2. 1 Experimental conditions tested in the CA electrospinning process.

Solvent system	**Concentration** (% w/w)	**Flow rate** (mL/h)
Acetone	17	1
Acetone/isopropanol (2:1)	17	1
Acetone/DMAc (2:1)	10	1
	13	1
	15	1
	17	0.025
		0.1
		0.25
		0.5
		1
		3
	18	1
	19	1

2.2 Novel Architectures of Electrospun Cellulose

2.2.1 Uniaxial Fiber Orientation. The uniaxial orientation of CA fibers was assessed by electrospinning process using a rotating collector at high speed. For this purpose CA solution of 17% (w/w) in acetone/DMAc (2:1) was electrospun, separately, on a grounded mandrel and disk.

2.2.1.1 Mandrel. An aluminum mandrel with 76 mm of diameter covered with aluminum foil was used as a collector in the electrospinning process. The CA solution was fed with a syringe pump (Harvard Apparatus) at a rate of 1 mL/h with a positive applied voltage of 25 kV from a high voltage power source (Spellman's CZE1000R). The environmental conditions were approximately 50 %RH and 20 °C. The

mandrel was grounded and placed at 10 cm from the needle of the syringe. The orientation of the electrospun fibers was studied with image analysis as a function of the linear velocity of the mandrel.

2.2.1.2 Disk. A rotating aluminum disk (100 mm in diameter and 3mm of thickness) with a flat edge (10 mm in width and 5 mm of thickness), see Fig. 2.1, was employed in the electrospinning process at a linear speed of 21 m/s. CA solution was fed with a syringe pump (World Precision Instruments, Inc.) at speed of 1mL/h through a stainless steel needle with an inner diameter of 0.643mm (Howard Electronic Instruments Inc.). A positive voltage of 25kV was applied with a high voltage power supply (Spellman's CZE1000R) at approximately 54% RH and 20°C. The electrospun material was collected on aluminum foil placed at the edge of the disk. The separation between needle and the edge of disk was 22 cm.

Figure 2. 1 Aluminum disk device used as rotating collector.

2.2.2 Fabrication of Microporosity by Laser Ablation. Porosity was created on the CA fibrous meshes using a direct-write 60W laser (CO_2 laser of 10 µm wave length, Universal Laser Systems V460) at standard room conditions. The laser has a CO_2 air-cooled cartridge, a 50 mm focus lens that provides a 127µm spot size at a distance of 2.5 in, and a high power density focusing optics attachment that allows the laser beam to be focused to a much smaller spot size (32 µm). The porosity was created using the vector mode of the device by controlling the power (W), speed (in/s), and intensity of the laser (pulse per inch, PPI). Different experiments were carried out in order to establish the adequate value of those parameters in order to create pores with the desired size and shape and to avoid thermal degradation of the material. Patterns composed of circles and circles formed by parallel lines were designed in AutoCAD. The porosity patterns were ablated on the CA samples by using an x-y axis stage.

Pores of approximately 300 microns in diameter, with horizontal separation between pores of 1500 µm and a vertical separation of 500 µm, were ablated on the electrospun CA using 6 W, 6.7 in/s, and 500 PPI. After laser treatment the scaffolds were regenerated to cellulose by saponification reaction with 0.05 M NaOH solution in ethanol at room temperature for 24 hr. The microstructural features of laser ablated samples were characterized by SEM (LEO (Zeiss) 1550 field-emission and Neoscope from Nikon Instruments).

2.2.3 Electrospun Fiber Coated Microfiber Filament. The CA nanofiber coated lyocell fiber (NFCLF) structure was fabricated using a technique designed by Thorvaldsson *et al* [62]. In this process, lyocell fiber, a textile yarn composed of cellulose, was placed between the collector and electrospinning syringe pump. A study to determine the parameters to produce random and aligned electrospun fibers on the lyocell substrate was carried out. A 3 mL disposable syringe was filled with 17% (w/w) CA solution in acetone/DMAc (2:1). The solution was fed by a syringe pump (World Precision Instruments, Inc.) through a stainless steel needle with an inner diameter of 0.643mm (Howard Electronic Instruments Inc.). The CA solution was deposited at a flow rate of 0.4 mL/h and 0.3 to 0.5 mL/h for the random and aligned nanofibers, respectively. A grounded copper tape of 1 cm x 1 cm was placed on a plastic disc that rotated around the lyocell fiber. The disc was placed at a distance of 22 cm from the tip of the needle. The voltage was set with a high voltage power supply (Gamma High Voltage Research, Inc.) to 25 kV for random and 30 kV for aligned nanofibers. A Teflon tube of 10 cm in diameter was used to guide the nanofibers onto the lyocell filament. The teflon tube was placed between the needle and the rotating disc. The random non-oriented nanofibers were deposited on lyocell microfibers that were previously wetted in DI water. In the production of aligned nanofibers the lyocell fiber was kept dried. The NFCLF was wound-up onto a rotating plastic wheel of 2 cm in diameter rotating at 10 RPM placed behind the rotating disk. The speed of the lyocell microfibers during the electrospinning was established as 3.7×10^{-3} and 10.5×10^{-3} m/s for random and aligned nanofiber, respectively. Electrospinning of CA solution was conducted in relative humidity equal or higher than 23% at 23 °C. The final parameter values used are summarized in Table 2.2. The NFCLF were dried in a vacuum oven under 50°C and 10 mTorr for 1 day to remove excess solvent. The regeneration of NFCLF was performed by covering the samples with a 0.05M solution of NaOH in ethanol for 24 hr at room temperature. Thereafter the samples were carefully rinsed in DI water several times to stop the reaction and to remove the remaining NaOH. The samples were stored in DI water until use. The surface morphology of the NFCLF specimens before and after regeneration treatment was characterized by SEM (JSM-5300, JEOL, Ltd.,

Tokyo, Japan). The samples were coated with a thin layer of gold (Fine Coat Ion Sputter JFC-1100, JEOL Ltd., Tokyo, Japan) before SEM analysis.

Table 2. 2 Conditions used during electrospinning of random and aligned NFCLF.

Parameter	Random nanofibers	Aligned nanofibers
Flow rate (mL/hr)	0.4	0.3-0.5
Throw distance (cm)	22	22
Voltage (kV)	25	30
Humidity (% RH)	≥23	≥23
Temperature (°C)	23	23
Collection speed (m/s)	$3.7x10^{-3}$	$10.5x10^{-3}$
Lyocell size (μm)	350	350

2.3 Electrospun Cellulose a New Member of Nanocellulose Family

2. 3.1 Pseudo-Kinetics of Cellulose Regeneration. Nanofibers of CA (Mn = 30,000, 39.8% acetyl groups, Sigma Aldrich) were obtained by electrospinning. CA powder was vacuum dried at 50°C and 10mTor prior to dissolution. Solution of CA (13%w/w) in acetone/dimethylacetamide (DMAc, 99.9%, Sigma Aldrich) (2:1) was loaded into a 10mL disposable syringe. The CA solution was fed at speed of 3 mL/h; a positive voltage of 25 kV was applied between the needle and the grounded collector that were 25 cm apart. Consistencies in electrospinning CA were achieved by regulating the RH in the system. The electrospun CA fibers were carefully removed from the aluminum foil by peeling from the edge of the mat and put into a vacuum oven under 50 °C and 10 mTorr for 1 day. The dried CA scaffold was immersed into 0.05 M NaOH solution in ethanol for 5, 15, 30, 45 min, and 1 day at room temperature, in order to remove acetate groups via alkali catalyzed saponification. The regenerated cellulose scaffolds were thoroughly rinsed and kept in DI water for further treatment. Fourier-Transform infrared (FTIR) spectroscopic analysis, 8700 Nicolet Thermo Electron, in transmission mode, was used in the wave number range of 4000-500 cm^{-1} to measure the relative degree of regeneration into cellulose of the electrospun scaffolds. Experimental FTIR spectra of solid samples were obtained by preparing KBr pellets with ratio of 1:99 (1 mg to 99 mg) sample-to-KBr, and scanned at a resolution of 4 cm^{-1} and averaged over 64 scans. Regenerated cellulose meshes were analyzed by SEM (LEO (Zeiss) 155) to study change in morphology due to deacetylation treatment.

2.3.2 Thermogravimetric Analysis. The presence of residual solvents and humidity in electrospun CA (ECA) and regenerated cellulose (EC) fibers was determined by thermogravimetric analysis (TGA, Perkin-Elmer TGA-7). The fibers were produced from CA solution of 17% Wt in acetone/DMAc (2:1). During the electrospinning process an electrostatic field of 25 kV/25 cm was applied at a flow rate of 1mL/h, the temperature and RH were 20 °C and 50 to 60%, respectively. The electrospun CA fibers were regenerated with 0.05 M NaOH solution in ethanol at room temperature for 1 day. The regenerated cellulose sample was carefully rinsed in DI water several times and dried in a vacuum oven under 50 °C and 10 mTorr for 1 day. Approximately 5.0 mg of each sample was analyzed from 25 °C to 600 °C at a heating rate of 20 °C/min under nitrogen flow rate of 20 mL/h.

2.3.3 Crystalline Structure. In order to analyze the crystalline structure of the electrospun fibers, X-ray powder diffraction (XRD, Bruker D8 Discover) was performed from 2θ values of 10 to 60 ° on samples of random oriented cellulose acetate, and 24 hr regenerated random and aligned cellulose.

2.3.4 Surface Area Analysis. The surface area of random oriented and aligned electrospun cellulose meshes were derived from N_2 adsorption-desorption isotherms at 77K with the Brunauer-Emmett-Teller (BET) equation using a surface area and porosity analyzer (TriStar 3000, Micromeritics, USA).

2.3.5 Tensile Properties. Young's modulus, strength at break, and strain at break of random oriented and aligned electrospun cellulose fibrous meshes were determined by a tensile tester Instron 5565A using a 100 N static load cell at 25 mm gauge length and cross-head speed of 5 mm/min. The samples were tested dry (samples were previously dried at room temperature inside a hood) at 22 °C and 45% relative humidity, wet in a water bath at 22 °C, and in physiological conditions in phosphate buffer saline solution (PBS) bath at 37 °C. The specimens were cut along the vertical direction of the electrospun fibers to a size of 20 mm width and 100 mm length. The thickness and weight of the fibrous meshes were 0.03 mm and 47 mg (11% variation) in aligned fibers and 0.10 mm and 60 mg in random oriented fibers (20% variation), respectively. The Young's modulus of the samples was derived from the slope of the initial linear part of the stress-strain curves.

2.3.6 Wettability. Water contact angle (θ) of CA and random oriented and aligned cellulose samples was determined by a FTA dynamic contact angle analyzer to evaluate the hydrophilicity of these materials. Samples were dried in a vacuum oven at 80 °C and 10 mTorr over night before characterization. The contact angle measurements were carried out in the electrospun fibrous meshes with size of 2 cm x 6 cm placed onto a glass slide.

2.4 Improvement of Bioactivity on Electrospun Cellulose Scaffolds

2.4.1 Ca-P mineralization

2.4.1.1 Surface Modification (CMC Adsorption). In order to generate carboxyl groups on the surface of cellulose nanofibers, the scaffolds were exposed to carboxymethyl cellulose (CMC) adsorption in two ways. Procedure 1 involved exposing the scaffold to a mixture of 0.01 M $CaCl_2$ solution and 250 mg of CMC (100 000 g/mol, DS = 1.2, Celco, Sweden) for 24 h. Procedure 2 consisted of exposing the scaffold to a mixture of 0.01 M $CaCl_2$ solution and 250 mg of CMC at pH 8 adjusted by addition of 0.1N NaOH, at 80 °C for 2 h. Subsequently, the scaffolds were treated with 0.1 M $CaCl_2$ solution for 24 h at room temperature for both procedures. The modified scaffolds were then placed into excess deionized water for 1 h and agitated every 15 min in order to rinse the material from ions like chlorine.

2.4.1.1.1 Characterization. *Dye Adsorption Treatment*. The cellulose fibers treated with CMC were suspended in a 0.1% toluidine blue solution (20 mL/0.01 g of sample). The suspension was agitated at room temperature for 3 hours; the stained fibers were washed thoroughly with ethanol (300 mL) and then water (50 mL) by filtration. The original (control) and CMC treated electrospun fibers were observed by optical microscope (Nikon Instruments). *Conductometric Titration*. The amount of charge introduced by CMC adsorption process was determined by conductometric titration, using a Mettler Toledo pH meter with a conductivity probe. The fibers of the CMC modified electrospun cellulose scaffold and controls were carefully separated with tweezers in DI water. Thereafter, the fibers were sonicated to aid in dispersion. The electrospun cellulose dispersion was pretreated with 100 mL of HCl 0.1N for 1 h at 300 rpm and room temperature followed Katz procedure [63]. The pretreated fibers were rinsed several times with DI water. The dispersion of the electrospun cellulose fibers (approximately 0.22 g of dry weight) for titration was prepared by the addition of 0.001 mol of NaCl, 5mL of HCl 0.1N and DI water to a total volume of 350 mL. The conductometric titration was carried out under nitrogen atmosphere. A volume of 0.25 mL of NaOH 0.1N was added every 5 min before and after the conductivity plateau zone was reached. In the conductivity plateau zone, 0.1 mL of NaOH was added in 5 min intervals. Normally, titration was stopped at approximately pH 10.5. The surface chemical composition of the scaffold nanofibers was quantified with a scanning photoelectron spectrometer (XPS) Microprobe PHI Quantera SXM with a highly focused monochromatic X-ray beam. A rectangular area of 1 mm by 0.1 mm was scanned on the surface of the samples.

2.4.1.2 Simulated Body Fluid Treatment. Simulated body fluid (SBF) solution was prepared according to Cüneyt Tas procedure and stored at 5 °C for no longer than a month during its use [29]. The chemical composition of SBF solution is listed in Table 2.3. A comparison between ion concentration in SBF solution used in this study and the human plasma is shown in Table 2.4. The SBF solution was prepared by adding the chemicals sequentially until complete dissolution of each salt, in the order showed in Table 2.3. Fifteen mL of HCl 0.1 N solution was added before the addition of calcium chloride, to avoid calcium chloride precipitation as suggested within the procedure. Finally, the temperature was increased to 37 °C and the pH adjusted at 7.4 by the addition of $(CH_2OH)_3CNH_2$ (0.5 g/L) and HCl (25 mL/L) to mimic physiological conditions. Regenerated cellulose scaffolds (45 min and 24 h) without surface modification, CMC treated scaffolds at the different conditions, and reference scaffolds at the conditions of the second CMC treatment (pH 8, 80 °C for 2 h) were treated with SBF solution. The SBF treatment consisted of the static exposure of 1 cm by 1 cm sections of the cellulose scaffolds to 15 mL of SBF solution at 37 °C. The SBF solution was refreshed every day during 1 week. After the SBF treatment was completed, the samples were rinsed in distilled water several times and lyophilized for further characterization.

Table 2. 3 Simulated body fluid solution chemical composition [29].

Order	Reagent	Amount (g/L)
1	NaCl	142.0
2	$NaHCO_3$	103.0
3	KCl	27.0
4	$Na_2HPO_4\ 2H_2O$	5.0
5	$MgCl_2\ 6H_2O$	1.5
6	$CaCl_2 2H_2O$	2.5
7	Na_2SO_4	1.0
8	$(CH_2OH)_3CNH_2$	0.5

Table 2. 4 Ion concentrations of SBF solutions and human plasma [29].

Ion	Human Blood (mM)	Present work (mM)
Na^+	142.0	142.0
Cl^-	103.0	125.0
HCO_3^-	27.0	27.0
K^+	5.0	5.0
Mg^{2+}	1.5	1.5
Ca^{2+}	2.5	2.5
HPO_4^{2-}	1.0	1.0
SO_4^{2-}	0.5	0.5

2.4.1.3 Phosphate Buffer Saline Solution Treatment. An alternative mineralization process was also investigated using PBS. The surface of cellulose fibers were modified with CMC (procedure 1) as previously described. The CMC treated cellulose scaffolds were exposed to phosphate buffer saline solution (PBS, Dulbecco's phosphate buffered saline with magnesium and calcium, PAA) at 37 °C for 1 week in order to coat the cellulose fibers with Ca-P crystals. The chemical composition of PBS according to Dulbecco *et al* is shown in Table 2.5.

Table 2. 5 Phosphate buffer saline solution chemical composition [64].

Reagent	Amount (g/L)
KCl	0.25
KH_2PO_4	0.25
NaCl	10.0
Na_2HPO_4	1.44
$MgCl_26H_2O$	0.12
$CaCl_2$	0.12

2.4.1.3.1 Characterization. The morphology of the mineralized nanofibrous scaffold was characterized by scanning electron microscopy (SEM, LEO Ultra 55 FEG and LEO (Zeiss) 1550 field-emission SEM). The composition and structure of the crystals produced by PBS mineralization process were analyzed by SEM (FEI Quanta 600 FEG)-Energy Dispersive X-Ray Spectrometer (EDX, Burker QUANTAX 400 with high speed silicon drifted detector). In order to analyze the crystalline structure of the electrospun scaffolds and determine the identity of the produced crystals, X-ray powder diffraction (XRD, Bruker D8 Discover) was performed from 2θ values of 10 to 60° for samples treated with SBF and PBS.

2.4.2 Adsorption of Xylogucan-RGD. The adsorption of xyloglucan (XG) modified with Arg-Gly-Asp (RGD) cell adhesion peptide (XG (46 kDa)-GRGDS, SweTree Technologies) was introduced in order to improve cell attachment on electrospun cellulose following Bodin *et al* procedure [27]. XG-RGD was dissolved in DI water at concentration of 2 mg/mL at room temperature for 1 h. The cellulose samples were immersed in 100 mL of aqueous solution containing 15% (w/w) XG-RGD corresponding to the dry weight of cellulose. The samples were incubated in the XG-RGD solution for 1 day at room temperature under low agitation. The samples were rinsed in DI water several times and dried for characterization.

2.4.3 Cationization Treatment (THAMP modification). Electrospun cellulose samples were chemically modified to introduce cationic charge and therefore to enhance the adsorption of cell adhesion proteins. The ionic charge was introduced through production of trimethyl ammonium betahydroxy propyl (THAMP). THAMP modification was carried out according to Watanabe *et al* protocol [58]. The samples were treated with 0.5M NaOH at 70 °C for 60 min. Thereafter, glycidyltrimethylammonium chloride (39.6 mmol) was added. The mixture was kept at 70 °C for 5 hours to obtain trimethyl ammonium betahydroxy propyl (THAMP) electrospun cellulose. Finally, the samples were rinsed twice with 0.1M HCl for 5 minutes and once with 0.1M NaCl 0.1M acetic acid/sodium acetate buffer solution for 30 minutes.

2.5 Evaluation of Cell Response on Electrospun Cellulose Scaffolds

2.5.1 Scaffold Sterilization Procedure. The EC scaffolds placed in a glass container with DI water were sterilized in an autoclave at 121 °C and 230 kPa for 30 minutes.

2.5.2 *In Vitro* Cytotoxicity Test

2.5.2.1 Minimal Essential Media Elution Test. The minimal essential media (MEM) elution test was designed to determine the cytotoxicity of extractable substances from medical devices. The amount of test material extracted was based on surface area or weight recommendations by ABSI/AAMI/ISO and USP standards. Test samples and controls were extracted in 1X MEM with 5% bovine serum for 24 to 25 hours at 37 ± 1° with agitation. Multiple well cell culture plates were seeded with a verified quantity of industry standard L-929 cells (ATCC CCL-1) passage 30 and incubated until approximately 80% confluent corresponding to 1.5 x 10^5cells/mL. The test extracts were filtered to avoid bacterial contamination and added to the cell monolayers in triplicate. The cells were incubated with the extracts at 37 ± 1° with 5 ± 1% CO_2 for 72 ± 3 hours. The cell monolayers were examined microscopically. The cells on the wells were scored as to the degree of discernable morphological cytotoxicity on a relative scale of 0 to 4 according to the criteria shown in Table 2.6. The results from the three wells were averaged to give a final cytotoxicity score value.

Table 2. 6 Qualitative morphological grading of cytotoxicity of extracts.

Culture conditions	Reactivity	Grade
No cell lysis, intracytoplasmic granules	none	0
Not more than 20% rounding, occasional lysed cells	slight	1
Not more than 50% rounding, no extensive cell lysis	mild	2
Not more than 70% rounding and lysed cells	moderate	3
Nearly complete cell destruction	severe	4

The United States Pharmacopeia and National Formulary (USP 87) states that the test article meets the requirements, or receives a passing score (pass) if the reactivity grade is not greater than 2 or a mild reactivity. The ANSI/AMI/ISO 10993-5 standard states that the achievement of a numerical grade greater than 2 is considered a cytotoxic effect or a failing score (fail).

2.5.2.2 Agar Overlay Test. The agar overlay test was designed to determine the cytotoxicity of diffusible components from material or solutions. A layer of agar was added over cell monolayer to act as a cushion to protect the cells from mechanical damage while allowing the diffusion of leachable materials. The tested articles were then placed on top of the agar layer and incubated. The cell monolayers were examined and scored based on the degree of cellular destruction. Six well cell culture plates were seeded with a verified quantity of industry standard L-929 cells (ATCC CCL-1) passage 30 and incubated until approximately 80% confluent corresponding to $1.5x10^5$ cells/mL. The agar overlay consisted of an equal mixture of 2X agar (1.0%) and 2X MEM + 10% bovine calf serum. Solid tested articles were placed directly on the solidified agar overlay testing ≥ 100 mm^2 per test well. Liquid or gel tested articles were applied to sterile filter discs testing no less than 0.1 mL per well. Powders, resins, or irregular materials were placed directly onto the solidified agar, testing no less than 100 mg per well. Positive and negative references controls were included with each assay. All tests were performed using three test wells per sample. After the addition of the tested samples, the cell culture plates were incubated above for 24 to 26 hours. Following incubation, cells were evaluated microscopically using the evaluation criteria outline in Table 2.7. The results from the three wells were averaged to give an average cytotoxicity score.

Table 2. 7 Reactivity grades for agar diffusion test and direct contact test.

Grade	Reactivity	Description of zone
0	None	No detectable zone around or under the tested article
1	Slight	Some malformed or degenerate cells under the tested article
2	Mild	Zone limited to area under the tested article
3	Moderate	Zone extending to 1.0 cm beyond the tested article
4	Severe	Zone greater than 1 cm in extension from tested article.

2.5.2 Osteoprogenitor Cells. Mouse osteoprogenitor cells (MC3T3-E1, American Type Culture Collection (ATCC) subclone 4, CRL-2593, passage 21) were expanded in α-modified minimum essential media (α-MEM, Invitrogen) substituted with 10% V/V fetal bovine serum (FBS, PAA) and 1% V/V antibiotic/antimyotic (A/A, Invitrogen) at 37 °C in 5% CO_2 and 95% relative humidity. After 3 days of expansion the cells had reached 80% confluency. The cells were washed twice with PBS (Dulbecco's phosphate-buffered saline without magnesium and calcium, PAA) and removed from the petri dishes by treatment with 0.05% V/V trypsin–EDTA (Invitrogen). Before cell seeding, the scaffolds were pre-treated for 12 h in α-MEM and incubated at 37 °C in 5% CO_2 and 95% relative humidity to equalize conditions. MC3T3-E1 cells were seeded using a pipette onto the cellulose scaffolds (6mm of diameter) with a density of 20 000 cells/cm^2 on each scaffold type. MC3T3-E1 cells were seeded on EC, mineralized EC, porous EC, and mineralized porous EC scaffolds. The experiment had 2 replicates for each category and the cell study ran for 3 days.

2.5.3 Neural-like Cells. Rat pheochromocytoma cell-line (PC12,) kindly provided by Prof. Andrew Ewing (Chalmers University of Technology, Gothenburg, Sweden), was used as neural cell model. PC12 cells were propagated in RPMI-1640 media (without l-glutamine and phenol red, PAA) supplemented with 10% horse serum (PAA), 5% fetal bovine serum (PAA) and 0.4% antibiotic-antimycotic solution (100X, Gibco). The media was changed every 2 to 3 days until confluency was reached. In order to differentiate PC12 cells the culture media composition was changed. PC12 cells were cultured in RPMI-1640 media, supplemented with 3% horse serum, 1.5% fetal bovine serum, 0.4% antibiotic-antimycotic solution and 50 ng/mL of nerve growth factor 2.5S (NGF, natural from mouse, Gibco) was added. The media was changed every 2 to 3 days. PC12 cells were incubated at 37 °C in 7% CO_2, and 100% humidity. Before cell seeding, XG-RGD treated, THAMP modified and non-treated scaffolds were washed twice with RPMI-1640 media and incubated in RPMI-1640 media for 3 days at 37 °C. After this process, the samples were divided into two groups. One group was only exposed to RPMI-1640 media and the other one had an additional treatment with laminin (natural from mouse, Invitrogen). For the laminin treatment, the growth media was removed from the wells and 50 μg/mL of laminin solution was added to each well. The samples were incubated for 5 hours at 37 °C. The laminin solution was removed and the scaffolds were incubated with RPMI-1640 media for 30 minutes before PC12 cell seeding. PC12 cells were seeded onto the scaffolds (8mm of diameter) at a density of 56 000 cells/cm^2, approximately. PC12 cells of passage 27 were used in the study.

2.5.4 Myoblast Cells. Mouse myoblast cell line (C2C12) was used to regenerate muscle tissue on random and aligned EC scaffolds. C2C12 cells were expanded in Dulbecco's modified eagle's medium with high glucose and L-glutamine (DMEM, Fisher Sci.), 10% fetal bovine serum (Fisher Sci.) and 1% penicillin-streptomycin (Fisher Sci.). The cells were washed twice with PBS and removed from the containers by treatment with 0.05% V/V trypsin–EDTA. Cells number was subsequently estimated using a hemocytometer and a microscope. C2C12 cells were differentiated in DMEM with 2% horse serum (Fisher Sci.) and 1% penicillin-streptomycin, after 80% of confluence (this took 5 days). The cells were incubated at 37 °C in 5% CO_2 and 95% relative humidity. In order to improve the adhesion of C2C12 cells to the cellulose scaffolds, adsorption of proteins from the culture media to the electrospun scaffolds was carried out. The random and aligned THAMP modified EC scaffolds were treated with DMEM and incubated over night at 37 °C in 5% CO_2 and 95% relative humidity. A cell density of 50 000cell/cm^2 was seeded onto modified (THAMP and culture media treated) and non modified random and aligned EC scaffolds (8mm of diameter). The cell study was carried out for 3h, 1, 7, and 14 days. Cells seeded on scaffolds for 3 hours and 1 day were only cultivated with growth media. Cells cultured on scaffolds for 7 and 14 days were incubated in growth the first 3 days and after that the media was changed to differentiation media for the rest of the cultivation time.

2.5.5 Cell Fixation. The culture media was removed from the cell seeded samples and the samples were rinsed twice with PBS. The fixation was carried out by incubation of the samples with 4 % V/V methanol free formaldehyde (Polysciences) for 30 minutes (MC3T3-E1) and 1 hr (C2C12 and PC12). Finally, the samples were washed twice with PBS to remove not-adhered cells.

2.5.6 Cell Staining. Cells were permeabilized in PBS containing 0.1% Triton-X 100 (Sigma-Aldrich) for 45 min. In order to visualize fixed cells on the scaffolds, the samples were stained with 4',6-diamidino-2-phenylindole (DAPI, Invitrogen) and rhodamine phalloidin (Invitrogen) to observe nuclei and F-actin of cytoskeleton, respectively.

2.5.7 PC12 Cell Viability Test. The proliferation of PC12 cells seeded on random oriented EC scaffolds was evaluated using a MTS (3-(4,5-Dimethylthiazol-2-yl)-2,5-diphenyltetrazolium bromide, Promega, Madison, WI, USA) assay after 1 day of cell culture. The culture media was carefully removed from the scaffolds and 84 µL of the MTS assay reagent (plus 416 µL of culture media) was added. The cell seeded scaffolds, 3 scaffolds of each kind, were incubated overnight with MTS assay reagent in PC12 cell growth

medium. During the incubation, the MTS tetrazolium yellow compound was enzymatically reduced by the PC12 cells into a purple formazan product. After 16 hours, aliquots of 120 µL (2 replicates from each scaffold) were transferred into the wells of a 96-well plate. The quantity of the formazan product was measured by absorbance at 490 nm using a spectrophotometric plate reader (Epoch Microplate Spectrophotometer, BioTek Instruments). An average value from 9 measurements for each scaffold type was obtained. The recorded absorbance of the control was subtracted from the calculated average value for each sample. The control consisted of the MTS reagent and the cell media. The absorbance measurements were directly related to the number of viable cells on the scaffolds through a cell density standard.

2.5.8 Cell-Scaffold Characterization. The morphology of PC12 and C2C12 cells on the nanofibrous scaffolds was characterized by SEM (JEOL JSM-5300 and LEO Ultra 55 FEG). Cell-scaffold interaction was also visualized by fluorescence phase contrast microscope (Leica DMI4000 Digital Microscopes Inverted and analyzed in the software Leica LAS AF).

Chapter 3. Electrospinning of Cellulose Acetate

The aim of this study was to determine the electrospinning parameters and solvents to adequately produce CA nanofibers that can be converted into cellulose with an adequate morphology, fibers size, and fiber size distribution to perform as scaffolds for tissue engineering applications.

3.1 Electrospinning Parameter Study.

Fiber size and fiber morphologies are impacted by a variety of polymer and electrospinning parameters [64]. Principal in controlling fiber size is the effect of concentration of the polymer in solution as fiber diameter scales with solution viscosity, which has been extensively studied [35, 36, 64-67]. Solvent choice also greatly impacts fiber size along with solution conductivity. Processing parameters specific to electrospinning such as flow rate of the polymer solution and field strength, impact fiber size as well [36, 64-66]. Electrospinning of cellulose acetate (CA) was studied in relation to factors of solvent composition, polymer concentration, and flow rate to better elucidate how the processing window impacts electrospun CA. This current study, builds from several studies regarding the parameters of CA electrospinning to quantify fiber size and distributions [6, 7, 68-71]. However, the effect of the flow rate on the morphology, fiber size, and fiber size distribution of the electrospun fibers has not been discussed and is scarcely mentioned in the majority of works. Literature resources regarding CA electrospinning fiber size and morphology are summarized in Table 3.1 and Table 3.2 contains a list of thirteen different solvent systems that has been used for electorspinning cellulose.

In this study acetone, acetone/isopropanol (2:1, w/w), and acetone/dimethylacetamide (2:1, w/w) were selected as solvent systems to dissolve CA. Acetone and isopropanol are highly volatile solvents with low boiling points, while dimethylacetamide (DMAc) is not. Each solution was prepared at a concentration of 17% (w/w), the selected flow rate was 1mL/h, and the applied electrostatic field during electrospinning experiments was 1kV/cm. Continuous electrospun CA fibers were obtained from all the solvent systems tested (see Fig. 3.1). No literature research has reported on the capability of acetone/isopropanol solvent system to produce electrospun CA fibers (see Table 3.2). Additionally, there is controversy in the formation of electrospun fibers from pure acetone solution. Liu and Hsieh [6]

(15% and 20% wt) and Tungprapa *et al* [7] (5%, w/v) have reported that is not possible to produce continuous CA fibers from pure acetone. However, Han and Gouma [71] and Son *et al* [70] have described electrospun CA fibers from solutions of concentrations of 17.5% (w/v) and 17% and 20% (w/w), respectively. The disagreement is due to the fact that acetone solution easily obstructs the tip of the needle during the electrospinning because the fast evaporation of acetone [7, 70]. Son *et al* mentioned that the fibers they achieved were produced previous to clogging of the needle tip [70]. In the present work, the tip was continuously cleaned during the electrospinning process. In this way, it was possible to create electrospun CA meshes of 10 cm x 10 cm with various thicknesses after 1, 2, or even 3 hours of electrospinning process. This procedure was also required during the electrospinning of CA dissolved in the solvent mixture of acetone/isopropanol due to similar issue. Nonetheless the capability of all solvents to produce continuous fibers of CA, a large difference in the morphology, fiber size, and fiber size distribution was observed in the fibers produced among them. Fibers produced from acetone and the mixture of acetone/isopropanol (2:1) exhibited a flat ribbon structure (Fig 3.1 A&B) in contrast to the system acetone/DMAc (2:1) that produced the common cylindrical fiber shape (Fig. 3.1 C). It has been established that fibers with ribbon structure contain a high molecular orientation which is the result of the rapid evaporation of the solvent [72]. When using acetone (Tb = 56 °C) or acetone/isopropanol (Tb_{mix} = 64.8 °C) mixture, a skin is formed on the surface of the droplet, and this skin is uniaxially stretched at the jet forming the ribbon-like structure when the rest of the solvent evaporates. With respect to the fiber size, acetone produced the higher average fiber size (2.77µm, see Fig. 3.1 A) followed by the mixture acetone/isopropanol (2:1) with an average size of 2.47µm (Fig. 3.1 B). The value of the fibers obtained from acetone solution is close to the value reported by Son *et al* [70]. Only the mixture acetone/DMAc (2:1) was able to generate CA fibers with an average fiber size in the submicron range (Fig. 3.1 C), with a range of values from 147 nm to 2.1µm. These values are comparable to the fibers described by Liu and Hsieh for the same solvent composition [6]. The mixture of acetone/DMAc (2:1) also produced the lowest distribution in size of the fibers, with approximately 84% of the fibers in the interval of 400 to 800 nm as illustrated in Fig 3.1 C. For this reason, with the purpose of optimizing the morphology, fiber size, and fiber size distribution of CA fibers, additional experiments relative to polymer concentration and flow rate were carried out for the solvent system acetone/DMAc (2:1).

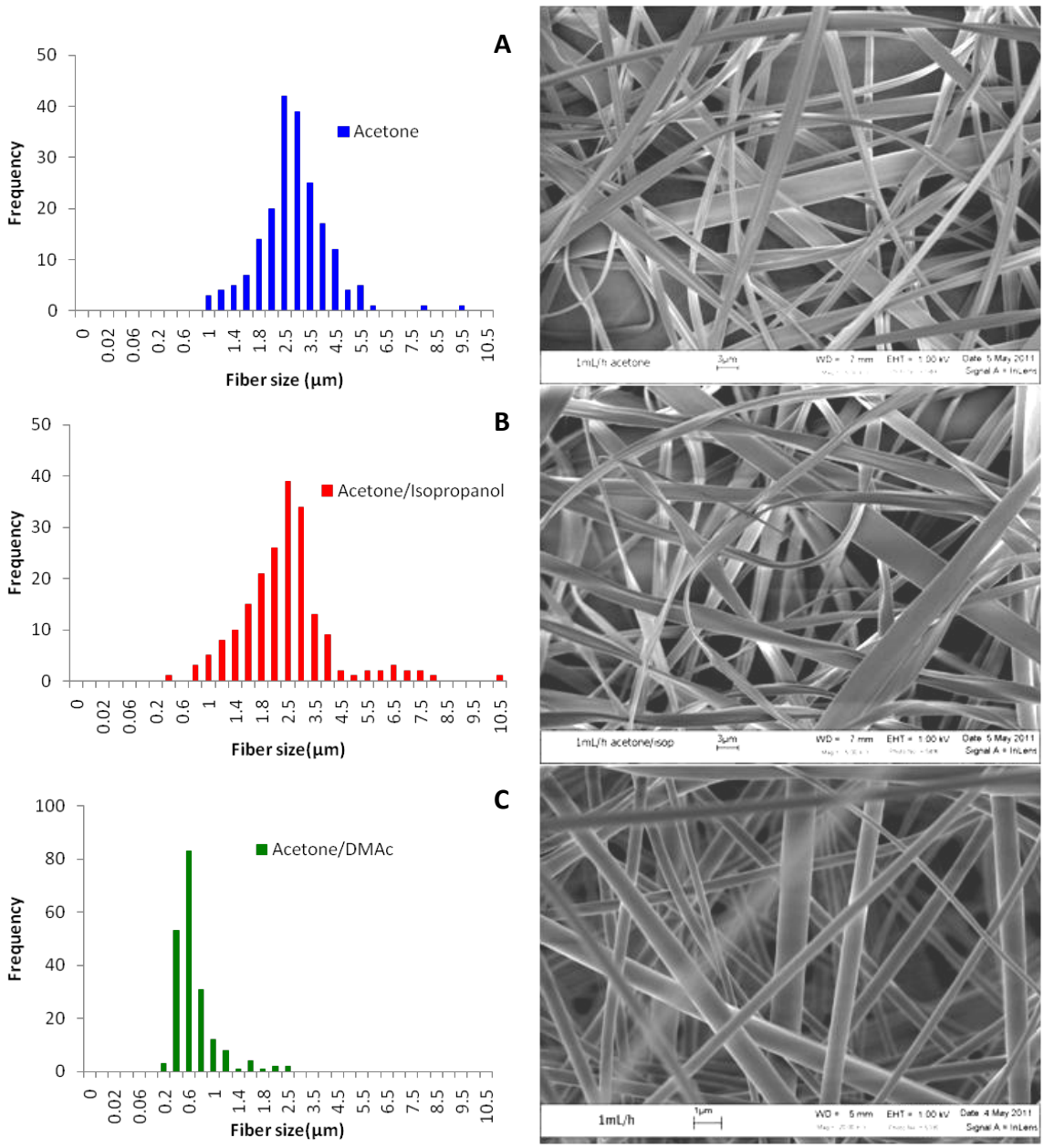

Figure 3. 1 Effect of solvent composition on the fiber size distribution and morphology of fibers produced from 17% CA (w/w) in: A) Acetone, B) acetone/isoporpanol (2:1), and C) Acetone/DMAc (2:1).

In those experiments, it was found that CA concentration has a large impact in the morphology of the electrospun fibers (see Fig. 3.2) as described in many different studies [65, 66, 71, 73]. Low concentration of CA produced high amount of beaded fibers whereas the increase in concentration to a specific value reduced the amount of beads. This response originates from the deficient polymer entanglement that results in instability of the solution jet [6, 65, 66, 68, 70]. Surface tension and net charge were held constant because polymer/solvent composition and electric field strength, respectively, were not modified; polymer entanglements, impacting the viscosity of the solution, is the main driving force in the creation of beads. Additionally, the shape of the beads changed from spherical to spindle-like from concentration of 10% to 15% and the size was increased as well, as documented by Fong for PEO [65] and also observed for CA [69, 70]. As shown in Fig. 3.2C at electrospinning at a concentration of 17% there was almost no beads. After increasing the concentration from 17% to 18% the beads were formed again, though the sizes of the beads were bigger and the amount of them was lower than the beads formed at 15%. Observed at 19% concentration there were large clusters, these clusters seemed to be the result of the fusion of several fibers (Fig. 3.2F). Therefore, as suggested by Fig. 3.2C, 17% of CA was considered the optimal concentration for the formation of ultrafine CA fibers. This result is consistent with Son *et al.* observations.

The flow rate of the solution, at the syringe pump, impacted bead formation (Fig. 3.3), fiber size and its distribution (Fig. 3.4). There was formation of beads and large clusters of CA though the initial polymer/solvent composition when the strength of electric field was held constant. The formation of beads and clusters was observed for the highest flow rate tested (Fig. 3.4A). That result is similar to that observed during electrospinng when CA concentration was above 17% w/w (see Fig. 3.2 F). It appears that the electric field was not high enough to produce smooth fibers as there was too much material at the droplet. Accordingly, the high flow rate (or high concentration) caused an increase in viscosity or/and surface tension due to a local accumulation of the polymer on the tip of the needle as evaporation of the solvent occurred. The clusters were reduced and disappeared by decreasing the flow rate as shown in Fig.3.3 (B to F).

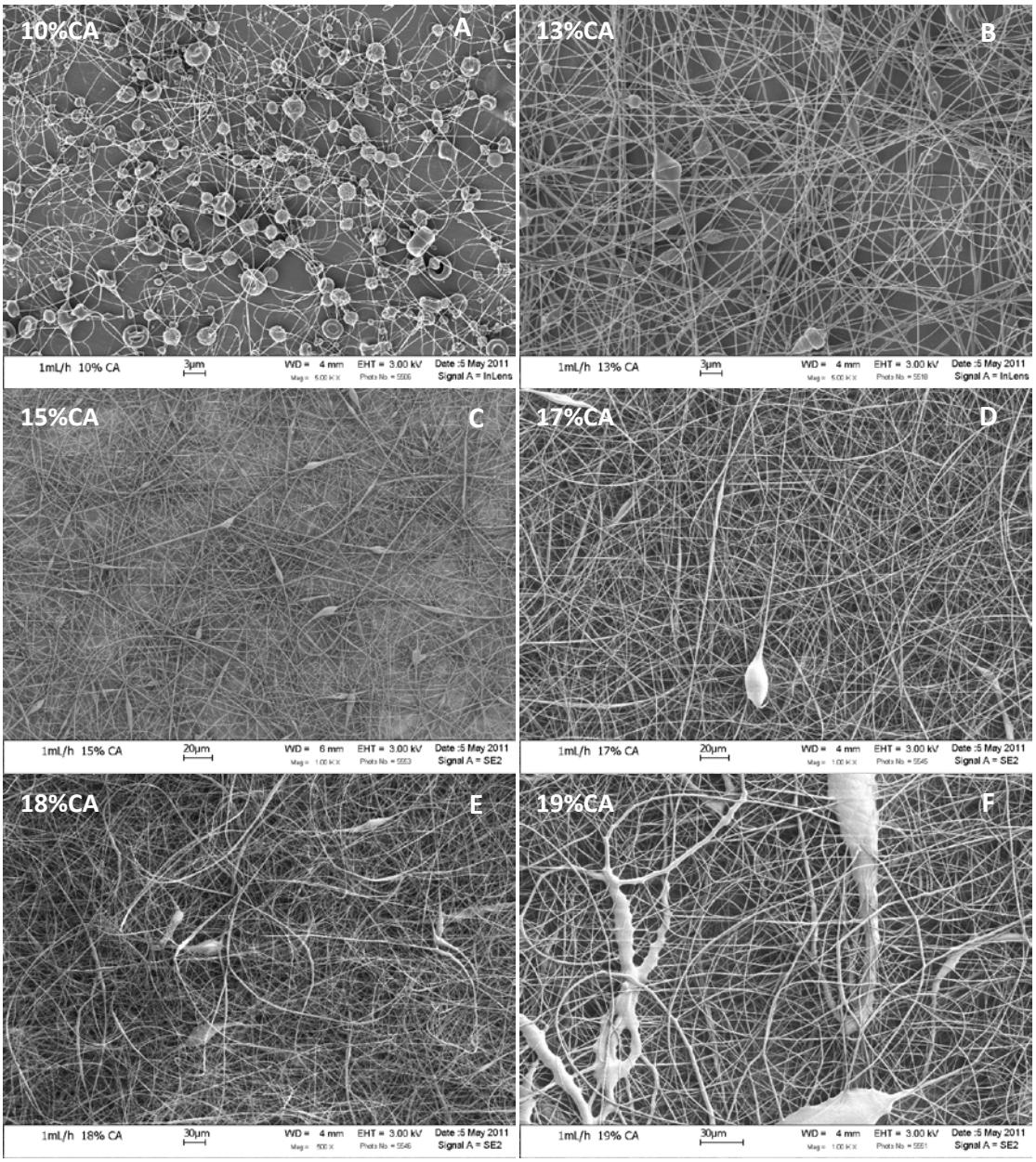

Figure 3. 2 Effect of CA concentration in acetone/DMAc (2:1) solvent system on the morphology of the electrospun CA fibers.

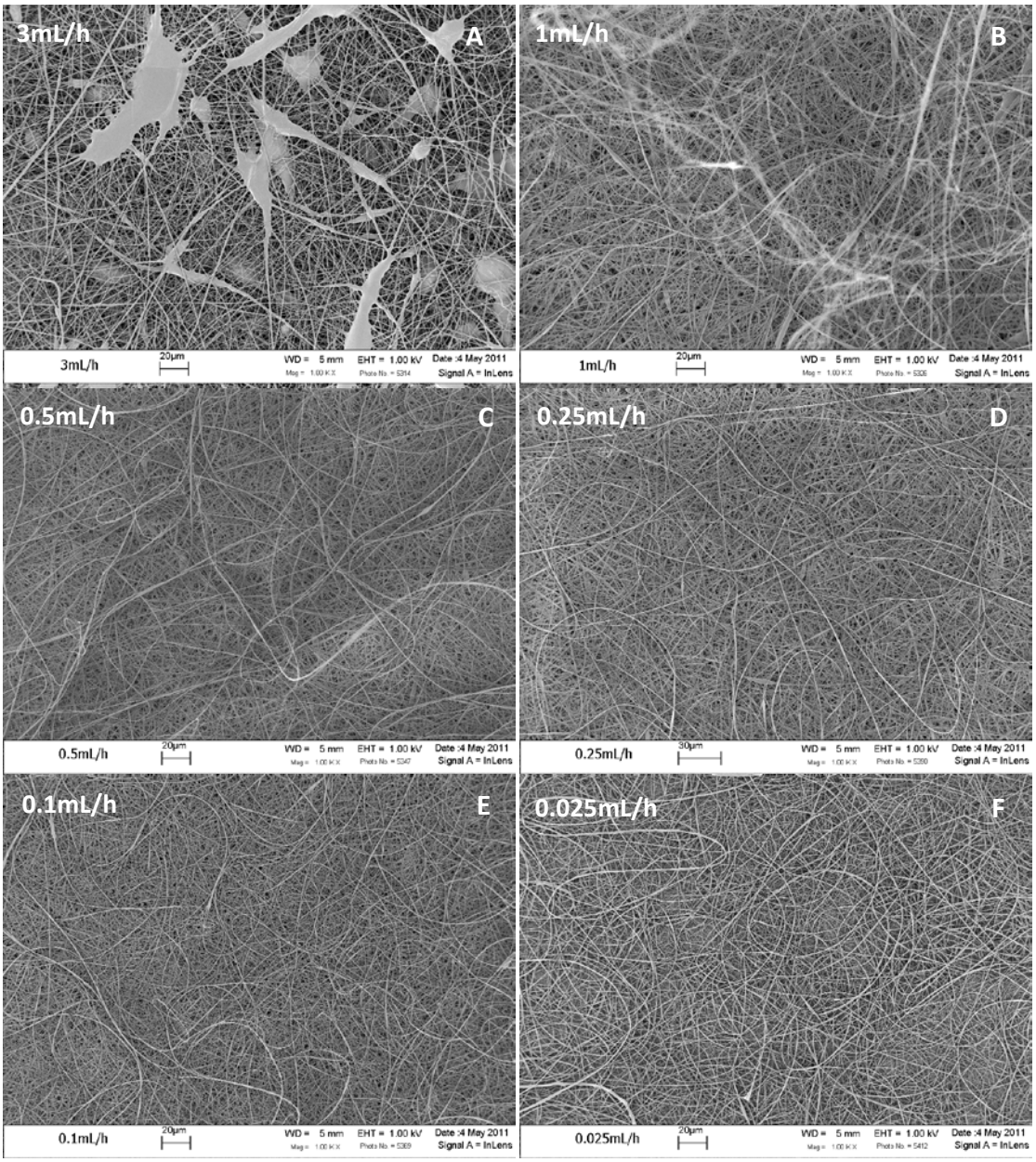

Figure 3. 3 Flow rate effect on bead formation for acetone/DMAc (2:1) solvent system.

The flow rate had a positive effect on the size of the CA fibers, i.e. there was a decrease of fiber size with the decrease in flow rate. Empirical observations support that smallest diameters take place at the lowest flow rates [35, 36, 71]. Currently, there is only one study that described the effect of the flow rate on CA fiber size and is concerning to acetone solvent system [71]. Despite that the relationship between these variable follows the conventional tendency, the reported values are inconsistent (much smaller average fiber size) than with those obtained by Son *et al*. [70] and the present work for the same

solvent system at similar CA concentration (see Table 3.1). In the present study, switching solvents, the average CA fiber size produced from acetone/DMAc solvent mixture did not follow a linear correlation with the flow rate (Fig. 34). The quantified fiber size on the sample produced at 3mL/h may be smaller than it should since the presence of beads and clusters skews the distribution of average fiber size. The phenomenon to be expected is that jet radius and flow rate (Q) have a non linear relationship, radius of the jet is proportional to $Q^{2/3}$ [36]. A power law dependency of 0.26 was found among fiber size and flow rate (Fig. 3.4). Munir *et al* have also indicated a power law dependency between flow rate and fiber size for polyvinyl pyrrolidone [36].

It has been discussed in literature that jet/fiber diameter depends on the flow rate [35, 36]. There are empirical equations that relate the jet radius and the flow rate. For instance, Oswald-deWaele Law has been used to describe polymer fluids [36]. The model for the prediction of the jet radius is:

$$h_r = 2[\varepsilon_O \gamma]^{1/3} \left(\frac{Q}{I}\right)^{2/3} \quad (3.1)$$

where h_r is the jet radius, εo the permittivity of a vacuum (A^2s^4/kgm^3), the surface tension(N/m), Q the flow rate (L/min), and I the electric current (A).

The terminal jet diameter was predicted using a model of a charged fluid jet in an electric field under conditions applicable to whipping instability [36]. The equation is as follow:

$$h_t = \left[\gamma \varepsilon \frac{2}{\pi(2\ln\chi - 3)} \frac{Q^2}{I^2}\right]^{1/3} \quad (3.2)$$

where h_t is the terminal diameter of the jet and $\chi \approx R/h$, R is the radius of curvature.

Equations 3.1 and 3.2 reflect that jet/fiber diameter not only depend on the solution properties but also the processing variable such flow rate and current. Nevertheless, the relation between the jet radius and produced dried fibers is not that simple and is impacted by factor such as solvent evaporation [36]. Munir *et al* [36] have studied the dependence of flow rate on average fiber diameter for different molecular weights and concentrations of polyvinyl pyrrolidone. They indicated that the dependence of fiber diameter on the flow rate followed a power law relationship.

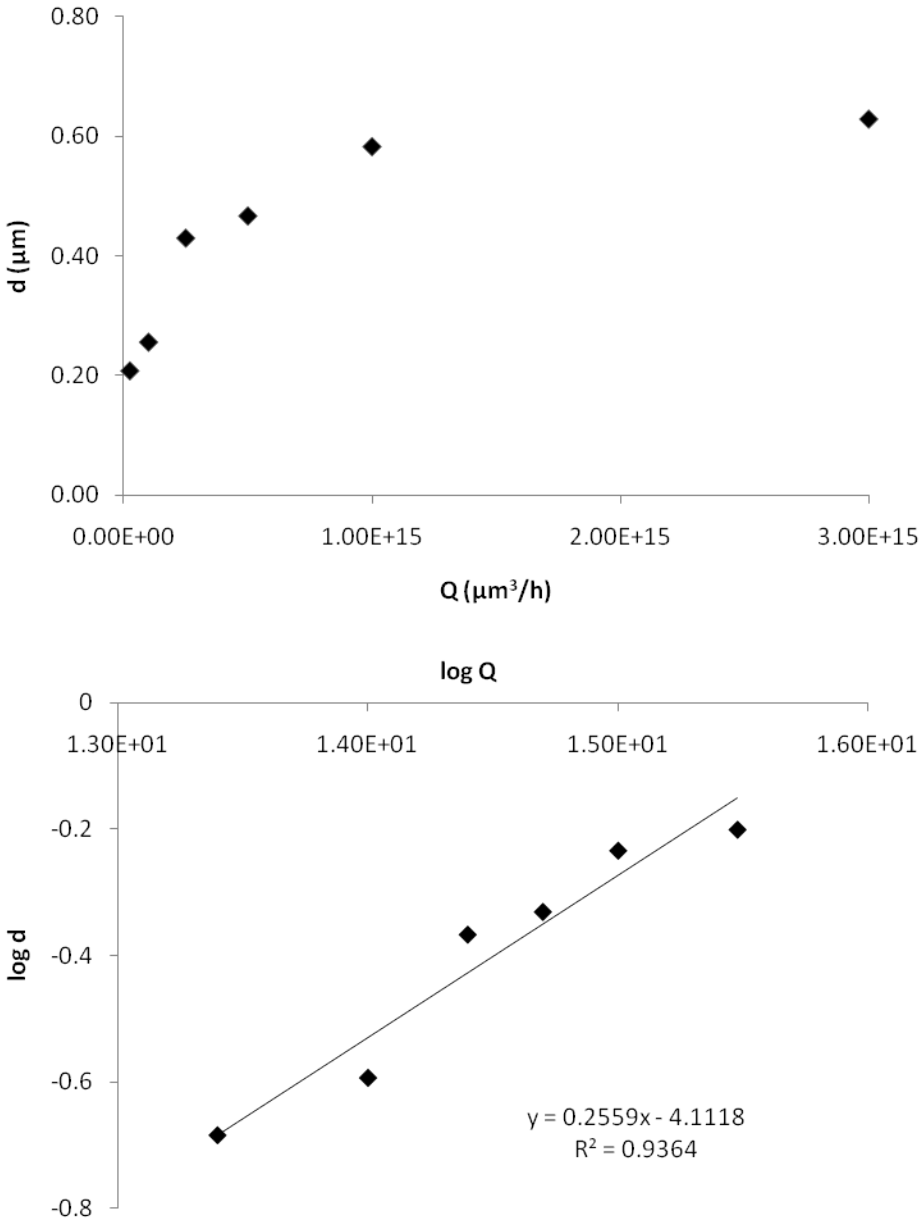

Figure 3. 4 Average fiber size diameter as a function of flow rate (Q) for 17% w CA in acetone/DMAc 2:1.

In addition, the distribution of the fiber size was also changed as a function of the flow rate (Fig. 3.5). An optimum value in the fiber size distribution was found at a flow rate of 0.5 mL/h where approximately 80% of the fibers had a size between 400 to 600nm (Fig. 3.5C). While the lower fiber size was obtained at 0.025 mL/h, this system included the highest fiber size distribution from 8 nm to 1.28 µm (Fig. 3.5F).

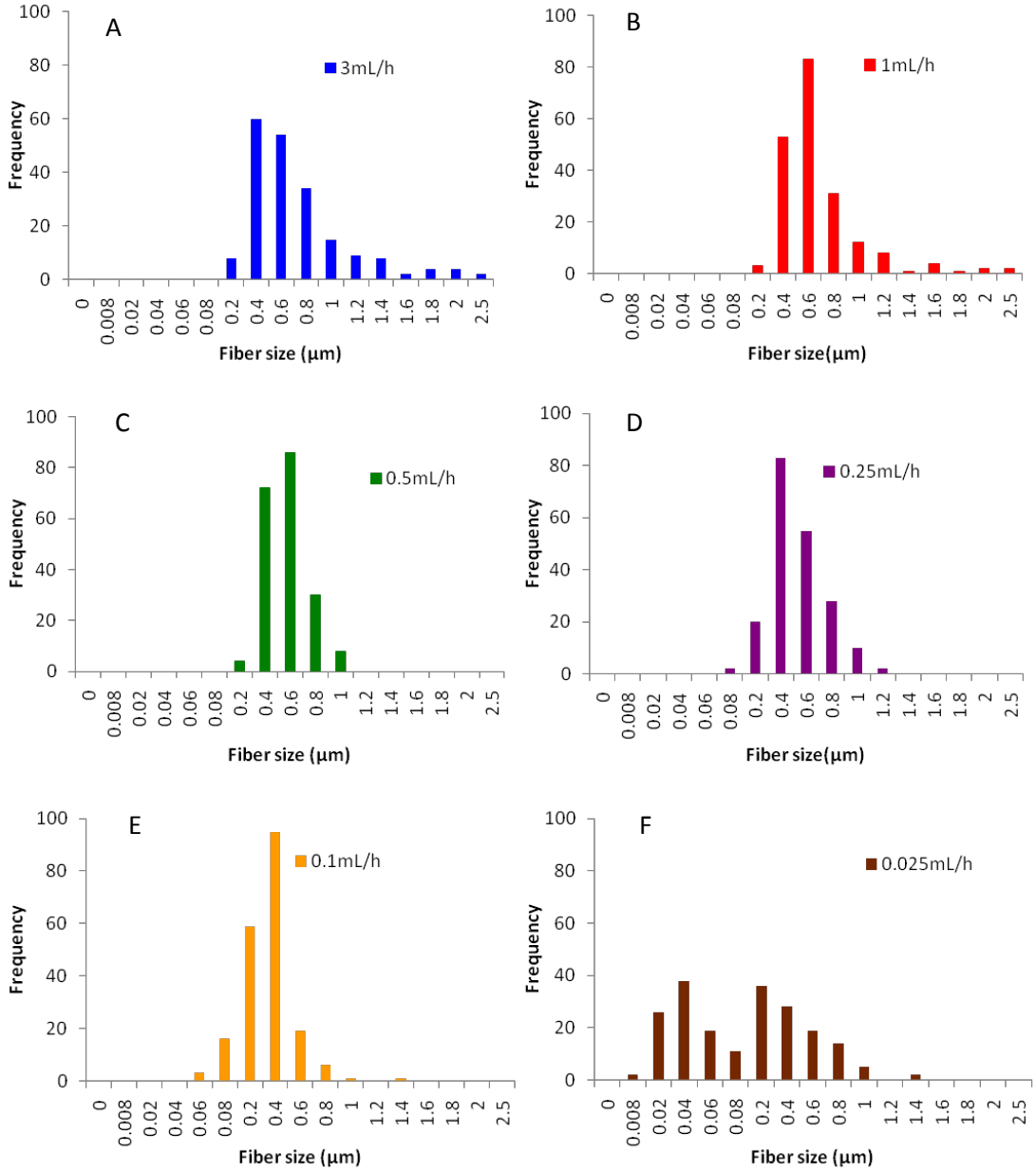

Figure 3. 5 Effect of flow rate for the solvent system acetone/DMAc on the fiber size distribution.

3.2 Performance of the Electrospun Meshes after Conversion to Cellulose

Another important criterion in the selection of the conditions to electrospin CA was the performance of the electrospun fibrous meshes after deacetylation treatment; since the ultimate purpose of the

electrospun fibers was to create nanofibrous cellulose scaffolds from them. Consequently, electrospun meshes fabricated at 3, 1, and 0.5 mL/h were deacetylated with alkaline solution (as described in Chapter 4). In this experiment it was observed that the nanofibers produced at 0.5 mL/h were not able to preserve their original network structure, since the fibers moved and aligned after deacetylation treatment (see Fig. 3.6 A&B). The alignment may be due to the wet tissue stretching as it is pulled from the solutions. Additionally, the material at low flow rates was difficult to handle when placed in water, which is a major drawback when performing tissue engineering experiments like cell seeding. In contrast, the nanofibrous meshes produced at higher flow rates (3 and 1 mL/h) were able to retain their physical structure, almost intact, after regeneration treatment and when exposed to water, as corroborated by SEM examination (Chapter 5, Fig 5.3).

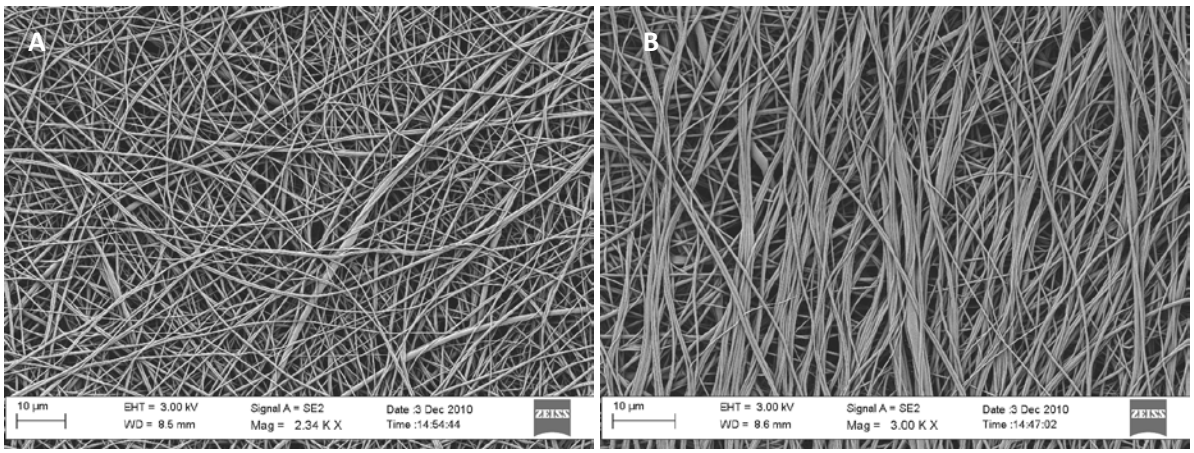

Figure 3. 6 Electrospun fibrous meshes produced at 0.5mL/h from acetone/DMAc solution. (A) CA mesh before deacetylation treatment. (B) Regenerated cellulose fibrous mesh treated with 0.05 M NaOH ethanol solution.

Similar regeneration experiments were carried out for the meshes produced from acetone and acetone/isopropanol solutions. The result was worse than the results in the low flow rate experiments for acetone/DMAc system, because the fibers were completely separated after the regeneration process (Fig. 3.7A&B). It has been mentioned in literature that when a solvent with relatively low volatility is used, for instance DMAc (Tb = 165 °C), certain amount of solvent remain within the fibers producing wet fibers. Because of the remaining solvent, a bonding via polymer diffusion is produced between intersecting fibers creating a strong interconnected porous structure [67, 73, 74]. This phenomenon explains the difference in physical stability after deacetylation process between the meshes produced from acetone versus the meshes produced from acetone/DMAc. That explanation, of “crosslinked” fibers, can also be used when a high flow rate is used (especially when DMAc is present), since the

amount of solvent is increased over time, compared to low flow rates, therefore there is more solvent residual adhering the fibers. It should be noted that the acetone/DMAc system appears as an interwoven mesh of individual fibers (3.1C). The effect of the high flow rate to bind fiber is evidence in Fig. 3.3A. For this reason, although the optimum conditions to electrospin CA, based on the morphology and fiber size distribution, was observed at flow rate of 0.5 mL/h, the practical flow rate selected was 1 mL/h. The existence of DMAc on the electrospun mesh after electrospinning process was corroborated by TGA analysis (Chapter 5, Fig. 5.5), the value corresponded to 5% of the total weight of the sample.

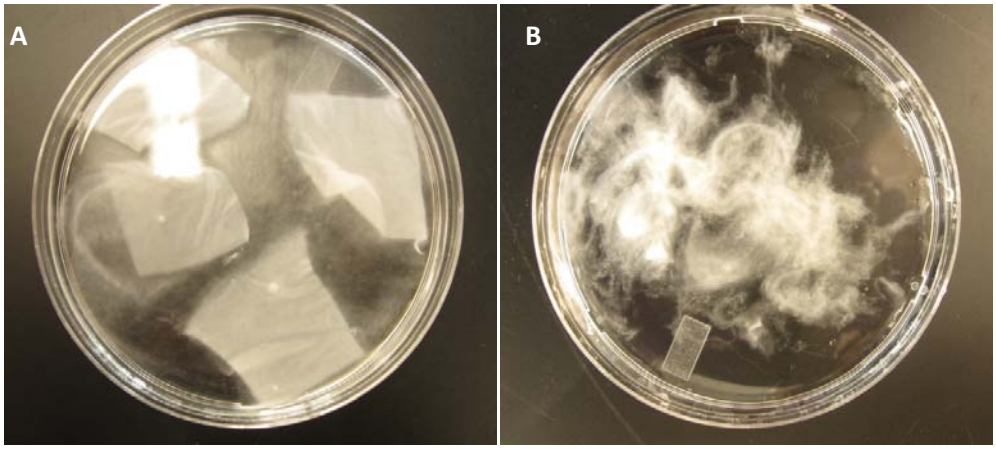

Figure 3. 7 Microscopic morphology of the electrospun fibers produced from 17% CA acetone solution (A) during deacetylation treatment and (B) deacetylated electrospun material rinsed in DI water.

Table 3.1 Literature resources on CA electrospinning parameters.

Authors	CA	CA concentration (%)	Solvents	Flow rate	Conditions	Average fiber size (μm)	Relevant findings
Liu and Hsieh (2002)[6]	Mn=30,000 DS=2.45	15, 20 (w/w)	Acetone		5-10 kV	-	Few fibers
			Acetone/DMAc				
		10	(2:1)	Not specified	10-15 kV		No fibers
		12.5			12; 15 kV		Small beads
		15			10; 15 kV	100nm-1 μm	Fibrous mat
		20			12; 15 kV		Fibrous mat
		25			12; 15 kV		Few fibers
Son *et al* (2004)[70]	Mn=30,000 DS=2.45	10-15 (w/w)	Acetone/water	5-20 mL/h	8-12 kV	2.3	Fibrous mat
			Acetone	5-20 mL/h	8-12 kV		
		9					Spherical beads
		13					Spindle beads
		17				2.25	Fibers
		21				3.23	Fibers
Han *et al* (2005)*[73]*	Mw= not specified DS= 3		Methylene chloride/ethanol				
			(100/0)				Porous fibers
		5 (w/w)	(90/0)	1mL/h	15kV/10cm	-	Porous fibers
			(85/15)				Smooth fibers
			(80/20)				Smooth fibers
Han and Gouma (2006)[71]	Mw= 29,000 Acetyl 40%	7.5 (w/v)	Acetone	1.8 mL/h	19kV		Dense beaded mat
		17.5	Acetone	9.6 mL/h	7kV	1.2	Lose fiber mat
Liu and Tang (2006)[69]	DS= 2.45 Mw,	(w/w)	Acetone/DMAc			Size distribution	
	30,000	15	(1:2)	Not specified		90-790nm	Large spindle beads
	35,000	15			8kV	90-430nm	Few conical beads
	40,000	15				90-550nm	Fibrous mat
	50,000	15, 10					No fibers

Authors	CA	CA concentration (%)	Solvents	Flow rate	Conditions	Average fiber size (μm)	Relevant findings
Tungprapa *et al* (2007)[7]	Mw=30,000 DS=2.45	5 (w/v)	Acetone		15 kV		Short and beaded fibers
		12	Acetone/DMAc (2:1)	Not specified		0.14±0.31*	Beaded fibers
		14			12kV/15cm	0.23±0.25	Fibrous mat
		16				0.26±0.20	Fibrous mat
		18				0.33±0.34	Fibrous mat
		20				0.37±0.28	Fibrous mat
Han *et al* (2008)[68]	Mn=30,000 DS=2.45	17 (w/w)	Acetic acid/water (3:1)	3 mL/h	15 kV	180nm	Fibrous mat

*Diameters of as-spun smooth or beaded fibers were measured directly from selected SEM images, with an average value for each sample being calculated from at least 50 measurements.

Table 3.2 Literature review of solvents employed in the electrospinning of CA.

Solvent composition	Fiber formation
Acetone [6, 7, 70, 71]	Discrepancy
Acetone/water [70]	Smooth fibers
Acetone/DMAc [6, 7, 69]	Smooth fibers
Acetic acid [6]	Few fibers
Acetic acid/acetone [6]	Beaded fibers
Acetic acid/water [68]	Smooth fibers
Chloroform [7]	Beads
Chloroform/methanol [7]	Smooth fibers
Dichloromethano [7]	Beads
Dichloromethano/methanol [7]	Smooth fibers
Dimethylformamide (DMF) [7]	Beads
Acetone/DMF/trifluoroethylene [43, 75]	Smooth fibers
DMAc [6]	No fibers
Formic acid [7]	Beads
Methanol [7]	Beads
Methylene chloride/ethanol [73]	Smooth fibers
Pyridine [7]	Beads

Chapter 4. Novel Architectures of Cellulose: Aligned, Microporous, and Scale Integrated.

Nanofibrous electrospun materials have been successfully used to mimic the ultrafine textured extracellular matrix (ECM) for tissue engineering applications [76]. However, cells live in a complex mixture of pores and ridges with architectures that go beyond the simple nonwoven mesh of electrospun fibers [77]. Electrospinning processes normally create random oriented nanofibrous matrices with high surface to volume ratio, and high degree of porosity [78-80]. Nonetheless, uniaxial orientation of fibers can be achieved in the electrospinning process by different methods that mimic certain tissue structures [37]. These methods include the use of collector at high rotation speed [81] or collector formed of two parallel electrodes with a gap between them where aligned fibers are deposited [37].

The major advantage of aligned, in contrast to random, nanofibrous scaffold is the enhancement of mechanical properties [81, 82]. Well aligned fibrous scaffolds are important in applications that involve mechanically anisotropic tissues [81]. Aligned nanofibers are also essential for directing cell growth in some tissues, for example in nerve regeneration where guided axonal growth is crucial [83]. It has been established that the alignment of the fibers can provide directional guidance for axonal growth by bridging long nerve gaps [83]. In case of skeletal muscle this tissue naturally consists of bundles of highly oriented muscle fibers in an extracellular 3D matrix to form an organized tissue with high cell density [84]. The parallel orientation of muscle fibers guarantees the generation of longitudinal force after contraction that is induced by motoneuron activity *in vivo* [84]. In the present work the alignment of electrospun CA fibers was created by using a high-speed rotation collector.

Regardless of the high level of porosity and specific surface area that exemplify non-woven electrospun materials, as the diameter of the electrospun fibers decreases, the fibers become more closely packed which results in reduced pore size [3, 80]. Deficiency of large pores can be an issue when using the electrospun membranes as scaffolds for tissue engineering since pore size and interconnectivity impacts the infiltration of cells within the scaffold [80]. It is also well known that pores positively influence tissue bridging by allowing inward diffusion of growth factors and ECM proteins, and outward diffusion of waste products [85].

Different approaches have been suggested such as porogen agents that include salt particles or chemical blowing agents, thermal phase separation, and lithographic patterning [62, 79, 80]. Microporosity has been effective to create porous electrospun membranes by means of laser ablation [78-80]. Using micro-ablation technique, electrospun tissue scaffolds with controlled porosity of suggested optimum pore size were designed in the present work and characterized via microscopy and spectroscopy. Another approach to improve porosity and pore size is to combine nano and microscale diameter fibers within the scaffold [62, 82]. It has been shown that is possible to electrospin nanofibers directly onto single microfiber continuous filaments [62]. The nanofiber coated microfiber structure successfully enabled cell infiltration [62]. This method offered the possibility of creating a hierarchical structure [82] and also enhanced the mechanical properties of reinforced scaffolds [86]. Nanofiber-coated microfiber scaffolds were fabricated in this work by coating cellulose microfibers (lyocel) with electrospun cellulose nanofibers for potential application in muscle and nerve regeneration. Conditions were studied to deposit the electrospun fibers in random and align fashion on the microfiber.

4.1 Uniaxially Oriented Fibers

Electrospinning of CA was carried out in rotating collectors in order to fabricate scaffolds with uniaxially oriented fibers. There are several methods to produce aligned fibers by the electrospinning technique. Currently, there are no literature sources reporting on the fabrication of aligned electrospun cellulose fibers. The electrospinning conditions selected, as suggested by the study in Chapter 3, were 17% concentration in acetone/DMAc at a ratio of 2:1; the solution was feed at a flow rate of 1mL/h at electric field of 1 kV/cm. Fibers were aligned using a collector consisting of either a rotating mandrel or rotating wheel.

4.1.1 Fibers Produced in a Mandrel

The mandrel velocity was varied in order to study its effect on fiber orientation as suggested by previous work by Courtney *et al.* [81]. In this setup the separation between needle and mandrel was 10 cm and

the experiments were carried out at approximately 50% RH and 20 °C. The produced CA fibers were analyzed by SEM (Fig 4.1 A to F).

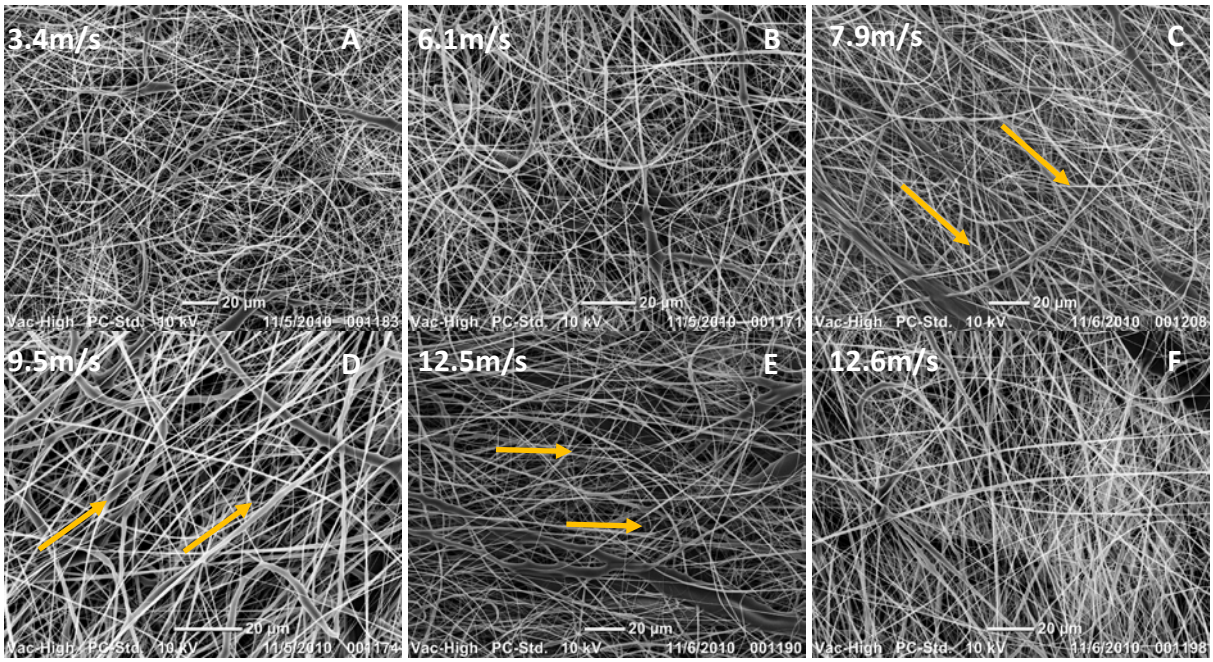

Figure 4. 1 Variation of electrospun CA orientation as a function of mandrel velocity. The arrows suggest the direction of the fiber orientation.

At velocities of 3.4 and 6.1 m/s (Figure 4.1 A, and B respectively) the produced fibers were randomly oriented. These images show fibers that have a loop-like structure throughout the image. These findings are in contrast to previous work that obtained aligned fibers at velocities equal or greater than 3.0 m /s for polyester urethane ureas (PEUU). From velocities of 7.9, 9.5 and 12.5 m/s (Fig. 4.1 C to E) some sort or orientation was observed as the loop structures were greatly reduced. Qualitatively the degree of fiber orientation was minimum. For electrospun PEUU the highest degree of uniaxial orientation was achieved at 13.8 m/s of linear velocity, which was not possible in the current study due to the restriction of mandrel size. For the lack of clear orientation, this device was considered not successful in the manufacture of highly aligned CA fibers and another device was tested. In general, the limitation of the degree of fiber orientation produced by the mandrel at high speed has been noted [37].

4.1.2 Fibers Produced on a Rotating Wheel

Electrospun CA fibers were collected on the edge of an aluminum wheel with an edge width of 10 mm. With the device, higher speeds were possible achieving a linear speed of 21 m/s. As described in Chapter 3, the separation between needle and wheel edge was 22 cm, and the experiments took place at approximately 50% RH and 20°C. The orientation of fibers produced in this collector was examined by SEM (Fig. 4.2 A&B).

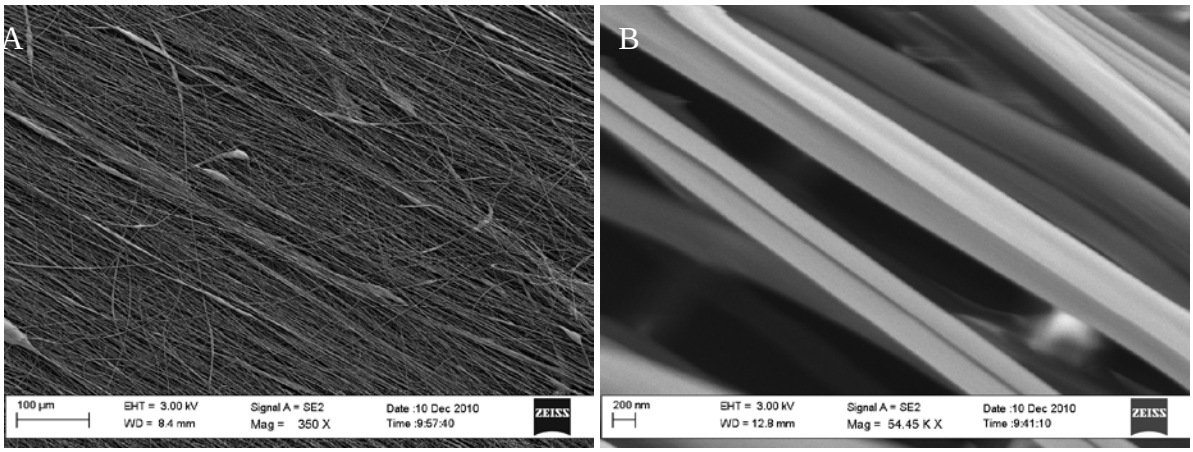

Figure 4. 2 Electrospun cellulose fibers collected onto an aluminum disk edge at a linear velocity of 21 m/s. A) Electrospun cellulose acetate fibers aligned in the direction of the disk rotation, and B) Morphology and size of the aligned cellulose acetate fibers.

The electrospun CA fibers produced in this device were highly aligned as illustrated by Fig. 4.2A. The morphology of aligned CA fibers can be seen in Fig. 4.2 B. The surface morphology of aligned fibers is similar to that of random oriented fibers (see Chapter 3). The average size and size distribution of the aligned CA fibers were determined using the same method as for the random oriented fibers. The fiber size distribution results are shown in Fig. 4.3. The average size of aligned fibers was 479 nm and 76% of fibers have a size in the range of 400 to 600 nm. There were only 0.5% of aligned fibers with a size greater than 1.2 µm. In contrast, random oriented fibers have 20% higher average diameter, with 8% less fibers in the range of 400 to 600 nm, and 3-fold increase in the total amount of fibers with size greater than 1.2 µm. These values suggest a difference in specific surface area for aligned fibers than for random CA fibers, while the SEM images show a qualitative difference in porosity. Aligned fibers pack

together better than random fibers (compare Fig. 3.1C and 4.2), therefore it may probably be expected a lower adsorption capability for aligned fibers; although there is more surface area, there is less space between fibers. In random architectures, this porosity is available for solutions to penetrate and travel within the material with the result of concentration gradients. Concerning cell-scaffold interaction this aligned architecture may be a subject for further study since the cells will be restricted to the surface, unable to penetrate and grow below the surface of the scaffold.

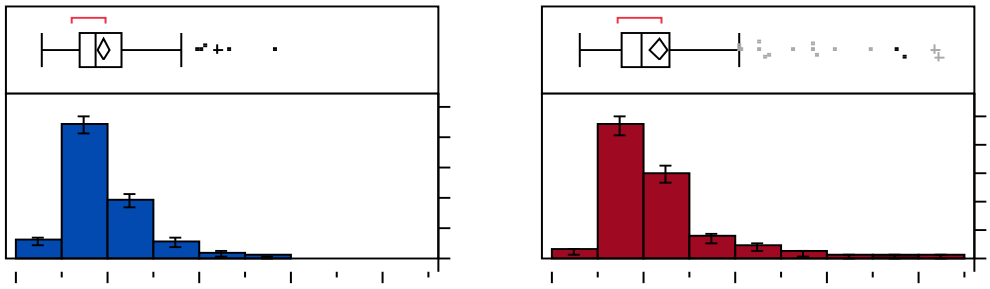

Figure 4. 3 Fiber size distribution of random oriented and aligned CA electrospun fibers.

4.2 Fabrication of Microporosity by Laser Ablation

In the literature, there are three sets of studies on the development of pores by laser ablation on electrospun membranes. Lim *et al* [79] and Rebollar *et al* [80] have described the parameters to create pores by a femtosecond laser on polycaprolactone (PCL) and PCL/gelatin membranes, respectively. It is thought that femtosecond laser can minimize polymer thermal degradation in contrast to conventional lasers due to the short time exposure [79]. McCullen *et al* [78] used a pulsed excimer laser on polylactic acid (PLA) electrospun scaffolds, they have found that cells were well spread and attached due to the micropores. Lim *et al* has suggested that cell spreading on laser ablated scaffolds is controlled by the pore walls. Additionally, increase in mineralization due to the presence of micropores has been observed [78]. Nevertheless, the capability of conventional lasers to produce microporosity without polymer degradation on electrospun membranes has not been evaluated. A summary of the different works on microporosity by laser ablation is shown in Table 4.1. In this work a CO_2 laser was used to create microporosity in a CA electrospun membrane. The surface morphology of the laser processed

samples was observed by SEM (Figs. 4.4, 4.5, 4.6, 4.8, and 4.10). Alteration of the chemical composition (degradation) of the electrospun material due to laser treatment was followed up by FTIR (Fig. 4.11). The laser modified scaffolds were regenerated to cellulose by treatment with 0.05 M NaOH in ethanol solution for 1 day at room temperature.

Table 4.1 Literature review on microporosity fabricated on electrospun scaffolds by laser ablation.

Authors	Laser type	Polymer	Conditions	Pore size (μm)	Cell behavior
McCuellen *et al* 2010 [78]	Pulsed excimer laser (Ar-F)	PLA collagen gel layered assembled	193nm, 25 ns pulse duration, 90mJ	300	Human adipose derived stem cells under osteogenic stimulation Cells were well spread and attached around and within the micropores Increase in mineralization of the laser ablated scaffolds after 21 days
Lim *et al* 2011 [79]	Femtosecond laser (Ti:sapphire crystal)	PCL/gelatin	775nm, 150 fs pulse duration, 2.5W	200	Mouse embriogenic stem cells No statistical difference in cell density was found after 1 and 2 days of growth on porous and non porous scaffolds Cell spreading on laser machined scaffolds was controlled by the pore walls
Rebollar *et al* 2011 [80]	Femtosecond laser (Ti:sapphire crystal)	PCL	800nm, 60-120 fs, 100-600μJ	90-200	No cell study was carried out
Present work	CO_2 laser	CA	10μm, 2-3.3 ms,6-12W	150-300	Mouse osteoblast cells (MC3T3-E1)

In the first experiment pores of 150 µm in diameter were created. For this purpose an AutoCAD file consisting of single lines of 0.0015 mm in length with a separation between lines of 0.009 mm was created in the program. The electrospun CA membrane was irradiated with the laser position controlled by an X-Y stage connected to the optical focusing head. The parameters used were 6W of power, 6.7 in/s laser scan speed, and 500 pulses per second. The resulting processed samples were imaged using scanning electron microscopy, shown in Fig. 4.4.

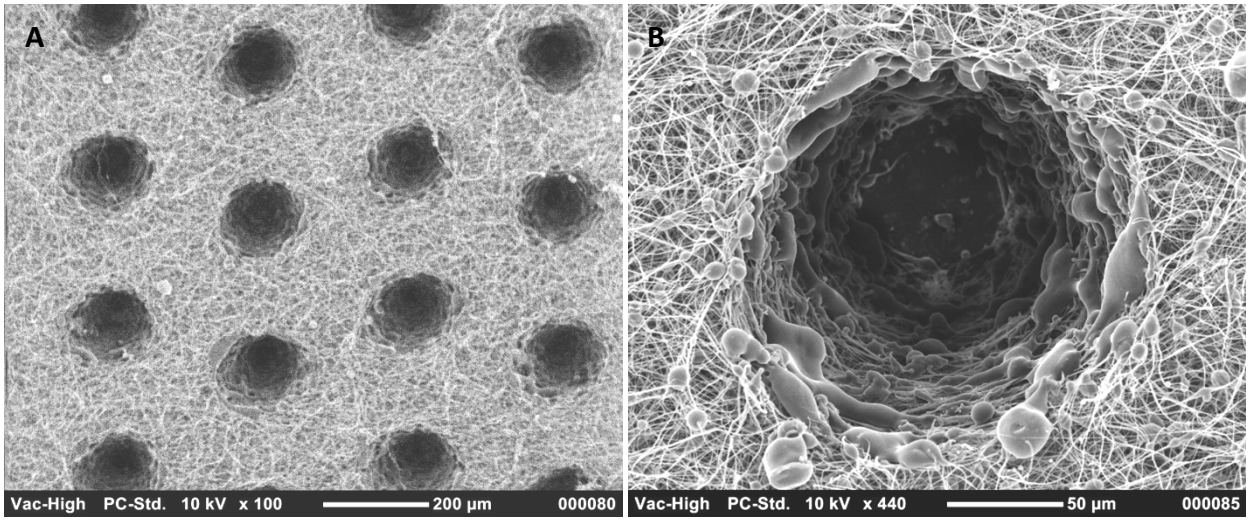

Figure 4. 4 CA membranes irradiated with 6W at 6.7 in/s and 500 pulses per second. A) Porosity pattern created of circles of 150µm in diameter. B) Magnification on edge of 150 µm pore revealing intact fibers.

Pores with circular shape and regular size were created with the pattern consisting of single lines by using the specified condition as illustrated in Fig. 4.4 A&B. There was no degradation of the fibers outside the irradiation zone as suggested by Fig. 4.4B where fiber structures are intact at the edge of the cavity. Furthermore, the laser penetrated the entire thickness of the material, with limited cellulose acetate residue deposited on the pore surface.

4.2.1 Pattern Consisting of Empty Circles

In order to ablate 300µm diameter pores an AutoCAD draw file was created with a pattern of unfilled circles of 0.01 inches of diameter and separation between circles of 0.01 inches. The same laser conditions used to create pores of 150µm were used in this experiment. It is evident in Fig. 4.5A&B, that

this patter was not successful when trying to create 300 µm pores, at least not at those laser conditions. As illustrated in Fig. 4.5 the laser was not able to remove the entire material to form the pores.

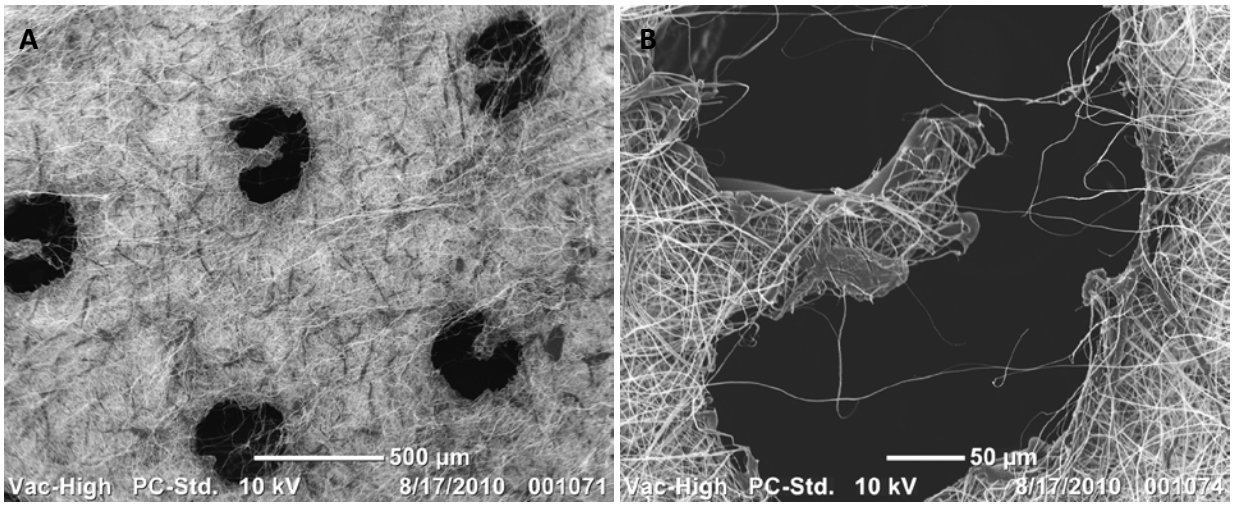

Figure 4.5 CA membranes irradiated with 6W at 6.7 in/s and 500 pulses per second.

Therefore, the power of the laser was increased to 12W, the velocity to 20.3 in/s, and pulses per second were decreased to 300 for the same AutoCAD draw file.

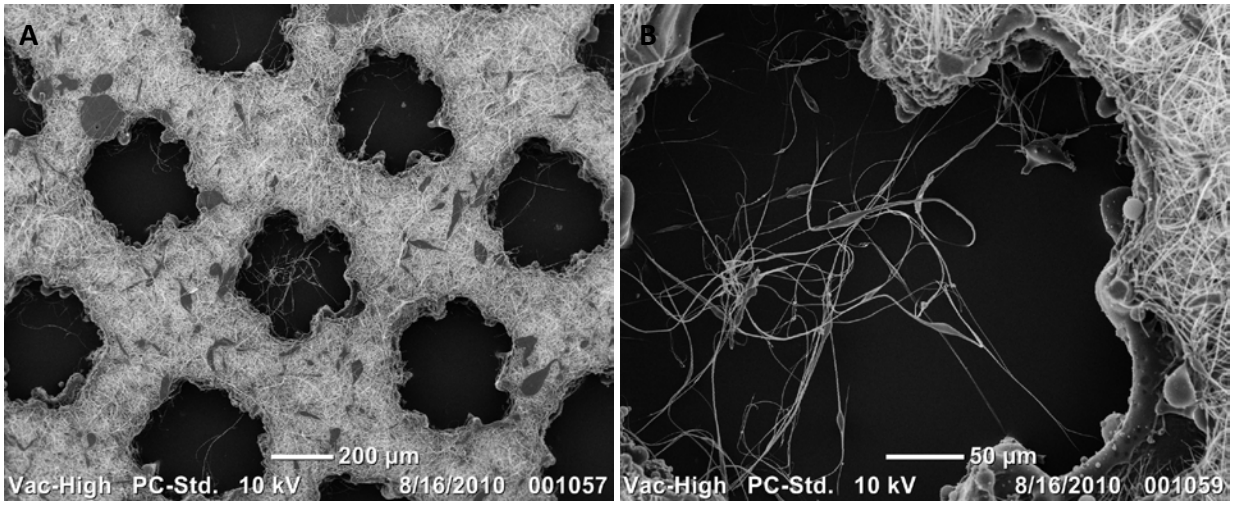

Figure 4.6 CA membranes irradiated with 12W at 20.3 in/s and 300 pulses per second.

Unfortunately, the shape of the pore was extremely irregular (Fig. 4.6A) and the fibers at the edge of the pore were melted due to the laser irradiation (Fig. 4.6B). Accordingly, another AutoCAD drawing was created; this file was composed of parallel lines of various lengths that together created the shape of a circle (Fig. 4.7 and 4.9).

4.2.2 Pattern Consisting of Parallel Lines

An AutoCAD draw file consisting of 7 parallel lines was created, in contrast to the unfilled circles, Fig. 4.7. This pattern was ablated onto electrospun mesh by the laser using 12W of power, 20.3 in/s, and 300 pulses per inch.

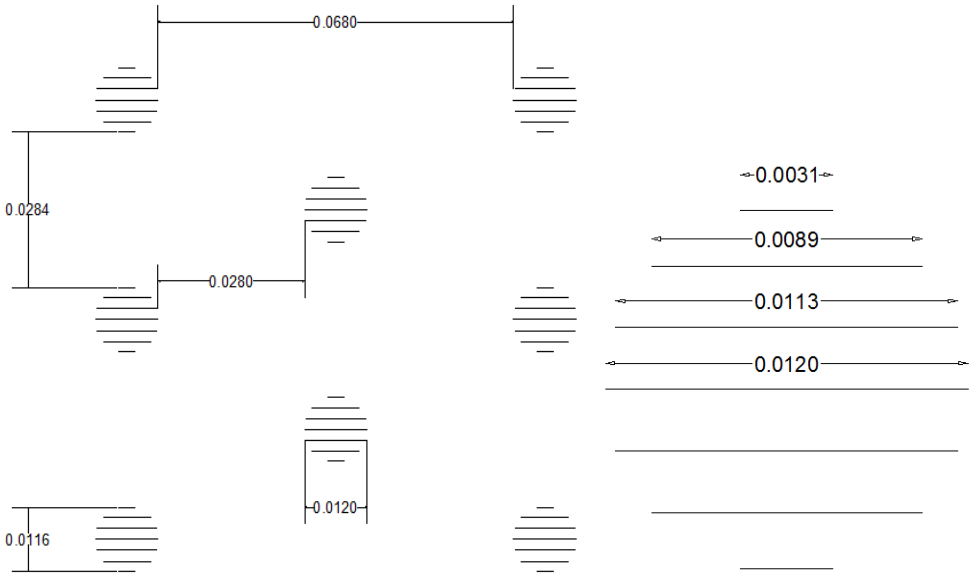

Figure 4.7 Pattern of parallel lines created in AutoCAD, the units used in the draw are millimeters.

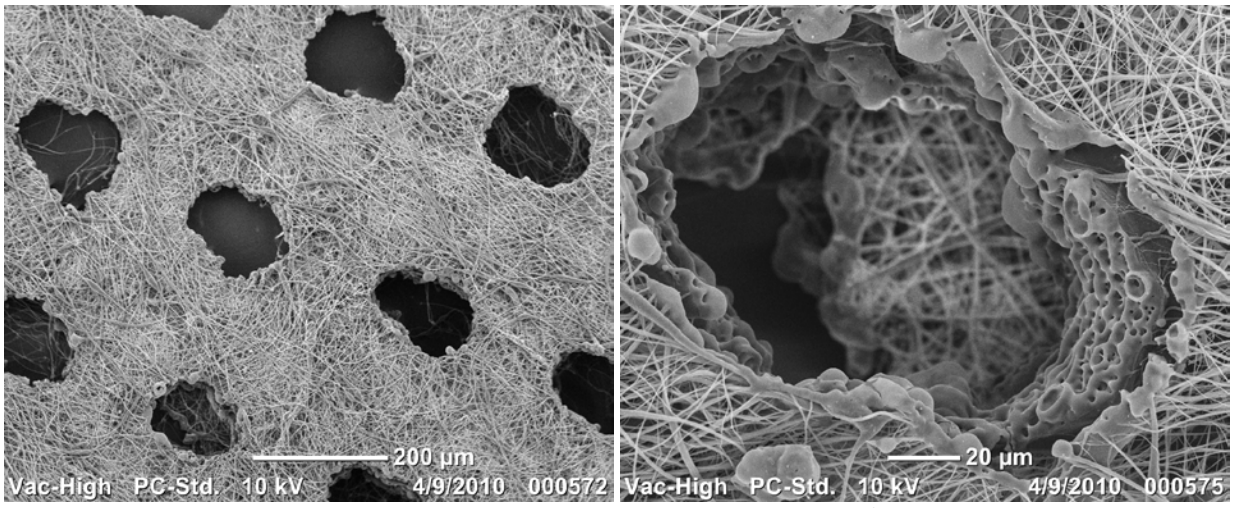

Figure 4.8 Laser ablated electrospun membrane at 12W of power, 20.3 in/s, and 300 pulses per inch.

The material was completely removed by the laser treatment; however the shape of the pore was an ellipse instead of a circle (Fig. 4.8A). Some of the fibers at the edge of the pore were melted by the laser processing (Fig. 4.8B) that was indicative that the parameters tested were not optimized. Therefore, in order to generate an accurate circular shape, more lines were added to the circular parallel line pattern. In this case 11 parallel lines with a separation between lines of 0.001 mm were created, Fig. 4.9.

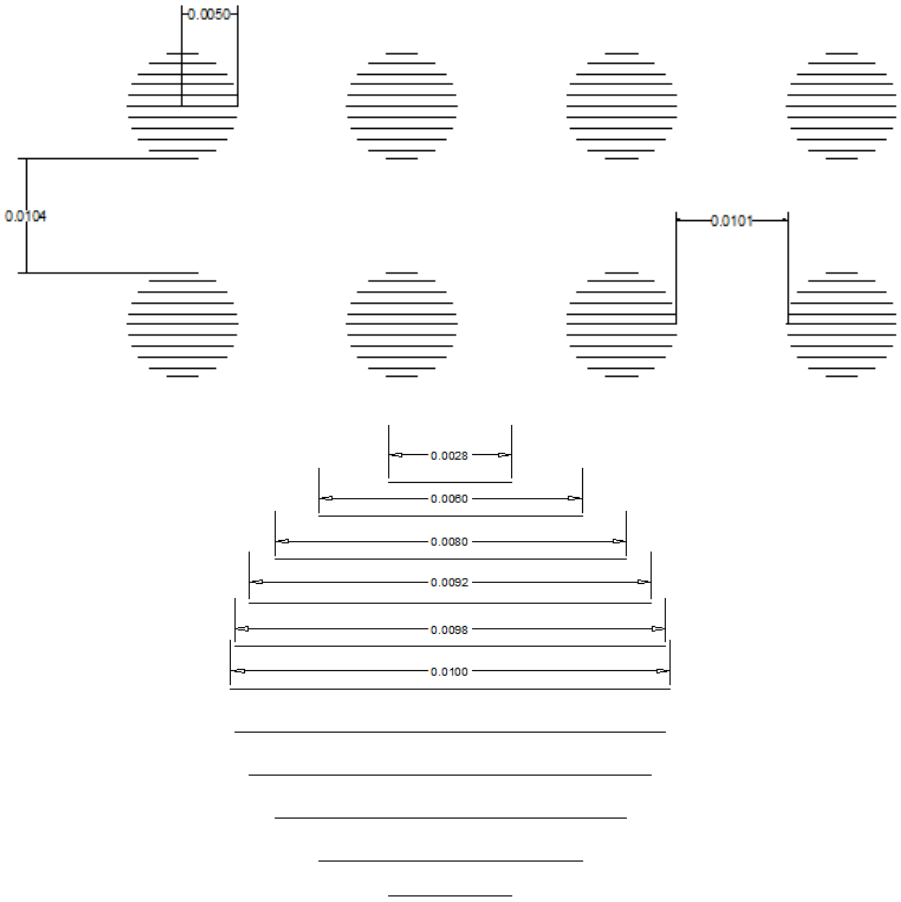

Figure 4.9 Pattern of parallel lines created in AutoCAD, the units used in the draw are millimeters.

The parameters of the laser in this experiment were 6W of power, 6.7 in/s, and 500 pulses per second. This file design produced pores with regular circular shape and size of approximately 300 µm (Fig. 4.10 A&B). It was possible to generate different amount of pores by changing the distance between pores, see Fig. 4.10 A&B. The pattern in Fig. 4.10 A has a horizontal separation between pores of 1500 µm and a vertical separation of 500 µm. In Fig. 4.10 B a pattern with separation among pores of approximately

200 µm was used. Variation in the porosity of a scaffold could influence its performance by changing properties such as wettability, tensile modulus, and mass transport coefficients.

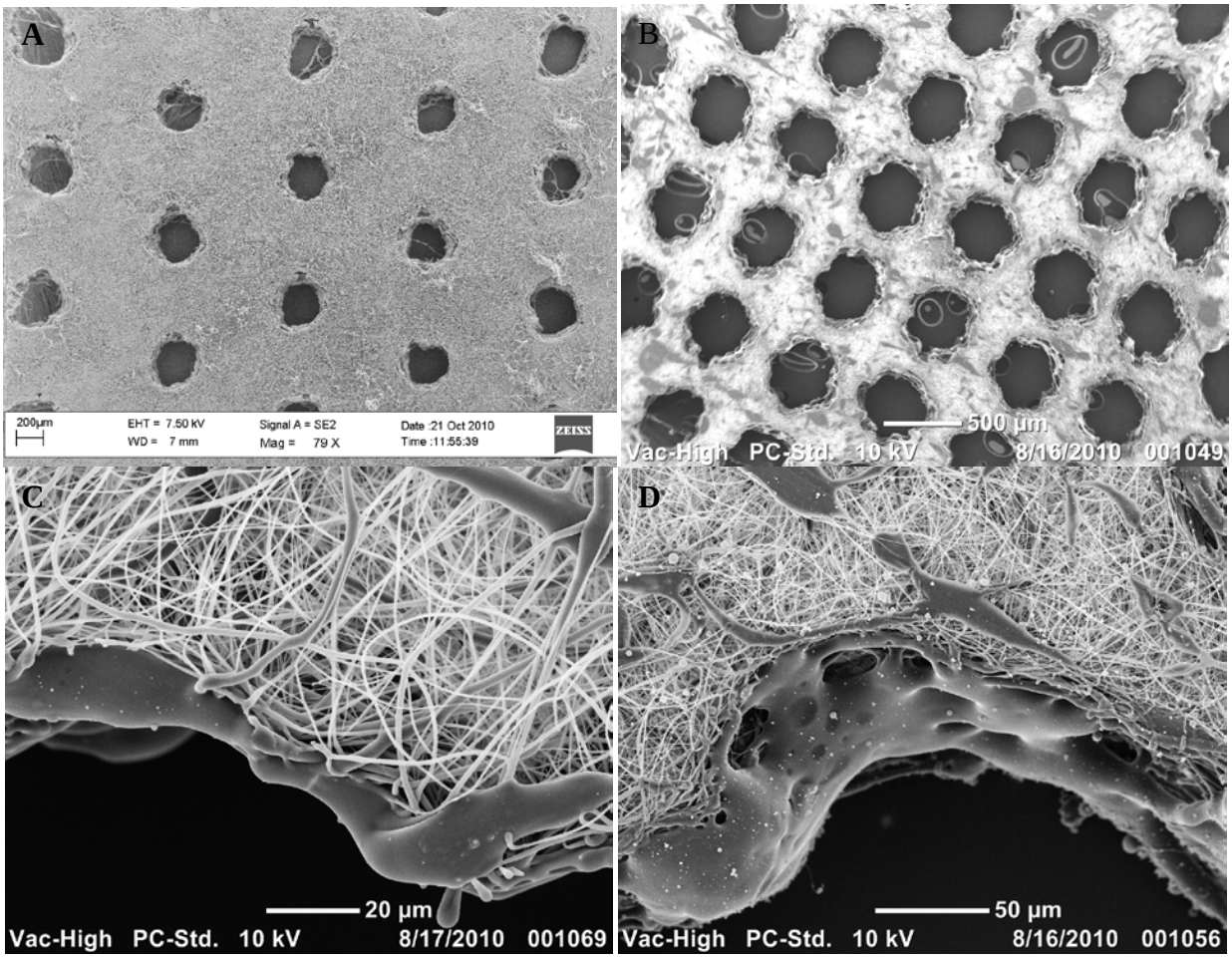

Figure 4.10 Micro-ablated electrospun cellulosic scaffolds. A) Pattern of horizontal separation between pores of 150µm and a vertical separation of 400 µm, B) pattern with separation among pores of approximately 200 µm, C) Higher magnification at the edge of the pore of pattern in A, and D) Higher magnification at the edge of the pore in pattern shown in B.

To evaluate the possibility of degradation of the electrospun cellulosic membranes due to laser treatment, non-modified and laser modified membranes were analyzed by FTIR. The results are shown in Fig. 4.11. FTIR spectrum (Fig. 4.11) of the CA membrane shows the characteristic bands attributed to the vibrations of the acetate group: the carbonyl stretching at 1750 cm^{-1} (νC=O), methyl bending at 1370 cm^{-1} (δC-CH3), and alkoxyl stretch of the ester at 1235 cm^{-1} (νC-O-C) [6, 43, 75]. The acetal linkages of the cellulose backbone can be observed around 1160 cm^{-1}, the methylene asymmetric stretching at 2853 cm^{-1} [87] and the broad hydroxyl group absorption at approximate 3400 cm^{-1}[6]. It can be observed, by comparison of the spectra, that no significant changes were induced by the laser

treatment, since there is not shift of peaks or presence of new peaks. Hence, FTIR results did not suggest any chemical modification due to the laser treatment, the non fibrous material observed at the edge of the pore (Figs. 4.10 C&D) could be the CA that was melted during laser ablation during the process. Consequently, it was concluded that is possible to create microporosity on CA electropun membranes by CO_2 laser with no bulk thermal degradation of the material. The relevance of this result lies in the decrease of the cost of scaffold fabrication by using a conventional laser and ease of manufacture of microporosity in contrast to femtosecond and pulse excimer lasers.

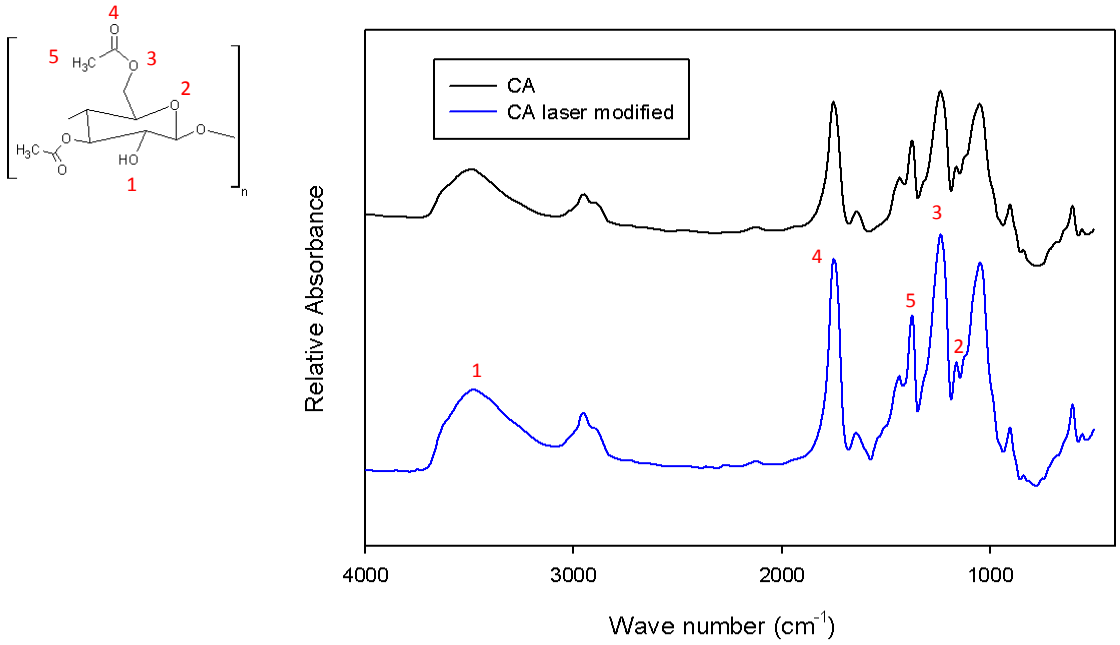

Figure 4.11 Electrospun cellulose acetate (CA) before and after laser modification.

4.3 Nano fibers Coated Lyocell Microfibers

CA nanofibers coated lyocell microfibrous scaffolds were produced by the technique described by Thorvaldsson and coworkers [62]. The fabrication of random and aligned CA nanofibers onto lyocell microfibers was assessed by microscopy. The surface morphological features were analyzed by SEM. The CA nanofibers deposited on lyocell fibers were deactetylated in NaOH 0.05 M in ethanol for 24 h at room temperature. The nano-micro scaffold was analyzed by SEM after deacetylation process to evaluate if the structure was preserved.

As seen in Figure 4.12 electropun CA nanofibers were successfully attached onto the lyocell microfibers. The CA electrospun fibers were randomly collected on the microfiber. CA random electrospun fibers were produced at flow rate of 0.4 mL/h, the diameter of the fibers was in the range of 400-600 nm, in agreement with the results of the study of the flow rate in Chapter 3 (Fig. 3.5). It was necessary to wet (distilled water) the lyocell fiber prior to electrospinning to obtain strongly attached electropun CA fibers. The lyocell microfiber had a diameter of 350 µm and it was composed of filaments, each with a diameter of 11 µm (Fig. 4.12 B).

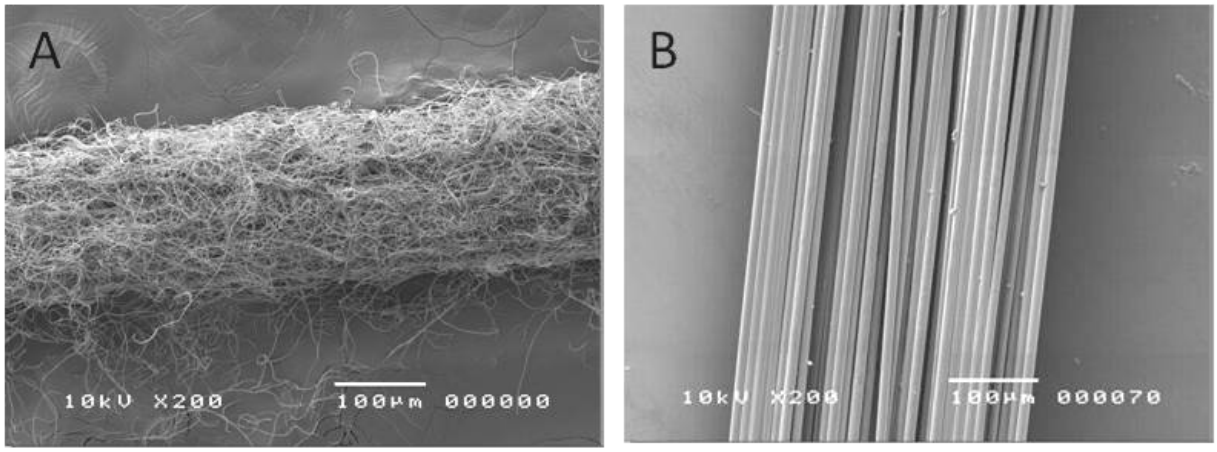

Figure 4. 12 Random oriented CA electrospun nanofiber coated lyocell microfiber (A). Lyocell fillament before nanofiber coating (B).

The alignment of the electropun nanofibers was created by modifying the velocity of the lyocell microfibers (collection speed) since velocity of the collector is known to impact fiber orientation as documented by Thorvaldsson *et al* [62]. In this case dry lyocell fibers were employed during the electropinning and the flow rate was from 0.3 to 0.6 mL/h. When using high collection speed the density of electrospun fibers decreased, hence the flow rate was increased to compensate. As suggested by the SEM images in Fig. 4.13 the parameters that produced some degree of alignment of the electrospun fibers was a collection speed of 1.05×10^{-2} m/s and a flow rate of 0.5 mL/h. The diameter of the aligned CA fibers collected onto lyocell fibers produced at those conditions was in the range of 450 to 600 nm. This structure has a potential application as scaffold for nerve and muscle regeneration due to its hierarchical structure and orientation of the nanofibers.

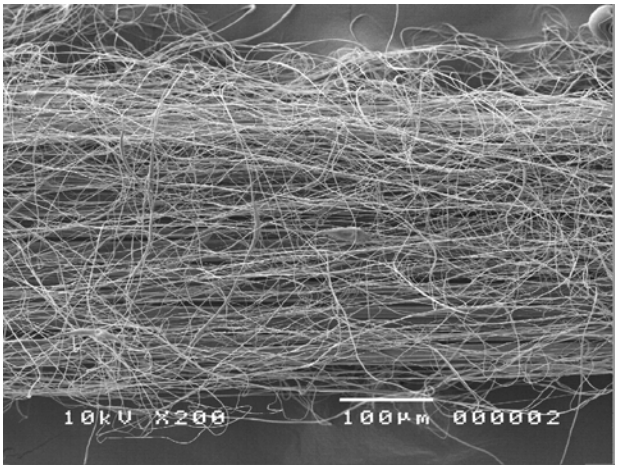

Figure 4. 13 Aligned CA electrospun nanofiber coated lyocell microfiber at different collection velocities.

The surface morphology of the nanocellulose coated lyocel fiber was characterized by SEM to evaluate any adverse effects on the cellulose fibers due to the deacetylation treatment. As suggested by the SEM images, there were no morphological changes of the fibers induced by this post-treatment (Fig. 4.14). The electropun fibers remained attached to the lyocell fiber (Fig. 4.14 A). The nanofibrous structure was intact and the dimensions of the fibers were preserved (Fig. 4. B&C). However, the electrospun mesh network structure appears as a tighter structure on the lyocell, must likely arising from intermolecular interactions, such as hydrogen bonding.

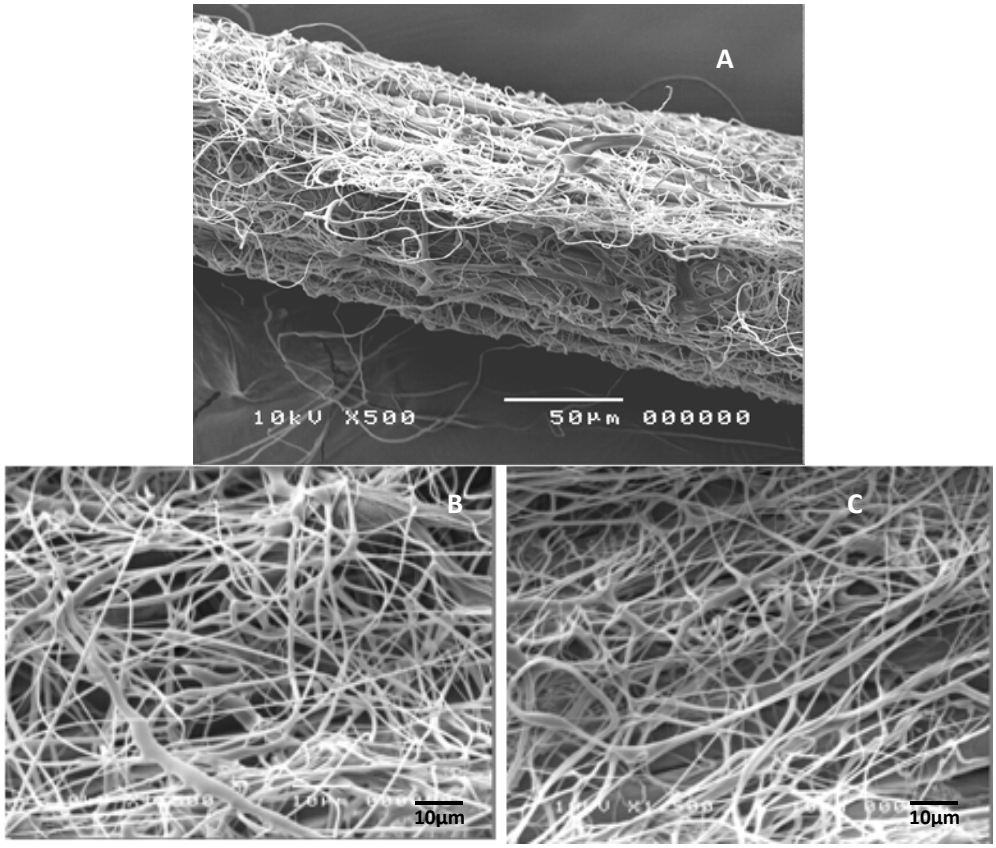

Figure 4. 14 Electrospun cellulose fibers onto lyocell microfiber after deacetylation process (A). Electropun CA fibers onto lyocell (B). Electropun cellulose fibers on lyocell after decateylation treatment.

Chapter 5. Electrospun Cellulose a New Member of Nanocellulose Family

The biological response to a material is highly affected by the proteins that attach to its surface [25]. Hydrophobicity is one of the most important parameters affecting the adsorption of proteins to a material in an aqueous environment, such as that found *in vivo* [25, 88]. In general, hydrophobic surfaces tend to adsorb larger amounts of proteins than hydrophilic ones. Therefore, it has been proposed that in order to increase blood compatibility, the incorporation of hydrophilic surfaces should be attempted [89]. It was suggested that metabolic functions of cells improves on hydrophilic membranes [90]. Neuron cells require hydrophilic surfaces-- highly hydrophobic surfaces such Teflon prevent neuronal growth [91]. Attachment of neurons is also prevented by surface coating substrates with alkane chains [91].

Mechanical properties of tissue scaffolds, such as strength and stiffness, are extremely important in that they should match, as much as possible, the properties of the tissue to be replaced [25]. The mechanical properties of bone are difficult to determine due to the anisotropy of this tissue. The elastic modulus reported for trabecular bone is around 0.01 to 0.9 GPa [92]. The mechanical forces experienced by cells in a scaffold are likely to be influenced by the mechanical properties of the scaffold construct [93]. Therefore, it is important that the scaffolds are designed so that they posses adequate mechanical properties to provide the correct physical stimuli to cells [93]. It was observed that myoblasts of the muscle display actomysin striation only on substrates with Young's modulus of approximately 12 kPa [94]. Neurons, mammary epithelial cells, and other epithelial cells isolated from soft tissue grow on materials with shear modulus around 100 Pa [95-97]. It is possible that the feedback of local substrate stiffness on the cell state has significant implications in development, differentiation, disease, and regeneration [98]. It has been shown that it is possible to direct stem cells lineages by varying matrix stiffness. In order to predict what tissue engineering applications will suit electrospun cellulose scaffolds and to further understand the behavior and performance of electrospun cellulose as biomaterial, it is crucial to evaluate its chemical, physical, surface, and mechanical properties. In this chapter the conversion of cellulose acetate to cellulose by deacetylation treatment as a function of time was monitored by FTIR and XPS techniques. The surface morphological features of electrospun fibers due to deacetylation postreatment was evaluated by SEM. The crystalline structure of regenerated cellulose fibers was elucidated by X-ray diffraction. Thermal degradation of electrospun CA and cellulose fibers was studied by thermogravimetric analysis (TGA) in order to determine the residual

dimethylacetamine (DMAc), the electrospinning solvent. Hydrophophilicity of electrospun CA and cellulose fibers was evaluated by water contact angle Sessile drop. Surface area measurements of random and aligned regenerated cellulose fibers were derived from nitrogen adsorption-desorption isotherms at 77K. The mechanical properties, the tensile mode, of random and aligned regenerated cellulose fibers were evaluated at physiological conditions.

5.1 Pseudo-Kinetics of Cellulose Regeneration.

Fibers of electrospun CA were regenerated to cellulose via alkali saponification with 0.05 M NaOH ethanol solution at room temperature using previously described procedures [6, 9, 43, 75]. In order to distinguish the degree of regeneration the time of deacetylation was varied for further studies of modification. The regeneration process was monitored by analyzing the scaffold composition using FTIR spectroscopy and XPS.

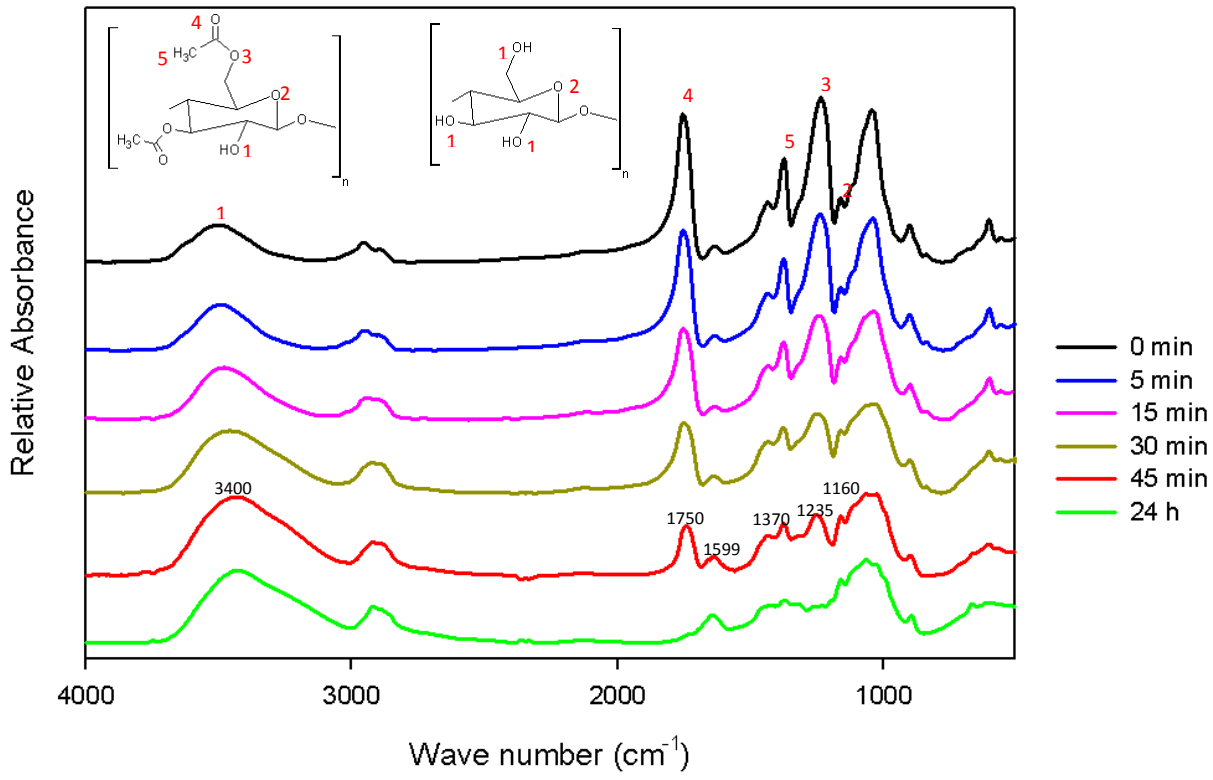

Figure 5. 1 FTIR spectra of CA and RC scaffolds hydrolyzed at different time.

FTIR spectra as a function of deacetylation time show characteristic changes in cellulose acetate when exposed to alkali (Figure 5.1). The spectrum of CA scaffold (0 min exposure to NaOH) has absorption peaks for carbonyl stretching at 1750 cm^{-1} (νC=O), alkoxyl stretch of the ester at 1235 cm^{-1} (νC-O-C), and methyl bending at 1370 cm^{-1} (δC-CH3), for groups of the acetate substituent [6, 43, 75]. The acetal linkages of the cellulose backbone can be observed around 1160 cm^{-1} and the broad hydroxyl group absorption at approximate 3400 cm^{-1} [6]. The intensity of absorption peaks at 1750, 1370, and 1235 cm^{-1} related to the acetyl group content decreased as the time of regeneration increased. It can be observed the broadening of the hydroxyl absorption with the increase in time of regeneration; this change illustrates the substitution of acetyl groups with hydroxyl groups. After 24 h of treatment, the carbonyl peak had completely disappeared (Figure 5.1), which supported the claim that nearly complete regeneration into cellulose of the electrospun fibers had been achieved at that point. Of particular interest in this work was the presence of carboxylate (COO^-) groups, due to its capacity to induce Ca-P crystal formation and increased the negative charge of cellulose that could probably improve the adsorption of cell adhesion proteins, indicated by the asymmetric stretching vibration at 1599 cm-1 for all samples (39). Furthermore, an increase in intensity of the carboxylate group was detected as result of the regeneration process, as observed in other studies [43, 75]. The carboxylate group formation may be attributed to cellulose scission and aerobic oxidation, a well-known process in alkaline hydrolysis of cellulose [99]. The time for complete regeneration differed with a previous study by Liu and Hsieh as they reported near complete deacetylation for electrospun CA for equal DS after 60 min of treatment with NaOH/ethanol at the same concentration [6]. However, the authors reported that there are still acetyl groups as the degree of substitution was found to be 0.15. Furthermore other studies have reported longer regeneration times at higher alkali concentrations were required [43, 75]. The inconsistency of regeneration times demonstrates the difficulty in describing the kinetics of heterogeneous deacetylation for electrospun cellulose acetate where different electrospinning parameters impact fiber diameter.

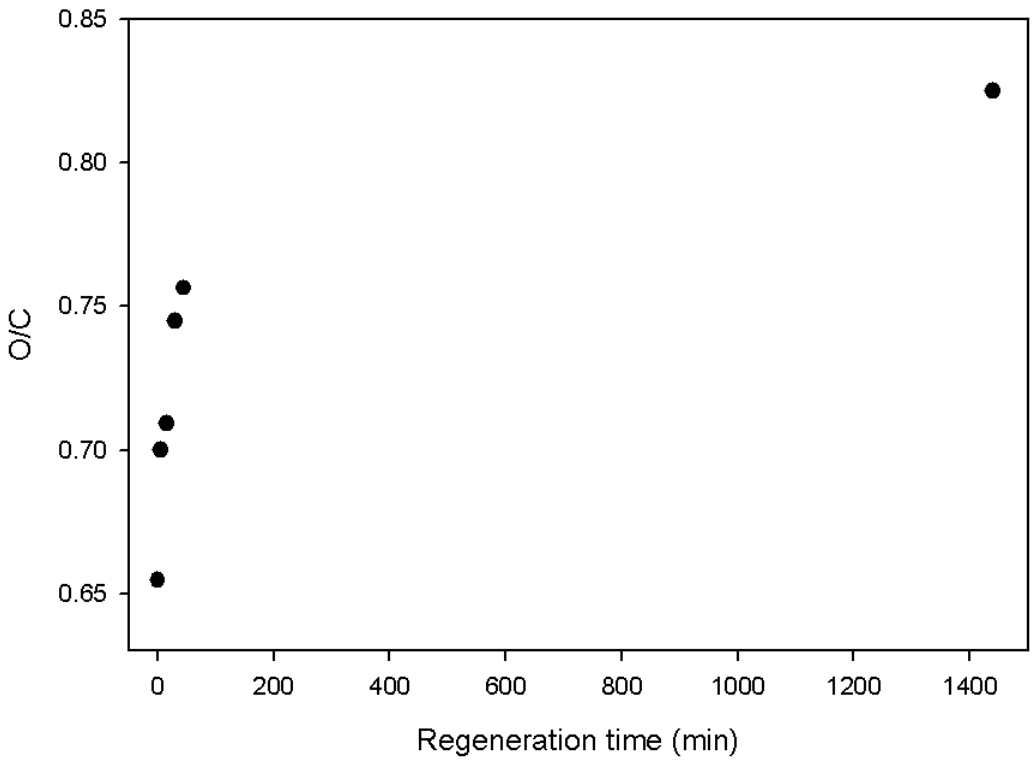

Figure 5. 2 Atomic O/C surface ratio of CA and RC scaffolds by XPS.

Surface chemistry of cellulose regeneration was analyzed by XPS. The XPS results (see Figure 5.2) showed an increase in atomic concentration of oxygen relative to atomic carbon with the increase in regeneration time. This increase is from the cleavage of the acetate groups that contain two additional carbon groups. This behavior supported the substitution of acetyl by hydroxyl groups due to the saponification reaction on the fibers surface. For 45 min and lower time regenerated samples, the fibrous mat still retains some acetyl groups within the first 10 nm of the fiber surface. Either the outermost surface is not fully saponified or the layer near the maximum probe depth is not. It was observed that at 24 h of hydrolysis the theoretical O/C ratio value for cellulose, according to [100] and, [101] had been reached. This value indicates that a complete surface regeneration of CA fibers into cellulose was accomplished at 24 h of deacetylation treatment. Surface and bulk regeneration of the CA nonwoven scaffold had shown a similar trend as demonstrated by FTIR and XPS analysis.

5.2 Fiber Morphology

The nonwoven mesh structure of CA was well preserved during the conversion into cellulose, as can be observed in the SEM images (Figure 5.3 A, B, C). There was no change in morphology of the fibers due to deacetylation treatment after 45 min (Fig. 5.3 B) and 24 h (Fig. 5.3 C). Furthermore, minimal swelling occurred in agreement with other studies for alkali-ethanol system [6, 68]. This result showed that cellulose-based scaffolds can be produced and designed from CA in order to take advantage of its expanded processability window compared to cellulose, including properties such as solubility, T_g, and T_m which can be influenced by either the degree of acetylation or the addition of a plasticizing agents.

X-ray analysis of the electrospun mats after regeneration (45min and 24hrs) shows changes in its morphological structure (Figure 5.4). The fiber sample after 24 h regeneration has sharp peaks associated with the crystal structure of cellulose II located at angles of 12°, 20°, and 22°, similar to what is shown by Fink and co-workers [102]. The cellulose II diffraction pattern was expected since the regeneration process was carried out by NaOH treatment. The 45 min regenerated cellulose sample only presented one broad signal at 20° and that peak was wider than that showed by the 24 h RC sample. The electrospinning process rapidly removes solvent preventing preferred packing of cellulose acetate chains. Control of the crystalline structure is expected to impact the *in vivo* stability and mechanical performance of the scaffold, providing a wider range of properties that can be controlled to impact scaffold performance by regenerating cellulose to varying degrees.

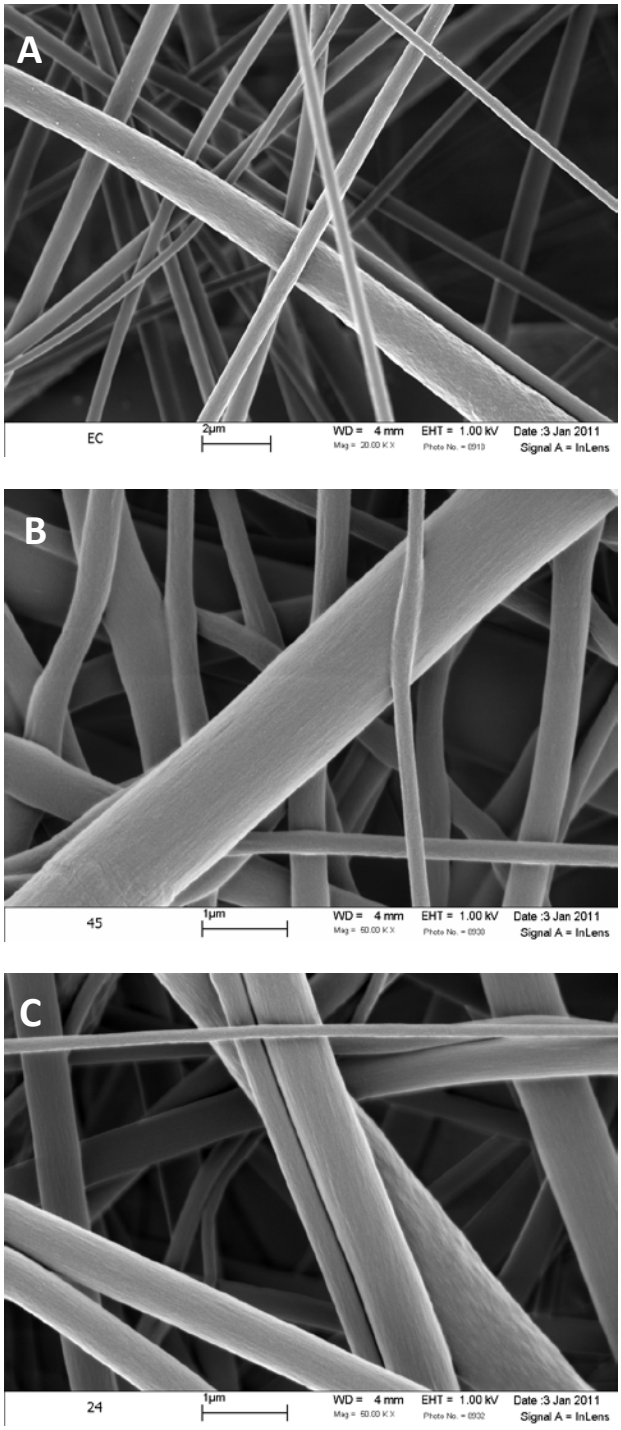

Figure 5. 3 Morphology of electrospun fibers during regeneration process. SEM images of A) CA and regenerated cellulose at: B) 45min and C) 24hr of treatment.

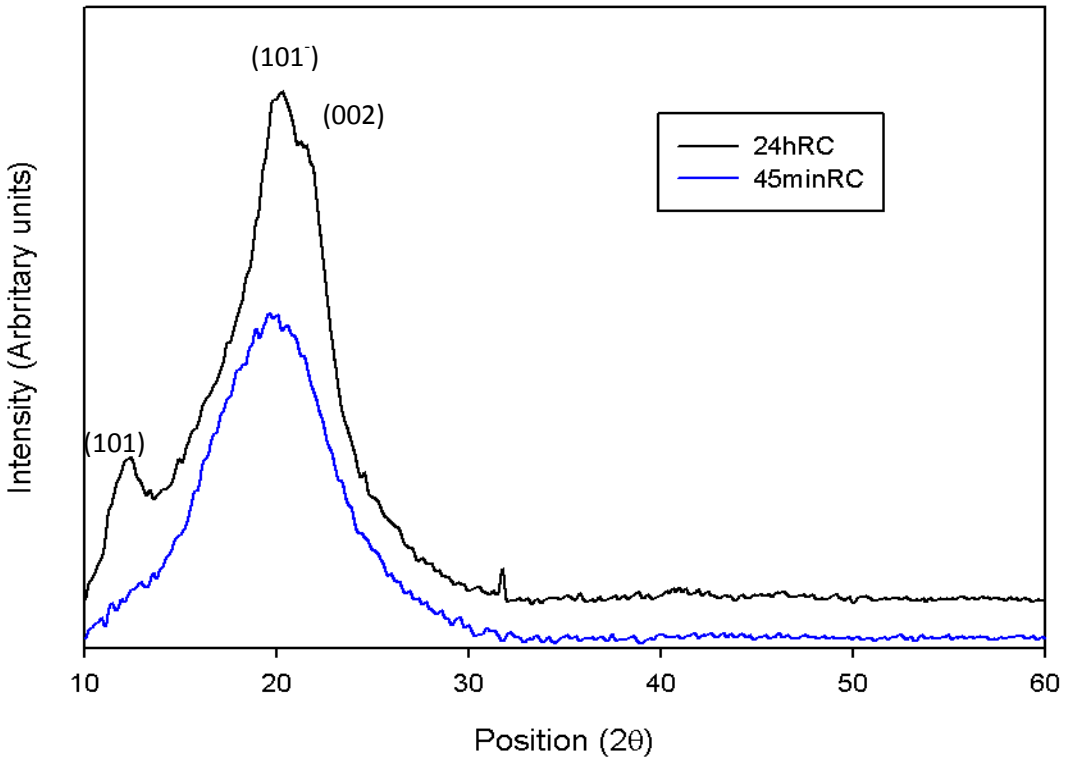

Figure 5. 4 XRD diffractograms of cellulose scaffolds regenerated 24 h and 45 min.

5.3 Thermogravimetric Analysis.

The thermal decomposition of electrospun CA and regenerated cellulose (24 hours treatment) membranes was analyzed by TGA with the purpose of determining the existence of trapped solvents, particularly dimethylacetamide (DMAc) due to its high degree of toxicity, from the electrospinning process and their hygroscopic behavior (Fig. 5.5). The thermal decomposition of electrospun CA and regenerated cellulose consist of a series of reactions. The first step of weight loss, from room temperature to 110 °C, can be related to the evaporation of residual adsorbed and absorbed water, the hygroscopic behavior. This is followed by the evaporation of DMAc around 170 °C. The last step ends near to 450 °C for cellulose and before that for CA, and is illustrated by the abrupt loss of mass that is related to the main thermal decomposition process [103-105]. The peak temperatures observed in the derivative of the TG values (DTG) curves corresponds to the temperature at which the rate of evaporation and decomposition reaches the maximum values [103].

The curve produced from the TGA and DTG of electrospun CA (ECA) shown 3% decrease in weight below 110 °C which corresponds to the water content, and 5.8% decrease from 110 to 170 °C where DMAc evaporation was expected to take place. EC registered a 3.3% of weigh in humidity. In contrast to electrospun CA the cellulose membrane (EC) did not exhibit any loss in weight from 110 to 250 °C which confirms that there was no detectable levels of DMAc present on the electrospun membrane after regeneration treatment. Since cellulose is an established biocompatible material [40, 52], this finding promotes the use of electrospun regenerated cellulose membranes as biomaterial due to the fact that there are no other substance apart from water and cellulose. On the other hand, an additional treatment, for instance vacuum drying or dialysis, is necessary for the electrospun CA membranes before to be in contact with any mammalian tissues.

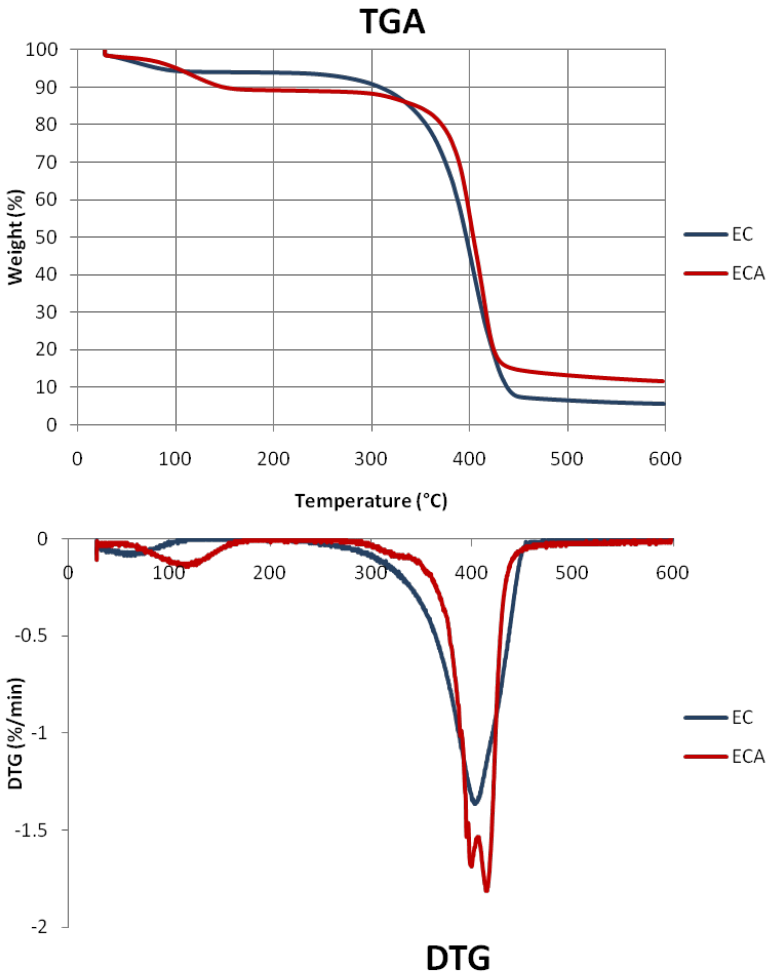

Figure 5. 5 TGA and DTG curves of electrospun cellulose acetate (ECA) and electrospun regenerated cellulose (EC) fibers.

5.4 Wettability.

Wettability measures the hydrophilic/hydrophobic character of a material based on the sessile contact angle measurement with a water probe. Wettability is a relevant property on the subject of biocompatibility, given that it has a major role on protein adsorption and cell interaction [25, 88]. The wettability of electrospun CA and regenerated cellulose membranes was evaluated by contact angle of a sessile drop of water (Table 5.1 and Fig 5.6).

Table 5.1 Water contact angle of aligned and random oriented CA and cellulose fibers, n=5.

Sample	Water contact angle
Random CA fibers	122.18 ± 0.04
Aligned CA fibers	119.90 ± 0.21
Random cellulose fibers	18.54 ± 5 .11
Aligned cellulose fibers	18.39 ± 3.18

The wettability between aligned and random oriented fibers was very similar in both CA and cellulose as illustrated in Table 5.1. A surface is hydrophilic if the value of the water contact angle is less than 90° and hydrophobic if the value is greater than 90° [106]. According to this criterion, electrospun CA fibers with values of 122.2° and 119.9° for random and aligned fibers, respectively, would be considered hydrophobic. Whereas electrospun regenerated cellulose fibers, with values of 18.5° and 18.4° in random and aligned fibers, fall in the hydrophilic category. A less hydrophilic nature of cellulose acetate compared to cellulose was anticipated attributable to the presence of methyl groups from the acetyl substituent. However, the value of the contact angle appeared to be high. The greater water contact angle value of a flat surface is no more than 120° [106]. It is commonly accepted that increased hydrophobicity results from the particularly rough microstructure of the surface in addition to its low free energy [106]. Wenzel's law states that the contact angle of a hydrophobic surface increases with enlarged surface roughness; while on a hydrophilic surface the contact angle decrease with increased surface roughness [107]. It has been observed that irregular CA membrane surface (102.2°) had a higher contact angle than flat film CA surface (54.3°) [108]. It was also reported that the water contact angle is higher in electrospun membranes than in solvent casting films within the same polymer composition [109]. Pure cellulose is hydrophilic with a water contact angle around 20° to 30° [110, 111]. In addition to surface roughness, the measurement of contact angle with dry cellulose is complicated by the

swelling effect caused by the contact with water, evidenced by the higher variability on electrospun cellulose membranes in contrast to CA membranes (Table 5.1). Cellulose swells, lowering the interfacial energy and decreasing the contact angle that justified the slightly lower obtained values. According to the wettability results, it could be expected less protein adsorption on electrospun cellulose fibers than on electrospun CA fibers and therefore a superior *in vivo* biocompatibility behavior. Also, it is suggested, that electrospun cellulose fibers could be a good substrate to grow neural cells.

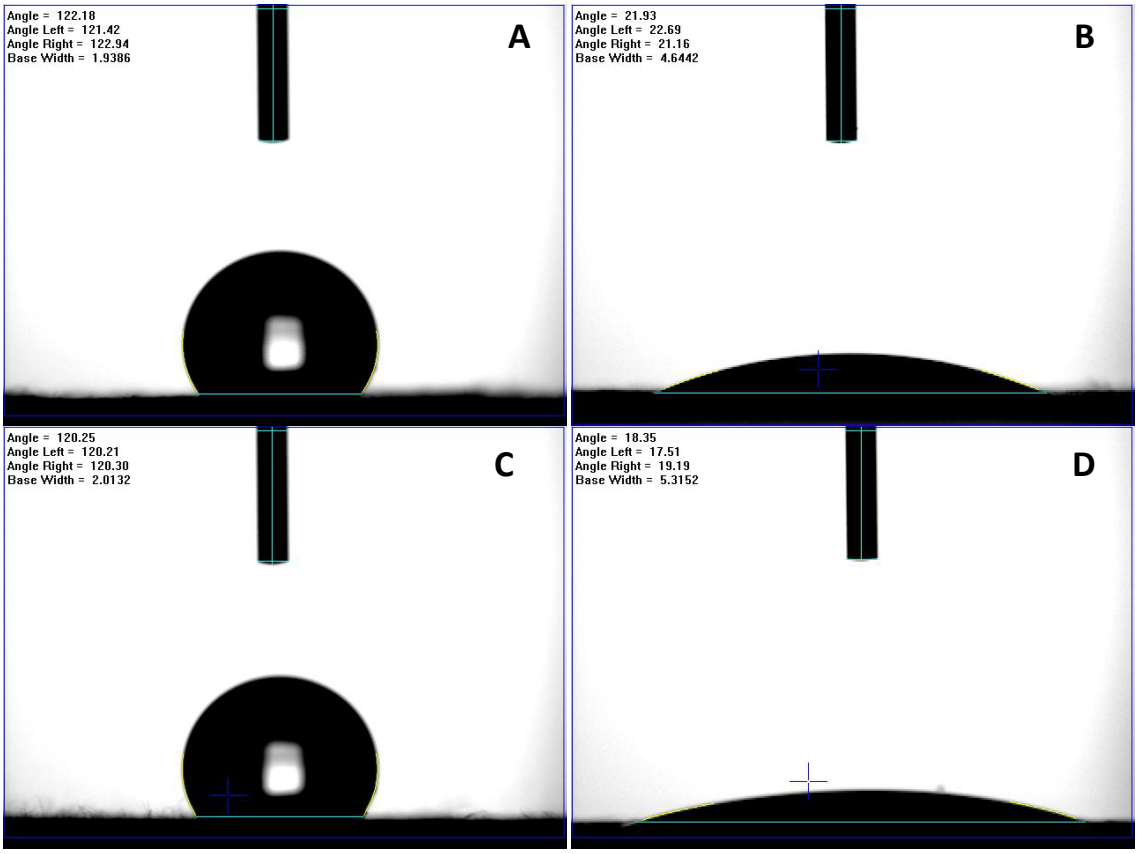

Figure 5. 6 Representative water contact angle images of random electrospun A) CA fibers, B) regenerated cellulose fibers, and aligned electrospun C) CA fibers, and D) regenerated cellulose fibers.

5.5 Surface Area Analysis.

The adsorption capacity of materials is generally proportional to their specific surface area. For this reason, the surface area of random and aligned electrospun cellulose fibers was measured by nitrogen adsorption-desorption method using Brunauer-Emmett-Teller (BET) equation (Table 5.2, Fig. 5.7 and 5.8). Adsorption isotherms are classified according to the strength of the interaction between the substrate surface and the adsorptive gas, and also by the existence or absence of pores[112] . Random and aligned cellulose fibers presented isotherms type II with almost no hysteresis (Fig. 5.7). A similar response to random regenerated electrospun cellulose have been previously reported [113]. Type II isotherms are distinctive of adsorption on macroporous adsorbents with strong affinities through a monolayer formation. According to the IUPAC classification macroporous materials have pore diameters greater than 50 nm [114]. The BET equation is expressed by:

$$\frac{1}{Q[(Po/P)-1]} = \frac{c-1}{Q_m}\left(\frac{P}{Po}\right) + \frac{1}{Q_m c} \quad (5.1)$$

Where P and Po are the equilibrium and saturation pressure of adsorbed material at the temperature of adsorption, Q is the adsorbed gas quantity and Q_m is the monolayer adsorbed gas quantity. c correspond to the BET constant described by:

$$c = e^{\left(\frac{E_1 - E_L}{RT}\right)} \quad (5.2)$$

E_1 is the heat of adsorption in the monolayer, and the heat of adsorption for the second and higher layers represented by E_L this value is also equal to the heat of liquefaction. Q_m and c values are calculated from the slope and intercept values of the BET plot.

The BET plots (Fig. 5.8) should give a linear line and the slope of that line is used to determine Q_m from which the surface area was calculated. In this manner using the parameter shown in Table 5.2, the specific surface area of random oriented fibers was 3.18 m^2/g from which 1.3 m^2/g was relative to pore area and 1.89 m^2/g to external surface area. In contrast, aligned fibers registered, 1.2 fold increase in surface area, 1.5 times less surface area associated to pores and 1.5 times higher external surface area. As discussed in Chapter 4, an enhanced surface area and reduced amount of pores was expected on aligned fibers because of the fiber packing and change in fiber diameter that was observed.

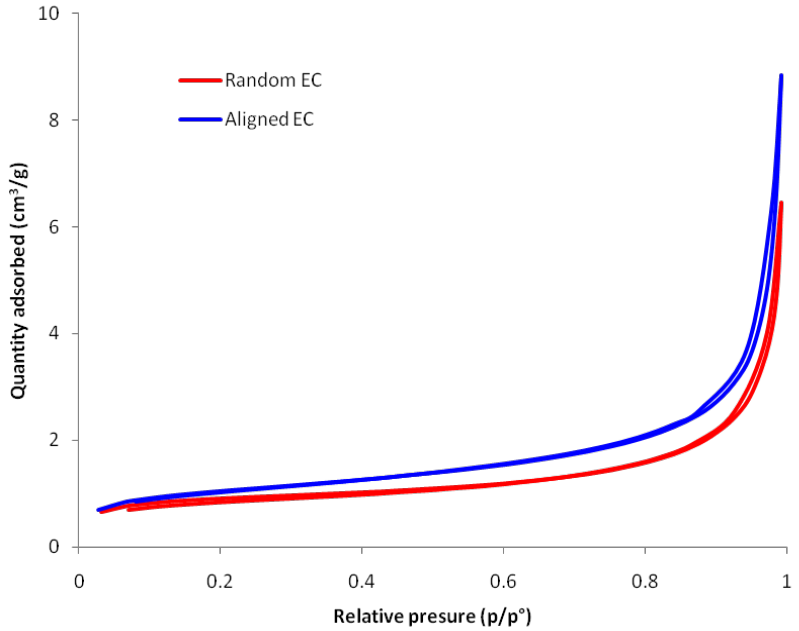

Figure 5.7 Nitrogen adsorption-desorption isotherms of random oriented and aligned electrospun cellulose fibers at 77 K.

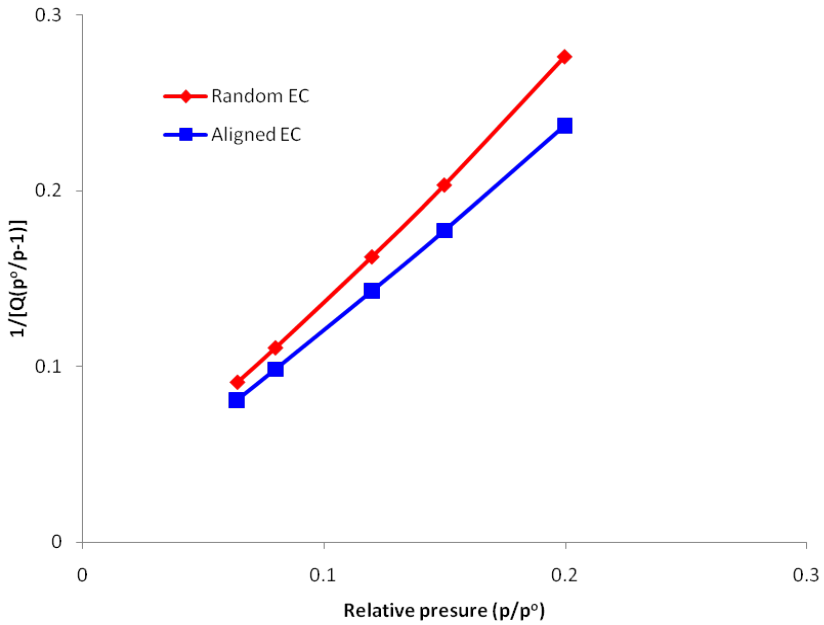

Figure 5.8 BET surface area plot of aligned and random cellulose fibers.

Table 5.2 BET equation parameters.

Sample	Slope (g/cm^3 STP)	Y-intercept (g/cm^3 STP)	C	Q_m (g/cm^3 STP)	Correlation coefficient
Random fibers	1.37 ± 0.02	0.00164 **±** 0.00331	1174.2909	0.7315	0.9995
Aligned fibers	1.15 ± 0.01	0.00668 **±** 0.00161	172.7331	0.8664	0.9998

Table 5.3 Textural properties of random and aligned fibrous membranes.

Sample	**Surface area** (m^2/g)	**Pore area** (m^2/g)	**External surface area** (m^2/g)
Random fibers	3.18 ±0.06	1.30	1.89
Aligned fibers	3.77 ± 0.04	0.85	2.92

5.6 Tensile Properties.

Stiffness of substrates used in applications for muscle or brain regeneration is critical. Accordingly, the tensile properties of electrospun cellulose fibers were determined in phosphate buffer saline (PBS, chemical composition of PBS is shown in Table 2.5 Chapter 2) solution at 37°C and pH 7.4 that resembles physiological conditions. The tensile properties were also evaluated for fibers dry at ambient temperature with 3.3% water content (TGA data, Fig. 5.5) and fibers immersed in a water bath. Dry and wet measurements were carried out at 22 °C to better understand the impact of physiological conditions on their tensile properties. Dry random electrospun cellulose acetate membranes were also evaluated by micro-tensile tester inside an environmental SEM chamber (Fig 5.10).

Typical stress-strain curves and calculated values of aligned and random nanocellulose fibers are presented in Figure 5.9 A&B and Table 5.4. The behavior of random electrospun fibers under tensile stress is shown in Fig 5.10. Overall, aligned fibers have higher stiffness and ultimate tensile strength than random oriented fibers for all the tested conditions. However, random fibers were more ductile, particularly when in aqueous media. The tensile strength of electrospun fibrous membranes can range

from 0.8 to 18.0 MPa depending upon the material composition [109]. Aligned dry fibrous membranes had outstanding elastic modulus of 355.6 MPa and tensile strength of 30.9 MPa but relatively low ductility (8.9%). Random electrospun dry membranes exhibited 3 times lower stiffness, 5 times lower tensile strength, and comparable ductility. The strain-stress curves of both fiber morphologies had an inflection in the beginning of the elastic region in dry conditions. The irregularity may be caused by the breakdown of few superficial fibers of the membranes. The stiffness and tensile strength reported by Lu and Hsieh [113] for dry electrospun regenerated cellulose membranes (random fibers) were 553 MPa and 21.9 MPa, respectively. The electrospun CA membrane was produced at similar conditions; however, the deacetylation process was carried out for much longer period of time that the used in the present work. They used smaller samples and a shorter gauge length. The discrepancy in tensile properties may be related to specimen preparation and performance of the evaluation. Mechanical properties within the same polymeric material are impacted by several factors such as molecular weight, crystallinity, fabrication process, architecture, in the case of fibers also fiber size, and porosity [25, 109]. In this work, the molecular weight and the fabrication process remained constant. It was observed a slightly difference in fiber size between aligned and random oriented fibers, discussed in Chapter 4. In the surface area characterization a decrease of 34% surface relative to porosity of aligned fibers relative to random fibers was observed, section 2.3.4, which may increase the tensile properties of aligned fibers in some extent. Increase of tensile modulus and ultimate strength with the increase of fiber alignment on electrospun membranes has been previously reported in several works [81, 115-117]. It has been observed that tensile testing induces alignment and decreases fiber diameter of random oriented electrospun membranes [117, 118]. The decrease in fiber size is dependent on the draw ratio as well as the nanofiber composition (if the polymer is above or below its T_g at the test temperature). Therefore, in random oriented fibers at the beginning of the test, only the fibers oriented parallel to the direction of the force, which is small, are holding most of the stress. As the test proceeds, there is an increase in the amount of aligned fibers at higher strain levels. At a critical point the electrospun mat resists the load causing an increase load bearing capacity, see Fig. 5.10. The aligned electrospun fibers do not undergo the orientation process, and the stress strain curve shows an immediate increase in slope at low strain values. The original uniaxial orientation of aligned fibers helps the tensile force distribute equally to all the fibers.

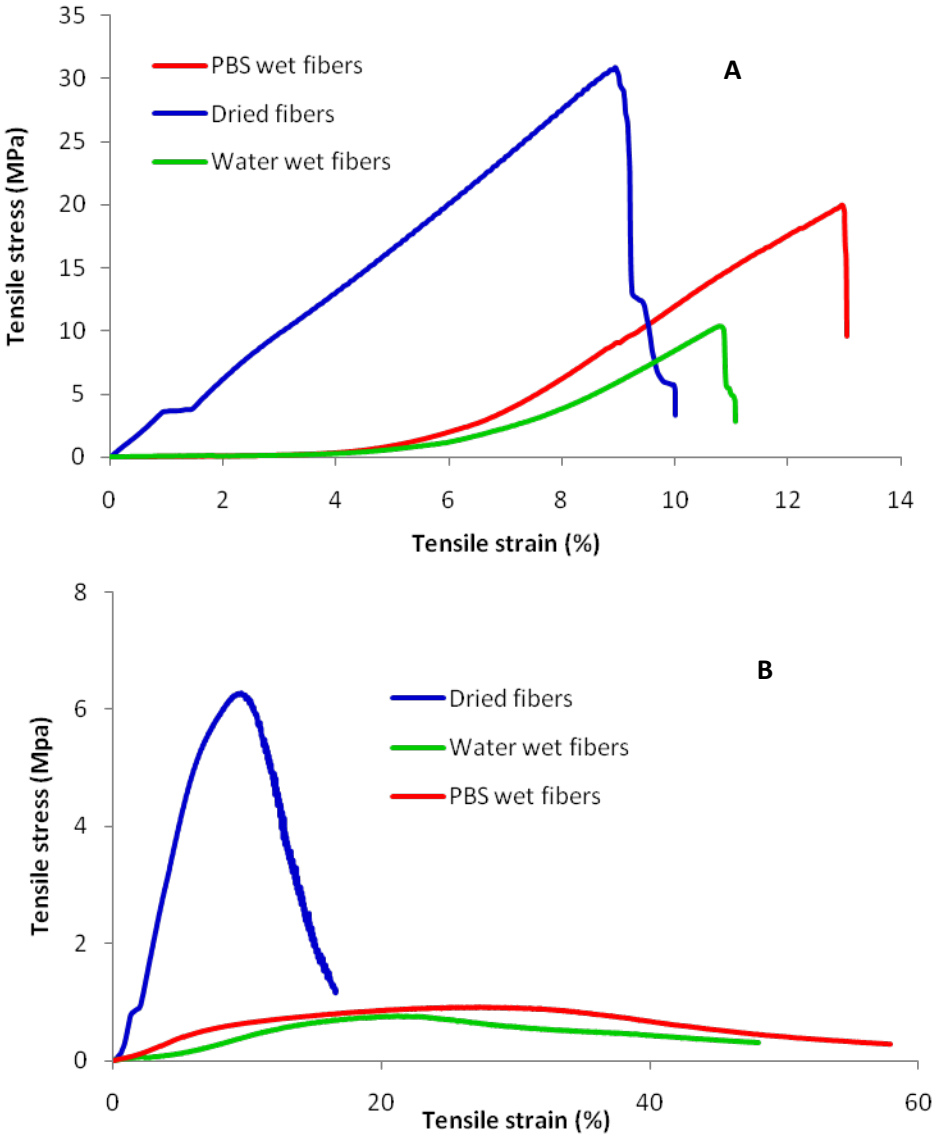

Figure 5. 9 Mechanical behavior of electrospun cellulose fibrous membranes composed of A) aligned fibers and B) random fibers at dry (22°C), water wet (22°C), and PBS solution wet (37°C) conditions.

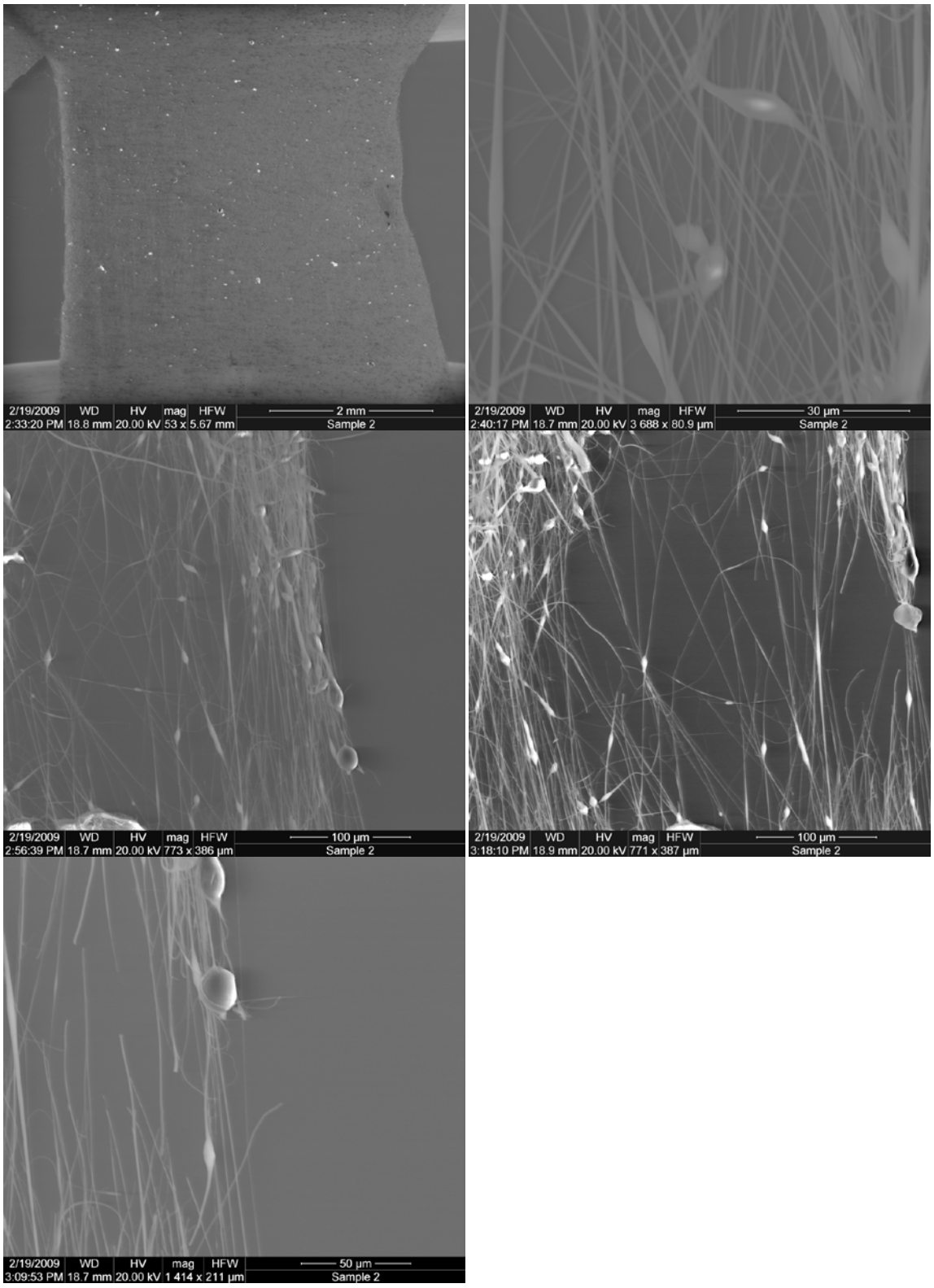

Figure 5. 10 SEM images of random electrospun cellulose acetate at some points in micro-tensile testing evaluation at ambient temperature.

Table 5.4 Tensile properties of electrospun aligned and random cellulose fibers, n=4.

Sample	**Young's modulus** (MPa)	**Ultimate tensile strength** (MPa)	**Elongation at break** (%)
Aligned dry	355.6 ± 154.9	30.9 ± 11.4	8.9 ± 0.5
Aligned PBS	302.9 ± 45.2	19.9 ± 2.3	12.9 ± 3
Aligned water	246.4 ± 94.7	10.4 ± 3.9	10.8 ± 0.9
Random dry	119.2 ± 92.9	6.3 ± 0.4	9.6 ± 2.3
Random PBS	9.4 ± 0.8	1.1 ± 0.1	36.1 ± 6
Random water	7.11 ± 3.1	0.8 ± 0.3	21.3 ± 7

It was observed that the addition of water at 22 °C and PBS solution at 37 °C decreased the stiffness and tensile strength of random and aligned fibers and increased the ductility in all the samples. It is well established that the increase in the testing temperature cause reduction in elastic modulus, a decrease in tensile strength and increase in ductility [25]. Random and aligned samples evaluated at same temperature in dry and water wet conditions have different tensile response. However, samples exposed to water and PBS solution at different temperatures presented a similar response that provides evidence that reduction on stiffness and tensile strength was mainly related to the aqueous environment and not to the change in temperature. When water is in contact with cellulose, water molecules penetrate the non-crystalline cellulose structure and interact via hydrogen bonds causing cellulose swelling. As a result, the intermolecular interactions between cellulose polymer chains are decreased and hence also their tensile properties making cellulose a more compliant material. Substances exerting this effect on polymers are called plasticizers. There is not a large difference of elastic modulus and strength between PBS and water wet for both aligned and random fibers. As illustrated in Table 5.4 there was a large variability in the tensile measurements, especially in the measurements at dry conditions. However, a trend in the different conditions can be observed. The elastic modulus and tensile strength decreased slightly when water was added relative to the case of PBS. Water molecules, within the PBS solution, interact with the dissociated inorganic ions. Though the amount of minerals in the PBS solution is small (1.2% w/w), the ions in some degree may prevent the swelling of cellulose structure which explains the observed behavior. On the other hand ductility had a higher increase in the presence of PBS at 37 °C than in the presence of pure water at 22 °C, which in this case is showing the change of ductility as a function of temperature. Finally, a larger sample size might

have resulted in more accurate measurements for the tensile properties of the electrospun fibers, and also the use of a better clamping technique to reduce the initial strain from the adjustment of the sample height. Biaxial tensile testing of the samples, due to its relevance in scaffold performance, is also suggested for future work.

Chapter 6. Improvement of Bioactivity on Electrospun Cellulose Scaffolds

The native extracellular matrix (ECM) is a three-dimensional network of biomacromolecules, and serves not only as a structural scaffold but also as an environment directing the actions of cells. Hence an ideal tissue engineering (TE) scaffolds should not only mimic the structure and compositions of ECM, but also be integrated with macromolecular bioactive agents in order to modulate the cell attachment, migration, proliferation, and differentiation [4]. In the TE field, it still remains a challenge to produce mature and functional tissues. Generally speaking, most of the tissue engineering scaffolds need to mimic the natural ECM environment in order to improve cell response. This is normally carried out by the addition of different components of ECM such as fibronectin, laminin, different types of collagen and growth factors. Cellulose is a biocompatible [40, 53] natural occurring polysaccharide made up repeating units of D-glucose. As a result this polymer exhibits a high amount of hydroxyl groups that can be used to either carry out physical adsorption or chemical reactions to create a variety of chemical moieties.

A key factor for a successful implantation in orthopedic applications is considered a close juxtaposition between bone and the implanted surface, which is known as osteointegration [46]. A strategy to enhance osteintegration is the surface modification of the scaffold with hydroxyapatite-like minerals [16, 20]. In addition, it has been reported that Ca-P minerals can enhance osteoblast cell adhesion to the scaffold [28, 57, 59]. Simulated body fluid (SBF) treatment is a widely reported procedure to create a surface apatite layer on biomaterials [16, 20, 29, 59]. Many studies have reported that a pretreatment of the substrate with Ca^{2+} containing solution is necessary to catalyze the calcium phosphate mineralization on the scaffold during subsequent exposure to SBF solution [20]. In the case of neural cells, it has been observed that they adhere poorly to different substrates [119-121]. As a result, surface modifications have been used in order to enhance cell attachment. Chemical modifications of cellulose biomaterials that have been used to introduce an ionic charge to cellulose membranes include trimethyl ammonium betahydroxy propyl (THAMP), diethyl aminoethyl (DEAE), aminoethyl (AE), and carboxymethyl (CM) functional groups [58]. Chemically modified cellulose membranes can be dipped into solutions of, for example, laminin, fibronectin or collagen, which are adhesion promoting proteins naturally occurring in the ECM of tissues [122], and the surface charge promotes adsorption of adhesion proteins from the solution onto the cellulose membrane. A study by Watanabe *et al* [58] showed that these chemical modifications improved L929 cell growth on bacterial cellulose (BC) compared to native

BC. It was also showed that THAMP modification, relative to the other treatments, resulted in the highest cell growth.

Fibronectin, as well as a number of other adhesion proteins are rich in the Arginine-Glycine-Aspartic acid (RGD) amino acid sequence, which is a fragment of the active site that binds to the integrin family of adhesion receptors[123]. RGD therefore plays an important role in cell adhesion. Adsorption of xyloglucan-RGD (XG-RGD) is a surface modification method that has been used to improve cell adhesion onto bacterial cellulose [27]. Xyloglucan is a polysaccharide that occurs in a wide range of land plants in the cell wall. Xyloglucan can thereby be used as a molecular anchor to bind chemical or biological functionalities, such as the RGD peptide, to cellulose [124]. It has been shown in a study by Bodin *et al* [27] that adhesion of human endothelial cells was enhanced when BC was modified with XG-RGD. Laminin contains the bioactive neurite binding sites Tyrosine-Isoleucine-Glycine-Serine-Arginine (YIGSR) and Isoleucine-Lysine-Valine-Alanine-Valine (IKVAV) [123, 125-128]. The peptide sequence of YIGSR can be used as an alternative to RGD for *in vitro* cell adhesion and IKVAV promotes cell adhesion, neurite outgrowth, differentiation of neural progenitor cells, and more. The use of both peptide sequences has a synergistic effect on neurite outgrowth[123]. Koh *et al* [125] investigated the effect of electrospun PLLA nanofibers coupled with laminin on PC12 neurite extension. Laminin was added to the nanofibers using three different modification methods; covalent binding, physical adsorption and electrospinning of blended laminin-PLLA nanofibers. The study showed that laminin-PLLA nanofibers had higher cell viability, attachment and proliferation compared with unmodified PLLA nanofibers. The neurite extension, after NGF treatment, was also significantly higher on the laminin-PLLA nanofibers. In addition, the blended laminin-PLLA nanofibers supported a higher neurite extension than the other two modification methods. The authors suggested that this was due to the fact that more laminin was attached onto the blended laminin-PLLA nanofibers [125].

There are several studies on the enhancement of muscle cells proliferation and maturation, specifically in mouse myoblast C2C12. Riboldi *et al* have studied the effect of diverse protein coatings (fibronectin, Matrigell®, and collagen) on block polyester urethanes (DegraPol®) [33]. They concluded that C2C12 cells adhered well on scaffolds coated with collagen type I and Matrigel ®. Matrigel® consists of different ECM components such as laminin, collagen IV, and entactin along with several types of growth factors

[129]. Fibronectin and laminin have also been used to improve the adhesion of muscle cells. Boonen *et al* cultured C2C12 cell on laminin and Matrigel ® coated substrates [130]. They concluded that in order to achieve optimal C2C12 cells maturation, laminin coated substrates should be used to modify the scaffold.

The aim of the present work was to investigate different surface modification routes to enhance adhesion and response of osteoprogenitor, muscle, and neural cells to electrospun cellulose scaffolds. With this purpose, the capability of electrospun cellulose fibers to induce nucleation and growth of calcium phosphate crystals under physiological conditions (bioactivity) was investigated. Further enhancement on the biomineralization process due to carboxymethyl cellulose (CMC) adsorption onto electrospun cellulose fibers was evaluated. In addition to the simulated body fluid (SBF) exposure, an alternative mineralization process was investigated by means of phosphate buffer saline solution (PBS). To our knowledge, this is the first time PBS procedure is reported for the mineralization of cellulose. A cationization reaction to produce trimethyl ammonium betahydroxy propyl (THAMP) cellulose in order to increase the adsorption of laminin and other ECM proteins was carried out. The EC scaffolds were also modified by adsorption of XG-RGD. The effect of Ca-P minerals and microporosity on osteoblast cell response was studied (Chapter 7). The increase in bioactivity due to THAMP modification and protein adsorption was evaluated using muscle and neural like cells (Chapter 7).

6.1 CMC Adsorption and Calcium Ion Content.

Carboxymethyl cellulose, an anionic derivative of cellulose, was adsorbed onto the electrospun cellulose (as described in Chapter 2, section 2.4). The degree of surface modification was qualitatively monitored by the adsorption of a cationic dye, toludine blue. Toluidine blue staining method was sensitive to detect the thin layer of CMC adsorption on the fiber surfaces. As observed in Figure 6.1, the cationic dye stained the CMC treated cellulose fibers indicating surface modification. For the control experiment lacking carboxymethyle cellulose, the dye was not adsorbed by the electrospun sample (Fig 6.1a).

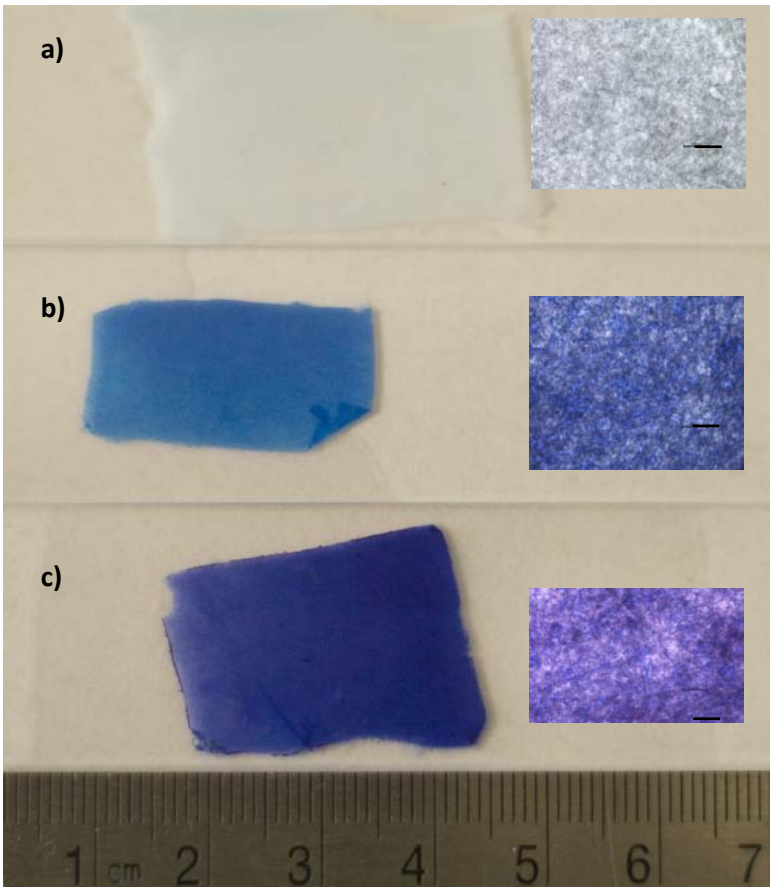

Figure 6. 1 Scaffolds treated with the cationic dye toluidine blue to qualitatively analyze CMC treatment a) 24h regenerated cellulose, b) 24 regenerated cellulose treated with CMC for 24h, room temperature pH 7, and c) 24h regenerated cellulose treated with CMC for 2h at 80°C and pH 8. Magnified surfaces are shown with the scale bar indicating 100 µm.

Conductometric titration was carried out to further quantify the carboxyl content introduced by the CMC adsorption process (see Table 6.1).

Table 6.1 Carboxyl content on regenerated and CMC modified electrospun cellulose quantified by conductometric titration.

Sample	COOH concentration (mmol/g of Sample)
Control	
24hr control (no CMC)	0.104
Procedure 1	
24hr CMC modified	0.240
Control treated at elevated temperature	
24hr treated at conditions of procedure 2 (no CMC)	0.111
Procedure 2	
24hr CMC modified	0.270

This technique revealed an initial concentration of COOH groups in the control regenerated cellulose sample, as observed by FTIR (Figure 5.1). The CMC modified samples registered a 2.3 fold increase for procedure 1 and 2.6 fold increase for procedure 2 in the carboxyl content. The adsorption of calcium ions to the cellulose is impacted by the anionic nature of the cellulose. Since the Ca-P crystal formation is influenced by the initial attachment of Ca ions to the cellulose fiber surface, XPS was performed to compare the efficiency of CMC treated versus unmodified samples to retain Ca ions after $CaCl_2$ exposure. The results are shown in Table 6.2. The atomic surface concentration of calcium for all the samples was less than 1%. The scaffolds for 45 min and 24 h of regeneration without CMC treatment presented the absence of/or lower concentrations of calcium. The regenerated cellulose controls treated at the conditions of procedure 2, without CMC, had a 4-fold increase in the calcium content for the 24 h regenerated sample. Additionally, in the presence of CMC, procedure 2 was more efficient than procedure 1 in calcium attachment, as there was twice the calcium amount for the 24 h regenerated samples and 10 times the calcium amount for the 45 min regenerated samples. These results suggest that Ca ion attachment to regenerated cellulose fibers surface can be enhance either by heat treatment or carboxyl group presence. It is also evident that 24 h regenerated samples are more efficient in the calcium loading than the 45 min regenerated samples.

Table 6.2 Atomic surface calcium concentration on regenerated and CMC modified electrospun cellulose soak in $CaCl_2$ solution prior to exposure to SBF.

Sample	C1s	O1s	O/C	Ca2p
Control				
45min RC control	56.16	43.84	0.78	0
24hr RC control	55.29	44.71	0.81	0.01
Procedure 1				
45min RC CMC modified	56.35	43.63	0.77	0.02
24hr RC CMC modified	55.54	44.29	0.80	0.18
Control treated at elevated temperature				
45min RC treated at conditions of procedure 2 (no CMC)	56.14	43.84	0.78	0.02
24hr RC treated at conditions of procedure 2 (no CMC)	55.73	44.23	0.79	0.04
Procedure 2				
45min RC CMC modified	57.45	42.36	0.74	0.20
24hr RC CMC modified	55.91	43.71	0.78	0.39

6.1.1 SBF Coating of Ca-P Crystals.

Regenerated scaffolds without CMC were exposed to SBF solution to determine if the fibers could be used to nucleate Ca-P crystallization. The samples shown in Figure 6.2 indicate that regenerated cellulose with a room temperature soak in $CaCl_2$ solution prior to exposure to SBF (Figure 6.2A, B), show marginal activity in forming crystals. This result suggested that regenerated electrospun cellulose can induce crystal formation under SBF treatment, albeit weakly (Figure 6.2A, B). It is seen in these images that random areas along the fiber surfaces show mineralized clusters, a micrometer or larger in diameter, for both regeneration times. The formation of minerals on the fibers may arise from the carboxylate groups formed during the slight oxidative degradation during alkaline saponification (Figure 5.1) and quantified by conductometic titration (Table 6.1). The samples that were exposed to elevated temperature in a slightly alkaline solution in the presence of $CaCl_2$, reveal additional mineralization (Figure 6.2C&D).

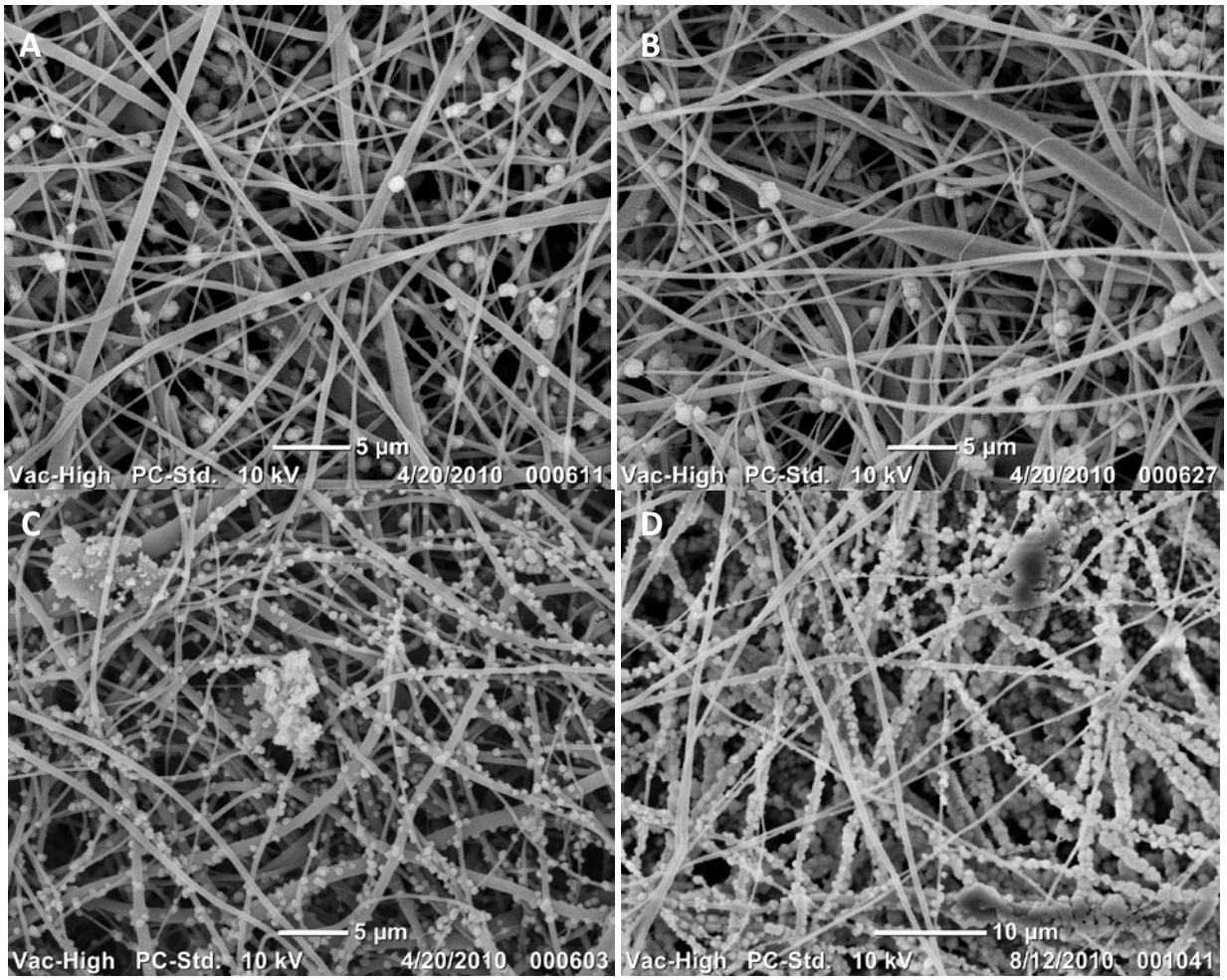

Figure 6. 2 SEM of mineralized scaffolds without CMC pretreatment A) 45 min regeneration time, B) 24h regeneration time , C) 45 minute regeneration time combined with treatment at 80°C, pH 8 for 2h and D) same as (C) but with 24hr regeneration time.

The additional mineralization may arise from greater loading of the Ca^{2+} ions on the fiber surface as seen in Table 6.1. While the time of regeneration for samples in Figure 6.2A and Figure 6.2B does not appear to influence the mineralization process, the degree of regeneration for the higher temperature soak does influence the mineralization process. Qualitative analysis of the images consistently shows increased mineralization for the 24 h-regenerated fibers, as the fibers are more decorated with mineralized clusters. Note that exposure of the 45 min scaffold to alkali at 80 °C causes additional saponification, but FTIR data shows that it retains acetyl groups (not shown). In summary, it appears that cellulose scaffolds treated with $CaCl_2$ at room temperature are weakly bioactive and this bioactivity, shown through mineralization, is enhanced after $CaCl_2$ treatment at elevated temperature. Cellulose fibers treated with CMC exhibits crystal mineralization (Figure 6.3).

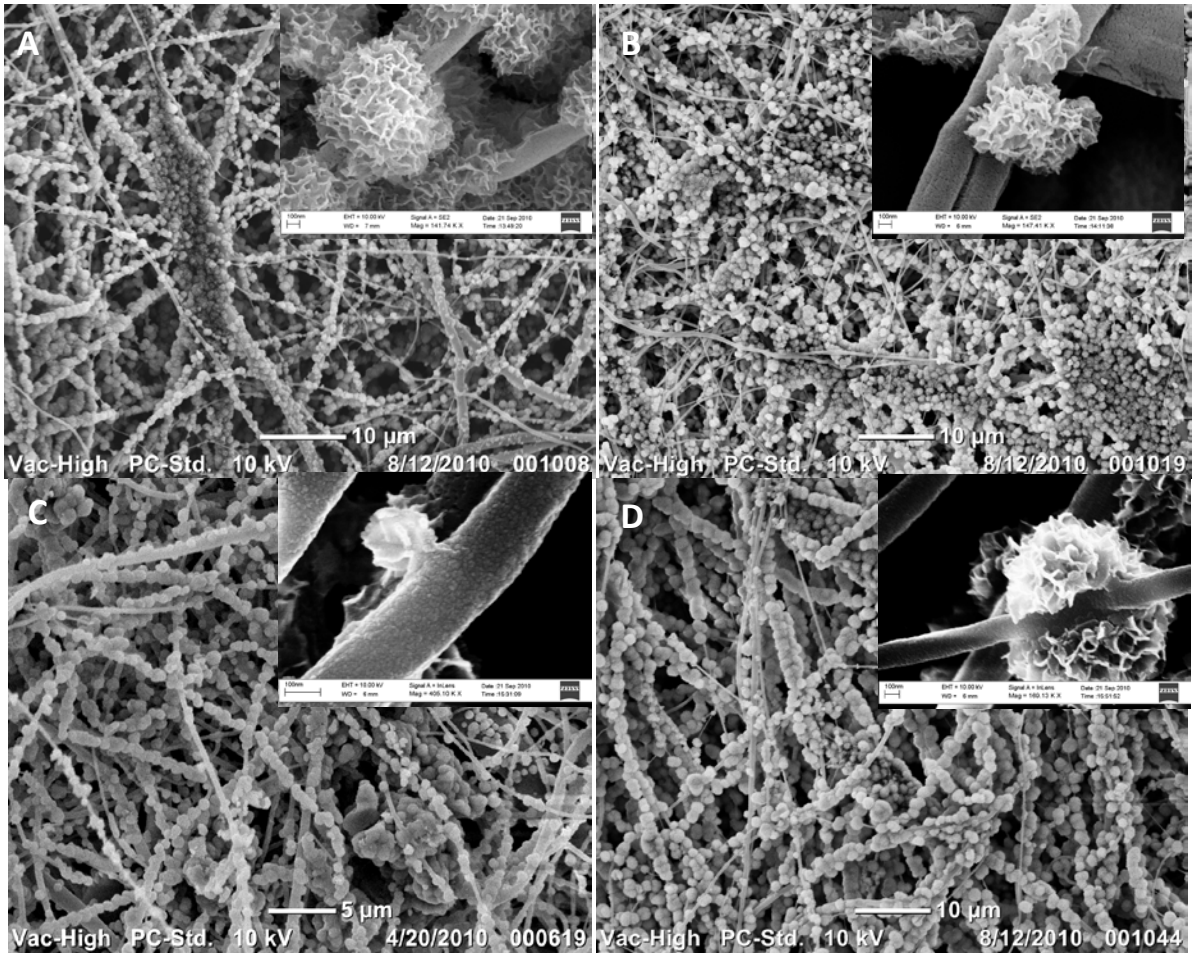

Figure 6. 3 SEM of mineralized scaffold with CMC treatment A) 45 min RC and B) 24h RC treated with procedure 1, C) 45 min RC, and D) 24h RC treated with procedure 2.

Both CMC treatment methods with either procedure 1 (adsorption at room temperature for 24 h) or procedure 2 (adsorption at elevated temperature and pH for 2 h) appear effective in inducing mineralization. In one of the inset images (Figure 6.3D), the mineral structure appears as a “blossom” on the fiber surface, while other images show the mineralization process proceeding further, continuing to wrap around the fiber providing a pearl-on-string type of arrangement. X-ray diffraction patterns were recorded to investigate the chemical structure of the mineralized scaffolds (Figures 6.4 and 6.5). Synthetic HA (Sigma-Aldrich) was analyzed by XRD and used as a HA reference. The synthetic HA was indexed using a powder diffraction files (see Figures 6.4 and 6.5). XRD peaks observed at 2θ equal to 25.8, 31.8, 32.9, 34.0, 39.7, 46.6, 49.4, and 53.1 correspond to HA as highlighted by the reference spectrum (Figures 6.4 and 6.5) [15, 131].

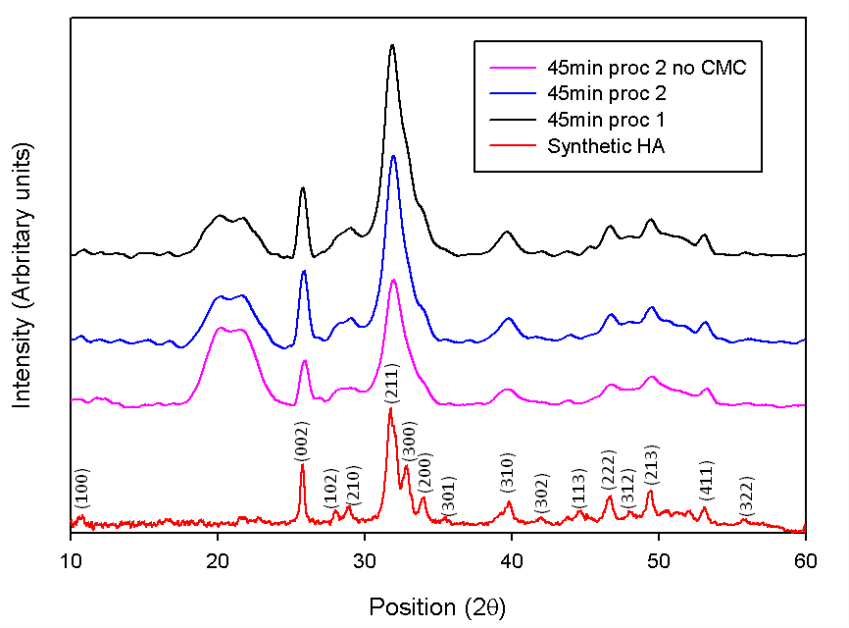

Figure 6. 4 Mineralized samples after 45 min regeneration exposed to SBF for 1 week.

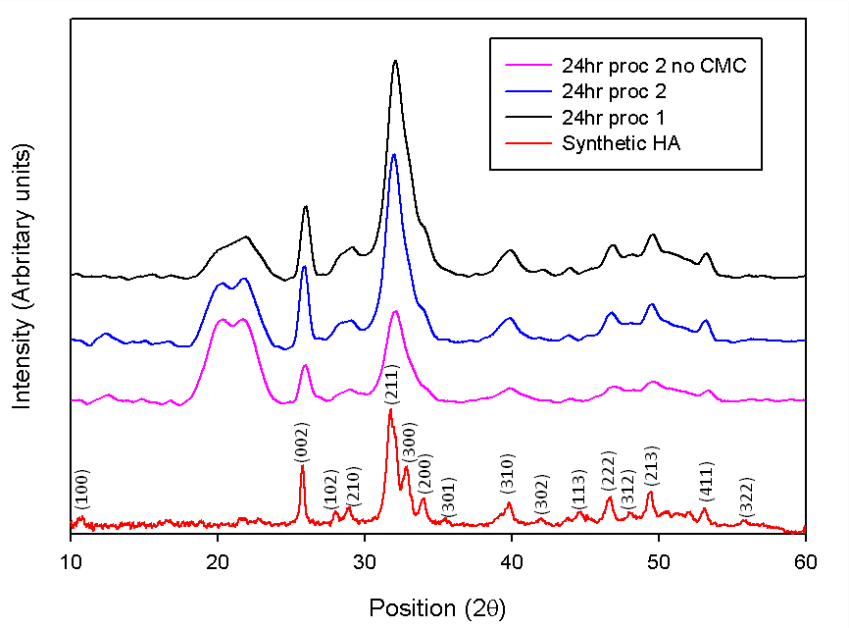

Figure 6. 5 Mineralized samples after 24hr regeneration exposed to SBF for 1 week.

The HA XRD peaks were observed for all the samples treated with SBF. This result clearly indicates that Ca-P crystals or deficient HA was formed on the electrospun cellulose fibers due to the SBF treatment. Moreover, limited differences were found within the diffractograms between the two mineralization

procedures (including the control sample of procedure 2). This data suggests a wide range of possibilities to achieve a mineralized scaffold with slightly altered structures from a single polymer material (cellulose acetate). Evaluation of the bioactivity due to mineralization *in vivo* needs to be performed to further compliment these *in vitro* studies.

Biomimetic mineralization was shown to occur *in vitro* on cellulose substrates that were surface modified via non covalent methods. For *in vivo* biomineralization, intermolecular interactions and ion solvation impacts crystal nucleation and ion transport to the surface impacts crystal growth. In the cellulose system, scaffolds with trapped calcium ions had created the nucleation sites that interact with phosphate ions during the simulated body fluid (SBF) treatment to produce Ca-P crystals. Evident of this mechanism was the differences in crystal growth for the control samples (no CMC) from procedure 1 and procedure 2 (Figure 6.2). Calcium contents prior to SBF treatment were greater for the samples that were treated at elevated temperature (Table 6.2). In fact, calcium content for the control treated at conditions of procedure 2 with 24 h regeneration was similar to the calcium content for the CMC treated sample from procedure 1 with 45 min regeneration. Comparing Figure 6.2d to Figure 6.3a, it is difficult to distinguish differences in crystal growth, further pointing to the presence of the calcium ions on the surface controlling crystal nucleation growth. The XRD data shows that most of the peaks related to hydroxyapatite are very broad (Figure 6.4 and 6.5). This result is similar to the diffraction pattern of extracted bone mineral from zebrafish fin rays that contain smaller sized and a lower degree of mineralization, relative to synthetic hydroxyapatite [132]. Hence, mineralized cellulosic scaffolds share similar features to the diffractograms from *in vivo* produced bone mineral. Another difference found in the XRD data for the scaffolds relative to the synthetic hydroxyapatite (Figures 6.4 and 6.5) is the broadening of the peak at 29° with increased intensity. Powder diffraction of amorphous Ca/P revealed a broad scattering peak located between 25 and 35° [132, 133]. On the basis of this data, it is suggested that amorphous Ca/P is also present within the SBF treated scaffold.

Since the electrospun cellulose fibers were not entirely coated with the calcium phosphate minerals produced by the SBF treated an alternative biomineralization method was studied. Phosphate buffer saline (PBS) solution is widely used in cell seeding procedures; however, its capability to form calcium phosphate minerals on scaffold surfaces has not been investigated up to now.

6.1.2 PBS Mineralization.

It has been reported that Ca-P mineralized surfaces can enhance osteoblast cell adhesion to the scaffold [28, 57, 59]. Following this approach, electrospun cellulose fibers and porous laser ablated electrospun cellulose fibers, previously modified by CMC adsorption and treated by $CaCl_2$ (procedure 1) as described in section 6.1, were treated with PBS solution. PBS solution treatment was used with the intention of producing Ca-P crystals in a better fashion that the produced by SBF treatment. The surface morphology of the fibrous scaffolds was analyzed by SEM (Fig. 6.6A, B, C, and D and Fig. 6.7 A&B). The composition and structure of the crystals produced by mineralization process were analyzed by energy dispersive x-ray analysis (EDX) (Table 6.3) and X-ray diffraction (Fig. 6.8). The surface of electrospun cellulose fibers was homogeneously mineralized after PBS solution exposure as suggested by Fig. 6.6B. The crystals had a flake like structure; the large amounts of crystals increased the fiber diameter, as can be observed by comparing images in Fig. 6.6 A&B. The high magnification inset image in Fig. 6.6C indicates an increase in surface area, where the 2-D flake-shaped crystals are extensions of small area of the fiber. By comparing images 6.3B and 6.6B it can be deduced that PBS treatment produced a more homogeneous mineral coating than SBF treatment.

The porous elecrospun scaffolds had a pattern of pores of 300 μm in diameter with horizontal separation between pores of 1500 μm and vertical separation of 500 μm as described in Chapter 4 (Fig. 4.10A). The surface structure of porous electrospun scaffold after PBS treatment can be observed in Fig 6.7 A&B. The pore size of the scaffolds was kept after mineralization treatment as suggested by Fig. 6.7 A. By comparing Fig. 6.7B and Fig. 6.8A with Fig. 6.6B can be noticed that crystal coating is very similar in porous and non porous scaffolds. Moreover, crystals on the porous electrospun cellulose scaffold were formed not only on the fibers of the surface but also within the pores (Fig. 6.8B). Regarding the elemental composition of PBS treated scaffolds; the main components detected by EDX were O, C, Ca, and P with traces of Na and Mg, data shown in Table 6.3. The atomic composition of these elements was slightly different for the non-porous and porous scaffolds. The concentrations of C and Mg were 1.4 fold and 1.6 fold higher, respectively, in porous mineralized scaffolds. In contrast to the fibers on the surface of the scaffold, the inner pore surface (within the same sample) has twice and 1.7 times higher concentrations of Ca and P without any Na and Mg. As a result the Ca/P ratio calculated from the EDX data for non-porous and porous mineralized scaffolds were 1.18 and 1.25, respectively.

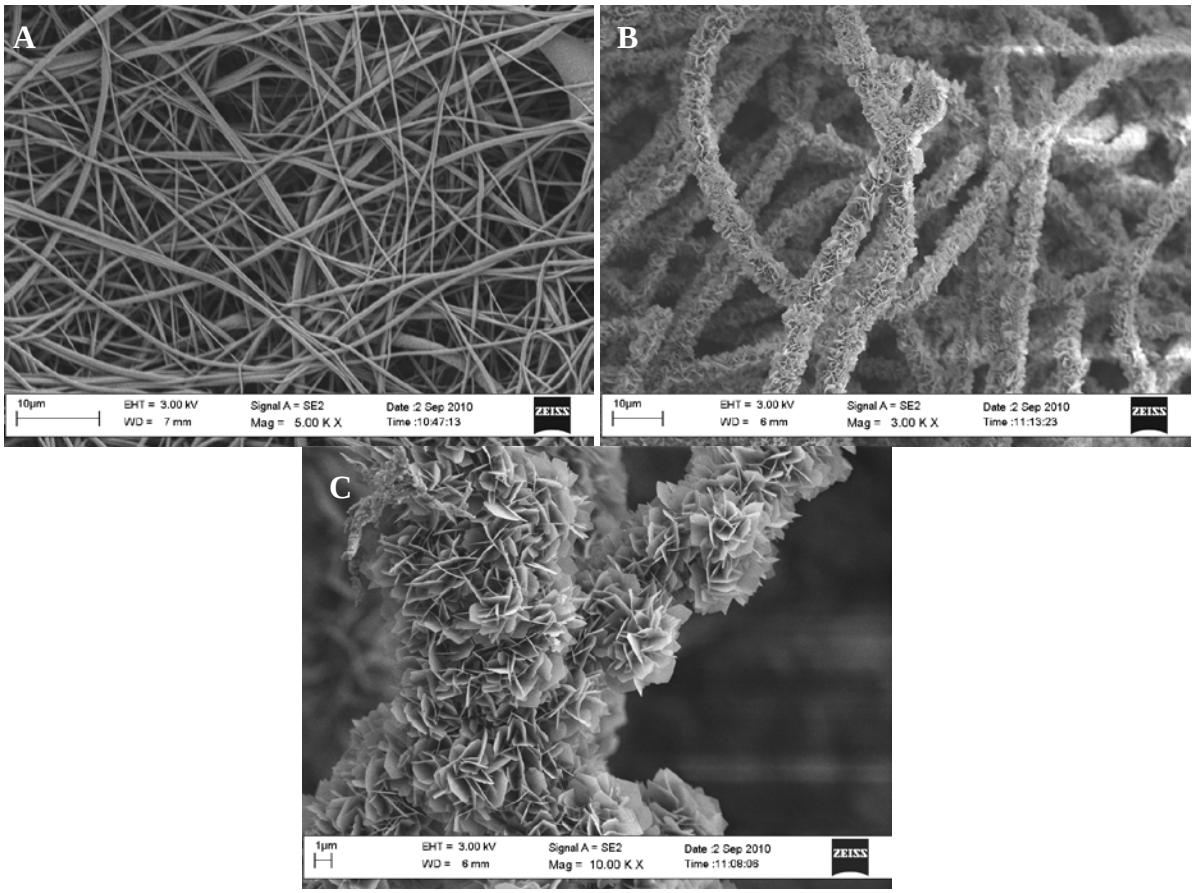

Figure 6. 6 Electrospun cellulose scaffolds. A) Control, B) Ca-P coated by PBS treatment, and C) Single fibers coated with Ca-P crystals.

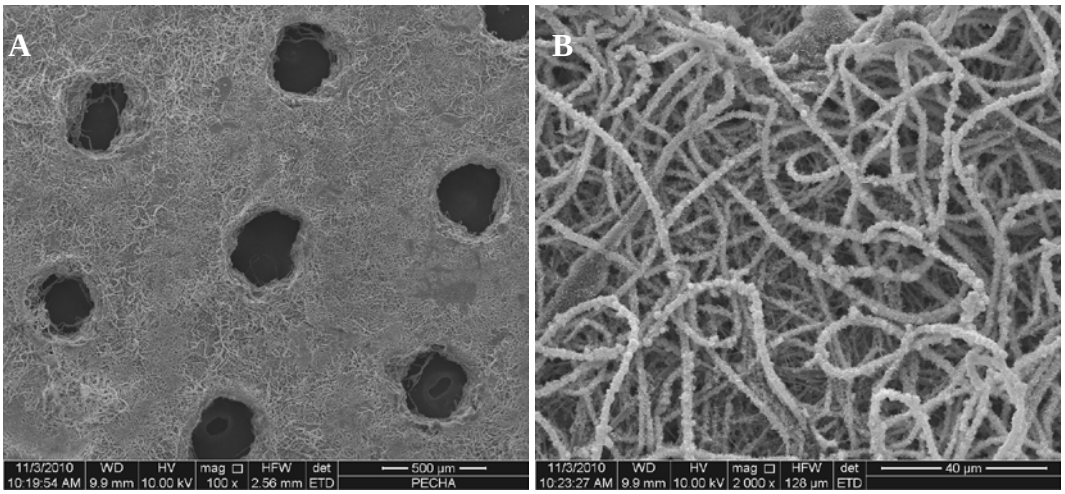

Figure 6. 7 Ca-P coated porous electrospun scaffolds. A) Microporosity, and B) Ca-P coated fibers.

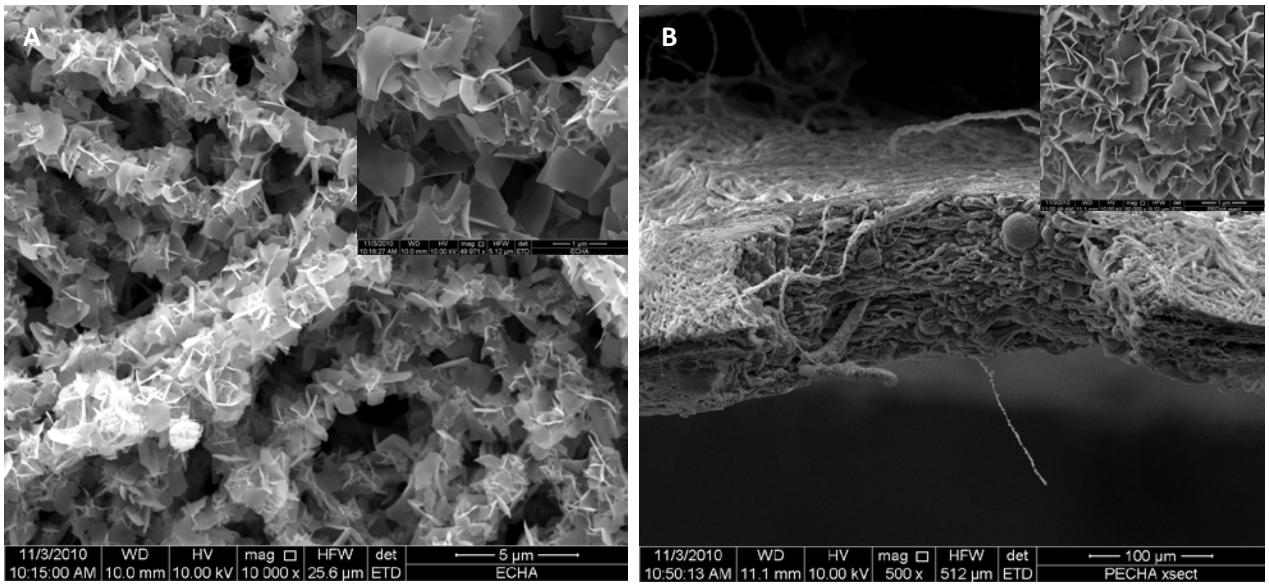

Figure 6. 8 Surface of electrospun scaffold mineralized in phosphate buffer saline for 1 week. A) Surface of scaffold, and B) Inner pore of micro-ablated sample. Inset images reveal higher magnification of the flake-like, high surface area, Ca-P minerals.

Table 6.3 Atomic composition of PBS mineralized scaffolds by EDX.

Sample description	C	O	Ca	P	Na	Mg	Ca/P
Mineralized EC	17.75	59.32	11.94	10.08	0.75	0.16	1.18
Porous mineralized EC	20.36	58.66	11.32	9.02	0.47	0.26	1.25
Porous mineralized EC cross section	14.71	46.72	23.47	15.05	0.03	0.05	1.56

Moreover, crystals lining the inner pore surface, the Ca/P ratio was 1.56, which is close to 1.67, the value of hydroxyapatite crystals [$Ca_{10}(PO_4)_6(OH)_2$] [134, 135]. This finding seems to agree with McCullem *et al* work that reported improved mineralization on laser ablated scaffolds [78]. The X-ray powder diffraction pattern of mineralized scaffolds showed the characteristics peaks of cellulose II structure, especially in non porous cellulose, and peaks pertaining to synthetic hydroxyapatite (Figure 6.9).

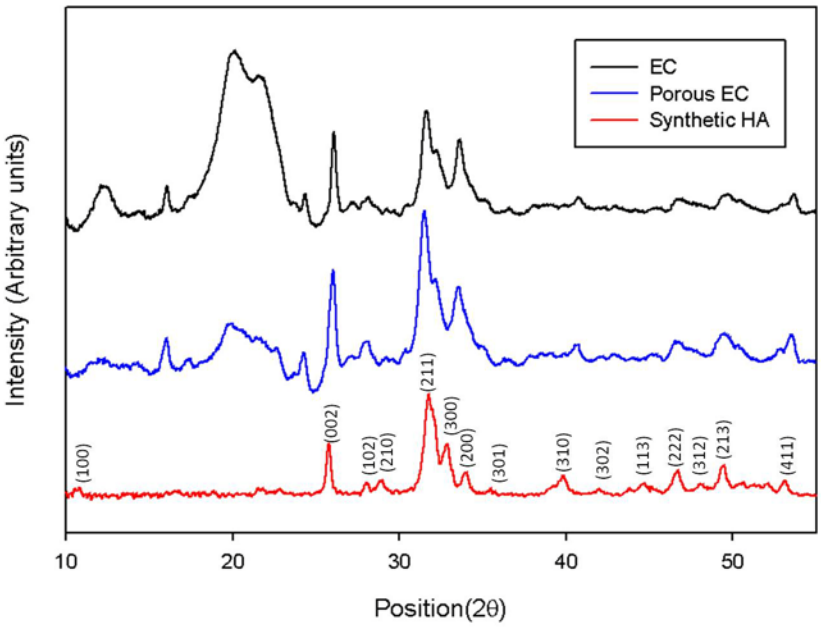

Figure 6. 9 Powder X-ray diffractograms of PBS mineralized electrospun scaffolds and synthetic HA.

Cellulose peaks in non porous mineralized scaffold were located at 2θ values of 12, 20, and 22 with a very similar structure to the non treated cellulose material (Fig. 5.4, Chapter 5). The diffraction peaks of PBS treated scaffolds, porous and non porous observed at 2θ equal to 25.8, 31.8, 32.9, 34.0, 39.7, 46.6, 49.4, and 53.1 correspond to HA as highlighted by the reference spectrum (Fig. 6.9). There was not observed a difference in the diffraction patterns among the scaffolds concerning to HA.

In contrast to the Ca-P minerals produced by the SBF treatment, minerals from PBS treatment presented less broad diffraction peaks from 31.8 to 34° (Fig. 6.5 and Fig. 6.9). Additionally, a shoulder in the peak at 31.8° that correspond to the peak from 32.9° was presented. The existence of sharp peaks may suggest that Ca-P minerals display larger crystalline size as a result of PBS treatment.

6.2 Adsorption of Xylogucan-RGD.

The adsorption of xyloglucan modified with the RGD sequence (XG-RGD) was carried out on random oriented electrospun scaffolds following Bodin *et al* procedure [27].The modification on the chemical composition of the cellulose scaffold was determined by XPS (Table 6.4). Alteration on the surface morphology of the scaffold due to the treatment was evaluated by SEM (Fig. 6.9).

Table 6.4 Atomic surface composition of random oriented EC fibers modified by XG-RGD treatment.

Samples	C1s	O1s	N1s
EC control	56.17	43.83	-
EC XG-RGD modified	55.93	44.07	-

There was no change in nitrogen surface composition due to the XG-RGD treatment as shown in Table 6.4 and Fig 6.10. XPS has limited sensitivity to detect the presence of nitrogen from the adsorption of XG-RGD on the electropsun cellulose fibers. Taking in to account that the surface of the electrospun cellulose is not flat, that the substrate, where XG-RGD was absorbed, is already compose of C and O in its majority and that XG-RGD is formed of C and O as well (approximately 89.2% w), it is understandable that XPS was not able to register an increase in nitrogen content. Bodin *et al* reported that the maximum adsorption of XG-RGD on bacterial cellulose was around 180mg/g and 3 times less on cotton linters, using a colorimetric technique [27]. They demonstrated that the observed enhancement on endothelial cell adhesion was due to XG-RGD adsorption and not to a non-specific adsorption of fibronectin from the culture media, as the QCM results had shown a decrease in adsorption of proteins from cell culture media on XG-RGD modified model cellulose in contrast to unmodified model cellulose.

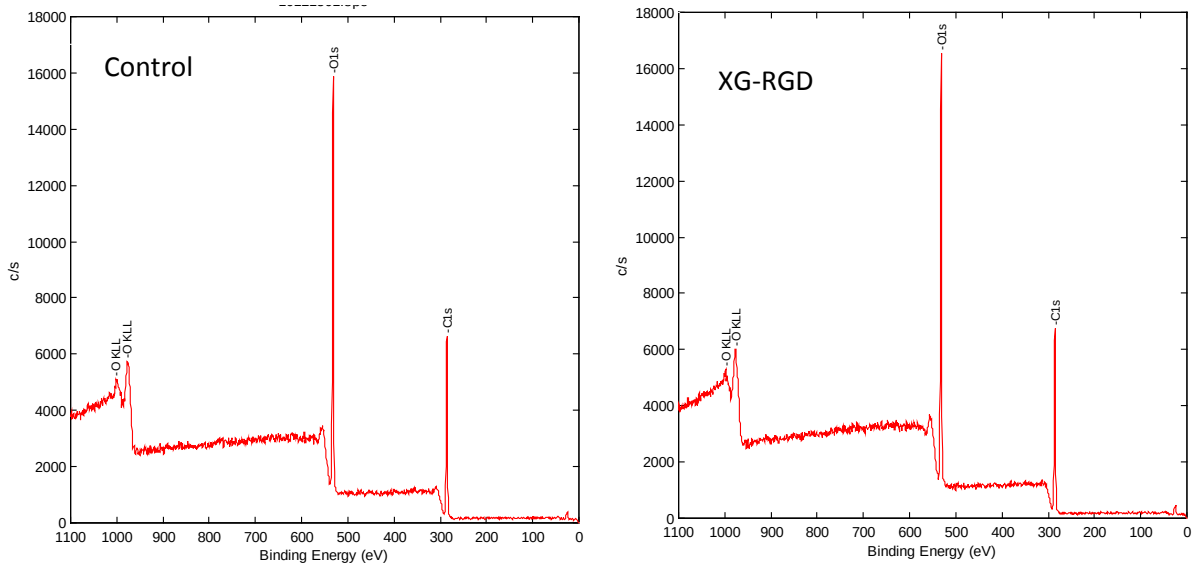

Figure 6. 10 XPS spectra of control and XG-RGD modified electrospun cellulose samples.

6.3 Cationization Treatment (THAMP modification).

The cationization treatment to produce trimethyl ammonium betahydroxy propyl (THAMP) cellulose was carried out on random and aligned electrospun cellulose fibers as described by Watanabe *et al* [58]. Change in the chemical composition due to the THAMP cationization reaction and protein adsorption from C2C12 culture media was evaluated by XPS (Table 6.6). Deconvoluted C1s peaks are shown in Appendix B. SEM was used to study the surface morphology of the unmodified and modified electrospun cellulose fibers (Fig. 6.9). These samples were used in the myoblast cell study in section 7.4, Chapter 7.

A change in chemical composition was observed because of the cationization reaction and also due to the THAMP and protein coating modifications (see Table 6.6). There was an increase in nitrogen content, less than 1%, for the THAMP cellulose sample. The deconvoluted C1s peak , C1/C2 value of THAMP modified random fibers had a 1.7 fold increase compared to the value of untreated random fibers. The increase is due to the presence of methyl groups associated with the ammonium from THAMP modification, confirming the accomplishment of the treatment. When the THAMP modified samples have the additional treatment with culture media, an increase in nitrogen of 6.83 and 7.18% in random

and aligned fibers, respectively, was observed. The O/C ratio decreased in random (1.6 fold) and aligned (1.7 fold) fibers that indicates the substitution of the hydroxyl groups. The C1/C2 ratios were 6 and 7.6 times larger in random and aligned fibers, respectively, verifying the presence of carbons from the proteins. This data suggest higher protein adsorption on aligned fibers near the surface than in random cellulose fibers, which was expected because of the larger surface area (discussed in Chapter 5). The XPS data supports that THAMP modification on electrospun cellulose and additional adsorption of proteins on THAMP modified samples did actually occurred, as observed in previous study [58]. However, Watanabe *et al* reported a five times higher amount of adsorbed protein on THAMP modified bacterial cellulose. This result could be because bacterial cellulose has a greater surface area than electrospun cellulose (79 m^2/g vs 3.7 m^2/g, see Chapter 5) and also due to the characterization technique that was employed to determine the amount of protein. In that study, the protein adsorbed on bacterial cellulose was dissolved from the membrane and quantified by a colorimetric technique. It was employed a bulk characterization technique instead of a surface technique as in the present work. This observation suggests that protein may also be absorbed within the scaffold, which can be relevant in increasing cell infiltration. The presence of sodium and chloride was also detected on majority of the samples (Table 6.6). The sodium of the control samples may be originated from the NaOH used in the regeneration process that was retained. After cationization reaction the samples were rinsed with HCl, NaCl, and acetic acid-sodium acetate buffer to neutralize the samples, as described in Chapter 2, which may explain the source for this case. The samples treated with the culture media after cationization were rinsed in PBS solution, which also contain Na and Cl.

6.4 Adsorption of ECM Proteins on Electrospun Cellulose Fibers.

Supplementary XPS measurements were performed on fully regenerated electrospun cellulose random fibers (untreated) and random cellulose fibers modified by several surface treatments (1. cationization reaction (THAMP); 2. THAMP followed by laminin adsorption: 3. XG-RGD adsorption; 4. XG-RGD and laminin adsorption; and 5. laminin coating). Results are shown in Table 6.7 and deconvoluted C1s peaks are presented in Appendix B. Those samples were used in the neural cell study in section 7.3 in Chapter 7. The modified samples were prepared as described in Chapter 2 (for each specific treatment), immersed in PC12 culture media and subsequently removed and dried directly with no further rinsing.

Unmodified random cellulose fibers exposed to PC12 media registered the presence of nitrogen, an increase in the C1/C2 ratio (13-fold), and a decrease in the O/C ratio (2-fold), see Table 6.7. These changes, as previously mention, revealed the adsorption of proteins onto the unmodified random cellulose fibers. When THAMP modified random cellulose fibers were exposed to PC12 media, there was an increase in N and decrease of O/C ratio. The C1s1/C1s2 ratio was 1.9 times larger in THAMP protein coated than in only protein coated fibers which is expected because the methyl group from the ammonium. THAMP modification was expected to facilitate protein adsorption via interaction of the zwitterionic amino-acids with the positive charged ammonium groups. RGD-XG culture media modification had 1.4 times higher O/C ratio and 1.9 times lower C1s1/C1s2 ratio than THAMP culture media treatment with very similar nitrogen content. However, it is difficult to make an absolute statement of which treatment was more effective in protein retention. Since, the C1/C2 may be larger because the methyl groups in the THAMP sample and the O/C ratio could be higher due to the hydroxyl groups from xyloglucan in the RGD-XG treatment. However, low adsorption of proteins in the XG-RGD samples may be most likely the case in accordance to Bodin *et al* study [27]. In all the laminin treated samples (laminin culture media, THAMP laminin culture media, RGD-XG laminin culture media) sulfur was detected in the binding energy range of 163.1-165.7 eV. Laminin molecule consists of three polypeptide chains that are linked by disulfide bonds [123, 125-128]. Hence, the presence of sulfur confirms the adsorption of laminin in the samples. Although, N and C1/C2 values are different among the laminin treated samples the similarity in sulfur content may imply that the adsorption of laminin occurred to the same extent. It should be noted that sulfur was detected in both RGD-XG laminin culture media and only RGD-XG culture media treated samples, which in this particular case makes uncertain the further adsorption of laminin. A tendency of the untreated samples to contain higher amount of nitrogen than the THAMP and RGD-XG pre-modified samples after laminin and laminin culture media post-treatments was observed.

Finally, the electrospun cellulose scaffolds modified by CMC, XG-RGD, and THAMP were analyzed by SEM in order to evaluate the presence of changes in their surface morphological features as a consequence of the treatments (Fig. 6.11 and Fig. 6.12).By comparing SEM images in Fig 6.11 from A to D, it can be observed that the treatments did not disrupt the nonwoven structure of electrospun cellulose scaffolds. Moreover, the topography of the fibers was retained as illustrate Fig. 6.12 A, B, C, and D; given that pockets or roughness on the surface of the fibers were not observed before or after

the treatments. This implies that the modifications employed in this work did not affect the fiber structure or cause any bulk modification.

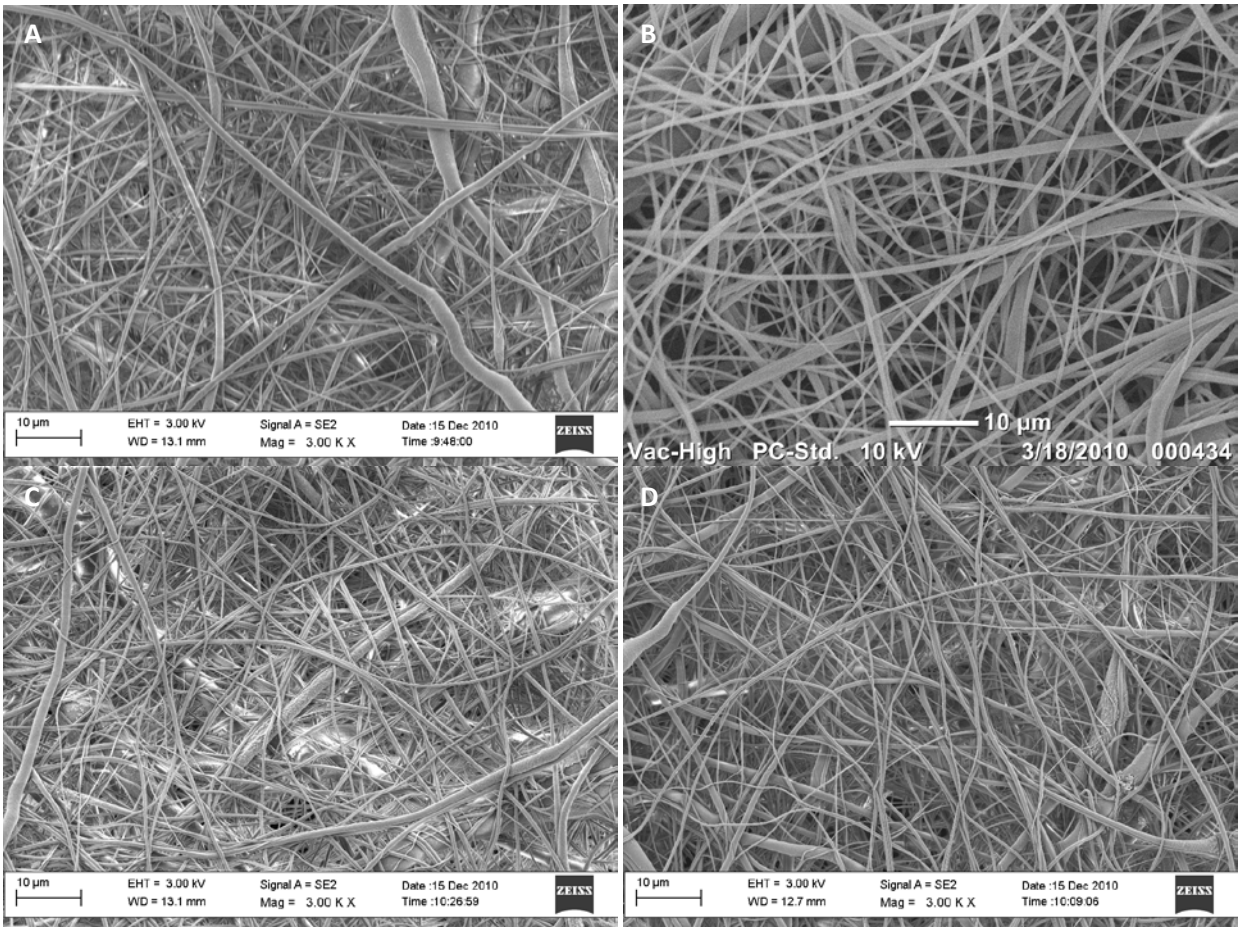

Figure 6. 11 Random oriented electrospun cellulose membranes. A) Control, B) CMC modified, C) XG-RGD treated, and D) THAMP treated.

The change of the bioactivity of electrospun cellulose scaffolds due to increase in ECM protein adsorption (from cell culture media) as a result of the THAMP chemical modification was evaluated using mouse myoblast cells (C2C12). In addition, the influence of aligned fibers on directing myotubes formation was assessed. Enhancement of electrospun cellulose cell adhesion due to THAMP modification and adsorption of laminin and XG-RGD was studied on neural like cells (PC12). The results are shown in Chapter 7. A summary of the treatments of electrospun cellulose fibers discussed in this Chapter is presented in Table 6.5.

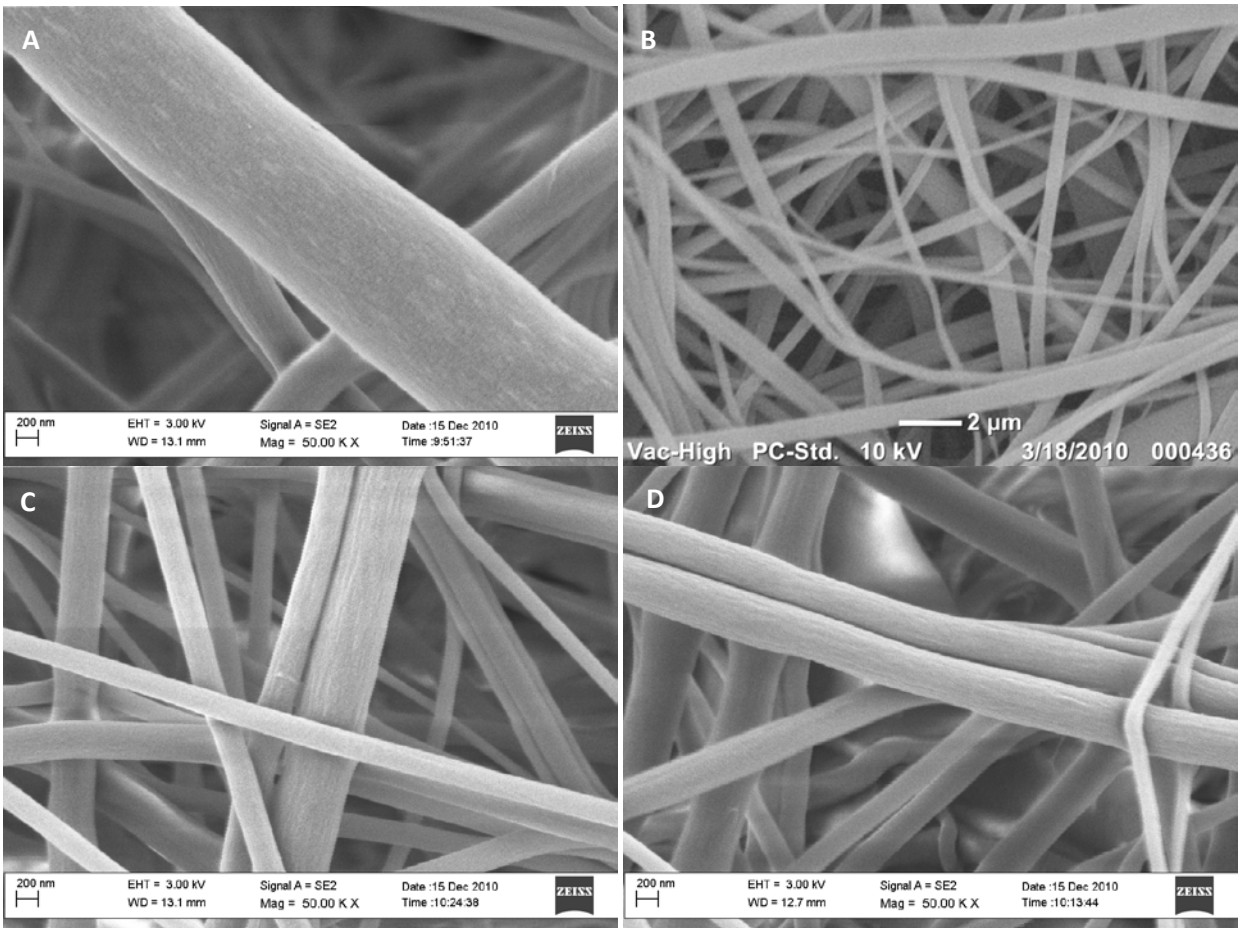

Figure 6. 12 Random oriented electrospun cellulose membranes. A) Control, B) CMC modified, C) XG-RGD treated, and D) THAMP tretaed.

Table 6.5 Surface modification of electrospun cellulose fibers.

Treatment	Modification	Functional group	Purpose	Target cell
CMC adsorption	Negative charge	(COO^-)	Ca-P nucleation	Osteoprogenitor
Xyloglucan-RGD	Uncharged	RGD sequence	Cell adhesion	Neuron
THAMP	Positive charge	$R\text{-}N^+(CH_3)_3$	Cell adhesion and ECM protein adsorption	Neuron/myoblast
Culture media adsorption		Amino acids	Cell attachment	Neuron/myoblast

R= -CH2- CH(-OH)- CH3

Table 6.6 Atomic surface composition of THAMP treated and C2C12 culture media protein coated random and aligned EC samples.

Sample	C	O	N	O/C	C1s1/C1s2	Na	Cl	Ca	S	P
Random cellulose fibers (untreated)	54.25	45.17	-	0.83	0.07	-	-	-	-	-
Aligned cellulose fibers (untreated)	55.30	44.10	-	0.80	0.08	-	-	-	-	-
THAMP modified random cellulose fibers	52.49	42.55	0.29	0.81	0.12	-	-	-	-	-
THAMP C2C12 culture media modified random cellulose[a]	54.11	28.65	6.83	0.53	0.42	5.92	4.50	-	-	-
THAMP C2C12 culture media modified aligned cellulose[a]	57.86	27.95	7.18	0.48	0.61	3.90	3.11	-	-	-

[a]Samples rinsed in PBS (without Ca and Mg).

Table 6.7 Atomic surface composition of THAMP treated and C2C12 culture media protein coated random and aligned EC samples.

Sample	C	O	N	O/C	C1s1/C1s2	Na	Cl	Ca	S	P
Random cellulose fibers (untreated)	54.25	45.17	-	0.83	0.07	-	-	-	-	-
Random cellulose with PC12 culture media[b]	62.70	26.35	9.68	0.42	0.91	1.08	0.20	-	-	-
Random cellulose laminin and PC12 culture media modified[b]	65.08	23.42	10.44	0.36	1.03	0.71	0.21	-	0.14	-
THAMP and PC12 media modified random cellulose[b]	70.04	21.04	8.47	0.30	1.69	0.45	-	-	-	-
THAMP laminin and PC12 media modified random cellulose[b]	67.15	22.72	9.51	0.34	1.14	0.48	-	-	0.13	-
RGD-xylogucan and PC12 media modified random cellulose[b]	62.54	27.02	8.93	0.43	0.87	0.91	0.22	-	0.15	0.22
RGD-xylogucan, laminin and PC12 media modified random cellulose[b]	63.92	24.85	10.02	0.39	0.99	0.91	0.19	-	0.12	-

[b]Samples were immersed in PC12 cell media and then removed and dried directly with no further rinsing.

Chapter 7. Evaluation of Cell Response on Electrospun Cellulose Scaffolds

In this chapter the evaluation of the *in vitro* biocompatibility of electrospun cellulose is described. The bioactivity of electrospun cellulose and its enhancement due to surface modifications was evaluated for three mammalian cell lines. Murine osteoprogenitor (MC3T3-E1) cells were seeded on electrospun cellulose scaffolds of random oriented fibers and the improvement in cell adhesion was studied for Ca-P coated and porous laser ablated scaffolds. The viability of neural (PC12) cells seeded on scaffolds of random oriented cellulose fibers and cellulose fibers with different surface treatments (THAMP modification, XG-RGD adsorption, and laminin coating) was determined. Myoblast (C2C12) cells behavior was evaluated as function of scaffold architecture, random and aligned nanofibers, and surface chemical composition (THAMP modification and protein coating).

7.1 *In Vitro* Cytotoxicity Test

The cytotoxic effect of electrospun cellulose fibers was evaluated *in vitro* on a culture of mouse fibroblast cells (L-929). Cytotoxicity was assessed by direct incubation of cellulose fibers extracts with the cultured cells (MEM elution test) and by diffusion of electrospun cellulose leachable substances over a cells monolayer (agar overlay test). The assessment was carried out by Nelson laboratories (Salt Lake City, UT, USA) in conformity with procedures established by United States Pharmacopeia and National Formulary (USP 87) and the ANSI/AAMI/ISO 10993-5 standards. The results as provided by Nelson laboratories are presented in Appendix C.

7.1.1 Minimal Essential Media (MEM) Elution test

In the MEM elution test a qualitative analysis of the morphology of the cells exposed to the electrospun cellulose fibers extracts was obtained (Table 7.1). The electrospun cellulose fiber extracts were compared with polypropylene (negative), latex (positive), and media controls as established by ANSI/AAMI/ISO 10993-5 standards. It was observed that cells exposed to the cellulose fiber extracts did not present formation of intracytoplasmatic granules, break down of cells (lysis), or reduction of cell

growth in any of the cellulose samples. Therefore, it was concluded that the extracts of electrospun cellulose fibers did not produce any cytotoxic effect on mammalian cells in conformity with the criteria established by United States Pharmacopeia and National Formulary (USP 87) and the ANSI/AAMI/ISO 10993-5 standards.

Table 7.1 MEM elution results of electrospun cellulose and controls[a].

Controls	Extraction Ratio	Amount tested/extraction solvent amount	Post extraction appearance	Scores				Result (pass/fail)
				1	2	3	Average	
Electrospun cellulose	0.2 g/mL	6.7 g/ 33.5 mL	clear	0	0	0	0	**Pass**
Polypropylene pellets (negative control)	0.2 g/mL	4 g/ 20 mL	clear	0	0	0	0	**Pass**
Media control	N/A	20mL	clear	0	0	0	0	**Pass**
Latex natural rubber (positive control)	0.2 g/mL	4 g/ 20 mL	clear	4	4	4	4	**Fail**

[a] MEM elution test was performed by Nelson laboratories

7.1.2 Agar Overlay

Electrospun cellulose fibers were tested for cytotoxicity on cultured cells by the agar overlay method for 24 hours; cells were evaluated microscopically and the "reactivity grade" of electrospun cellulose due to leachable substances was determined by the criteria established in the ANSI/AMI/ISO 10993-5 standard. Electrospun cellulose fibers were evaluated with negative and positive controls, results are summarized in Table 7.2. There were no degenerate cells around or under any of the three samples in contact with the electrospun cellulose fibers. Consequently, the degree of cytotoxicity of leachable of electrospun cellulose fibers was graded as zero. The negative and positive controls displayed the expected behavior, which validate the electrospun cellulose cytotoxic results.

Table 7. 2 Agar overlay results of electrospun cellulose and controls[b].

Sample	Amount tested	Grades			
		1	2	3	Average
Electrospun cellulose	≥ 100 mg per well	0	0	0	0
Polypropylene pellets (negative control)	≥ 100 mm^2 per well	0	0	0	0
Latex natural rubber (positive control)	≥ 100 mm^2 per well	4	4	4	4

[b] Agar Overlay test was performed by Nelson laboratories

The results from MEM elution and agar overlay tests confirmed that there are not cytotoxic extractable or leachable substances presented in electrospun cellulose fibers at levels that can be harmful or pose any adverse effect on mammalian cells. This group of tests confirms the feasibility of producing cellulose fibers by electrospinning and deacetylation processes for potential use as substrates for cell growth. There are several studies regarding *in vitro* cytotoxicity of electrospun cellulose based fibers that complement these results. An MTT (3-(4,5-Dimethylthiazol-2-yl)-2,5-diphenyl phenyltetrazolium bromide) assay on human fibroblast and human keratinocytes cells was carried out for electrospun cellulose and electrospun cellulose acetate (CA) with 24 and 11 % content of acetyl content. It was observed that the proliferation ability of both types of cells was not affected by any of these materials [136]. The viability of human fibroblast cells was also evaluated by XTT (2,3-bis(2-methoxy-4-nitro-5-sulfophenyl)-5-[(phenylamino)carbonyl] -2H-tetrazolium hydroxide) assay for CA electrospun fibers and CA fibers loaded with gallic acid [137]. The viability of CA fibers was 72.04 ± 5.91% in contrast to the control (plastic well plates) with 100% of viable cells and decreased with the increase in gallic acid content. It has been also reported the cytotoxicity (indirect evaluation) of CA fiber mat and CA fiber mats loaded with curcumin on normal human dermal fibroblast by a MTT assay [138]. It was found that the CA fiber mat provided the best support in attachment and proliferation. All these observations confirm that there are not extractable substances in harmful levels for mammalian cells derived from the electrospinning process of CA and the post regeneration treatment. In addition to the indirect contact evaluation of cytotoxicity of electrospun cellulose, in this work electrospun cellulose scaffolds were seeded with osteoprogenitor, myoblast, and neural like cells. The cytotoxic effect of cellulose fibers and cellulose modified fibers (Ca-P coated, laser ablated, and CA-P plus laser ablated) by direct

contact with osteoprogenitor cells was observed after three days of cell culture. PC12 cell viability after one day of cell seeding was evaluated by MTS (3-(4,5-Dimethylthiazol-2-yl)-2,5-diphenyltetrazolium bromide) assay for random electrospun cellulose and different surface treatments that were performed with the objective of improving cell adhesion.

7.2 Osteoprogenitor Cells

Osteoprogenitor cells (MC3T3-E1) were seeded on electrospun scaffolds to investigate the scaffolds for potential cytotoxicity (by direct contact) and cell adhesion. The seeded cells were fixed to the scaffolds with formaldehyde after three days of culture and were stained to highlight the cell nuclei and F-actin of their cytoskeleton (Figs, 7.1 A, B, C, and D).

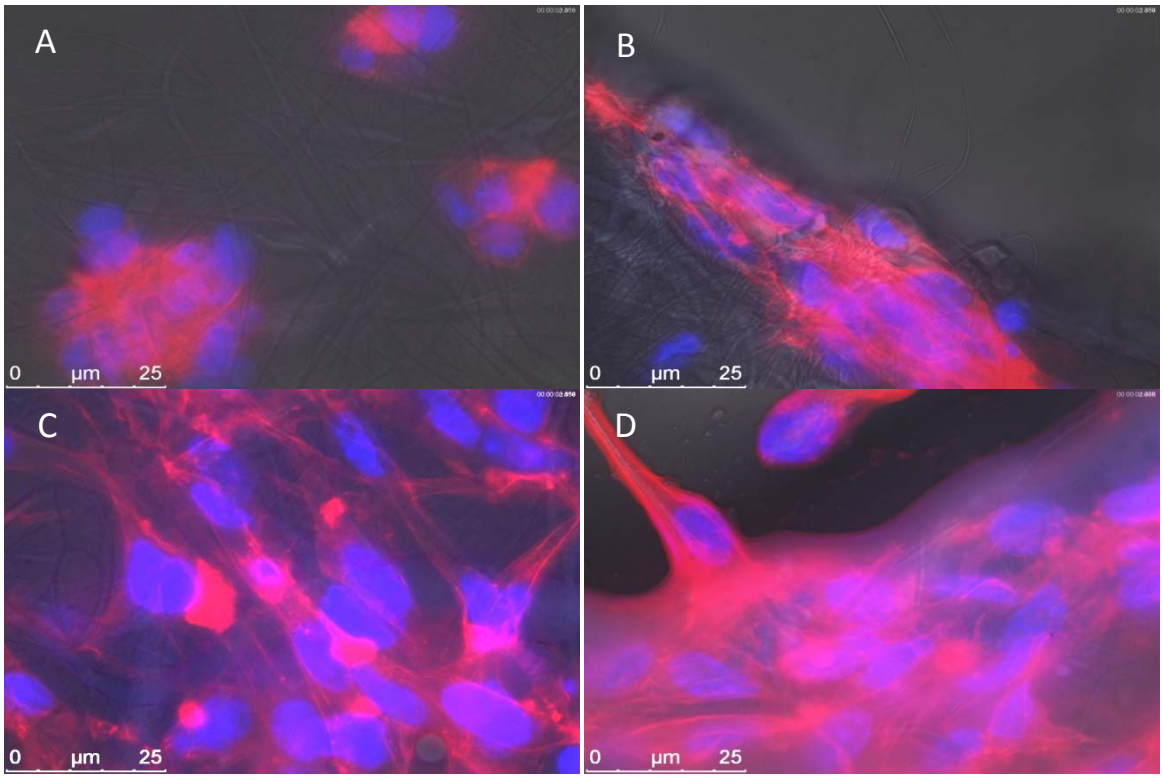

Figure 7. 1 MC3T3-E1 cells seeded on electrospun cellulose scaffolds with their nucleus dyed with DAPI, and F-actin stained with rhodamine phalloidin. A) electrospun cellulose scaffold, B) electrospun cellulose scaffold with cells lining the microablated pore, C) mineralized electrospun scaffold, and D) mineralized electrospun scaffold with cells lining microablated pore.

Most of the cells cultured on non-modified electrospun material displayed cluster like morphologies (Fig. 7.1A). Microscopy results indicated limited adhesion, as there were many regions of the scaffolds that did not host any cells. Additionally, the cells exhibited a round shape and the F-actin was not significant indicating minimal stretching of the cells. Cells cultured on the laser ablated porous scaffold showed cell clustering at the pore edges and within the pores. More F-actin appeared in the images for the cells near to the pores with some stretching evident as the nuclei were elongated (Fig. 7.1B). A large difference in cell adhesion was observed for both the mineralized samples relative to the samples that were not surface modified. Cells were stretched over the surface, indicative of good cell adhesion (Fig. 7.1 C, D). This result suggested that cells cultured on mineralized scaffolds have less difficulty to bind to the cellulose scaffold material. Groups of cells were well-stretched, lining pores of the mineralized scaffolds (Fig. 7.1D). A greater amount of F-actin is highlighted lining the pores, as there is excellent cell clustering and copious amount of cytoskeleton. On the mineralized surface without the pores, there is cell stretching, but there are distinct areas amongst the cells showing minimal overlap of F-actin. These results suggest that cells within the pores can better form cell clusters, and this cell gathering results in additional cytoskeleton growth and stretching. Cell adhesion on porous, Ca-P coated, porous and Ca-P coated, and uncoated cellulose scaffolds was qualitatively determined by counting the number of cells from the fluorescent micrographs at 3 days after seeding. The number of cells was related to the scaffold area analyzed in order to obtain cell density, Fig. 7.2. The size of the cells was also measured in order to quantitatively evaluate cell spreading due to morphology (porosity) and surface composition of cellulose scaffolds, Fig. 7.3. Porous cellulose presented a higher average cell density than plain cellulose scaffolds, which coincides with what is reported in literature [78, 79]. It has been suggested that the pores are the driving force that promotes cell adhesion on laser ablated scaffolds [78, 79] that is clearly represented by Fig. 7.1B. Attachment of MC3T3-E1 cells was further enhanced by the presence of Ca-P minerals. It is well known that Ca-P minerals have a positive effect on osteoblast cell spreading [28, 57, 59]. However, the novelty of this work was to produce Ca-P in a new fashion. As reported in Chapter 6, the PBS treatment produced a homogeneous coating of flake-like crystals around the cellulose fibers with slightly different crystalline structure. The Ca-P morphology produced by PBS treatment was well accepted by osteoprogenitor cells expressed by the enhanced adhesion as suggested by Figs 7.1 C and 7.2. Regarding the porous Ca-P coated scaffolds, the performance was not as expected since the cell density was comparable to that of plain cellulose. The real area (since there are open pores 300 microns in diameter) with cells of the porous scaffolds was smaller than for the rest of the scaffolds. Overall, the variability of the average values of cell density was particularly large. However, this data gives a general

idea of the cell response obtained by fluorescence microscopic characterization. The large variability in cell density was observed in plain cellulose scaffolds and porous cellulose scaffolds (Fig 7.2). In the case of porous scaffolds, as already explained was due to variability of area between micrographs. Regarding the untreated cellulose surface, it is speculated that the variability may arise from the presence of negative charges (COO^-) that were identified by FTIR and quantified by conductimetric titration in Chapter 5. That negative groups may increase adsorption of culture media proteins (Chapter 5) in some specific areas and not on the whole scaffold surface thus creating a variation in cell proliferation.

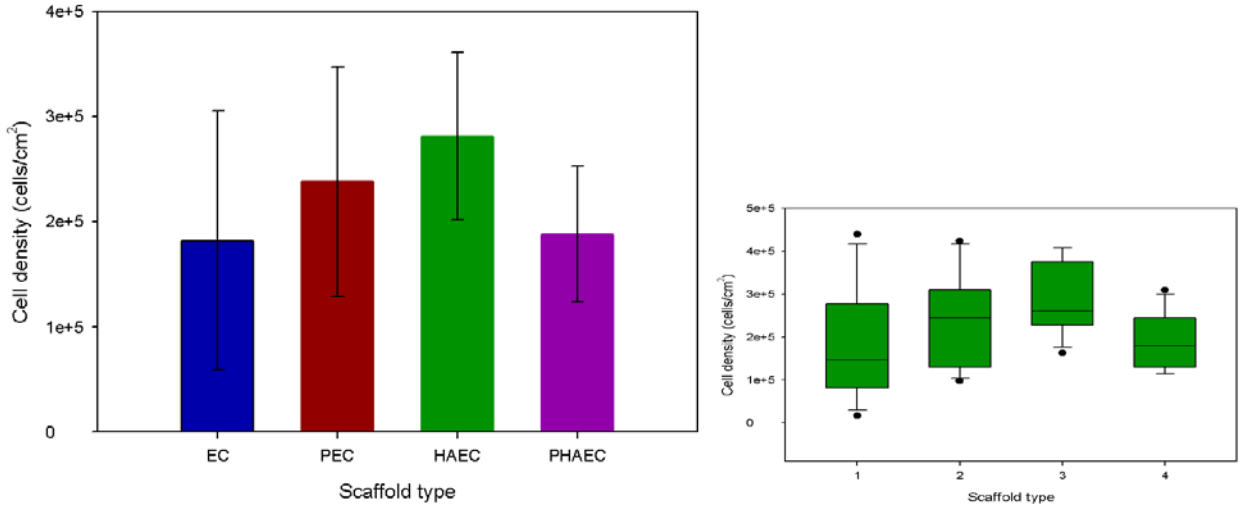

Figure 7. 2 Cell density and cell density distribution on different random cellulose fibrous scaffolds.

Regarding the size of MC3T3-E1 cells for the different cellulose scaffolds (Fig. 7.3), it can be suggested than cells seeded on Ca-P modified scaffolds were better spread across the materials that those found on untreated cellulose as observed on Figs 7.1 A&D. The expected increase in size of cells from porous scaffolds with respect to cell size on plain cellulose was not observed. This result is noted by the observation that 95% of cells seeded on porous cellulose had a size between 10 to 20 microns, with 93% of cells in the same size category for plain cellulose. Cell average size on Ca-P coated and porous Ca-P coated were very similar suggesting that spreading was equivalent. However, the amount and morphology of the cytoskeleton is also relevant on cell adhesion and hence is evaluation would give additional clues to determine whether or not the addition of porosity changed cell attachment on Ca-P coated scaffolds. As observed in cell density quantification, the variability produced in the measurements of cell size was also large. Consequently, in future work, a cell proliferation assay is

necessary to clarify the importance of addition of microporosity on osteoprogetinor cells adhesion and proliferation.

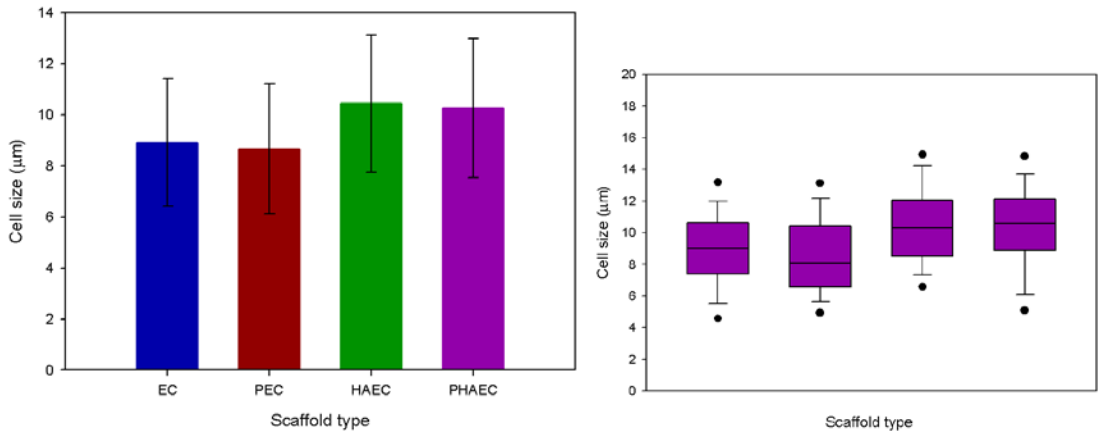

Figure 7.3 Cell size and cell size distribution on different random cellulose fibrous scaffolds.

7.3 Neural Cells

The interaction of rat pheochromocytoma cells (PC12) seeded on scaffolds of fully regenerated electrospun cellulose random fibers (untreated) and random cellulose fibers modified by a number of surface treatments (1. cationization reaction (THAMP); 2. THAMP followed by laminin adsorption: 3. XG-RGD adsorption; 4. XG-RGD and laminin adsorption; and 5. laminin coating) was visualized by SEM (Fig. 7.4 and 7.5). As evidenced by Fig. 7.4 the structure of the scaffolds after surface treatments and cell seeding was well preserved. Electrospun cellulose fibers and all the different surface treatments supported the growth of PC12 cells. The morphology of the PC12 cells on the different cellulose surfaces was round and the cells gathered in clusters, which is the normal behavior of PC12 cells before differentiation towards neural form by adhesion of nerve growth factor (NGF) and expected after one day of cell growth. Based on the SEM images, the THAMP modification seemed to be the most promising in adhering PC12 to the cellulose surface (Fig. 7.4E).

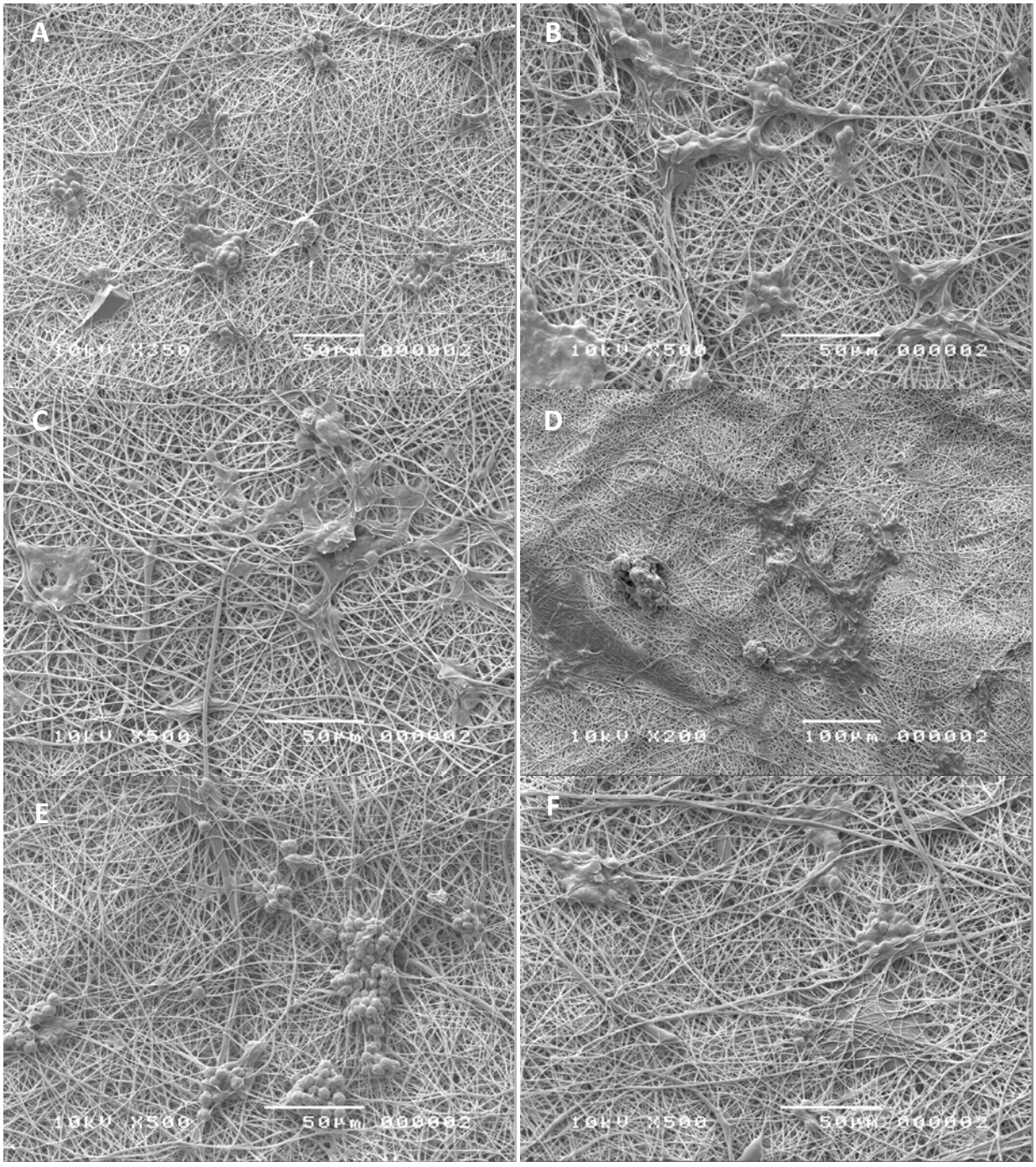

Figure 7. 4 SEM images of PC12 cells seeded on electrospun cellulose scaffolds during one day. A) Untreated cellulose fibers, B) Laminin treated cellulose fibers, C) XG-RGD modified fibers, D) XG-RGD and laminin treated fibers, E) THAMP modified cellulose fibers, and F) THAMP modified and laminin treated cellulose fibers.

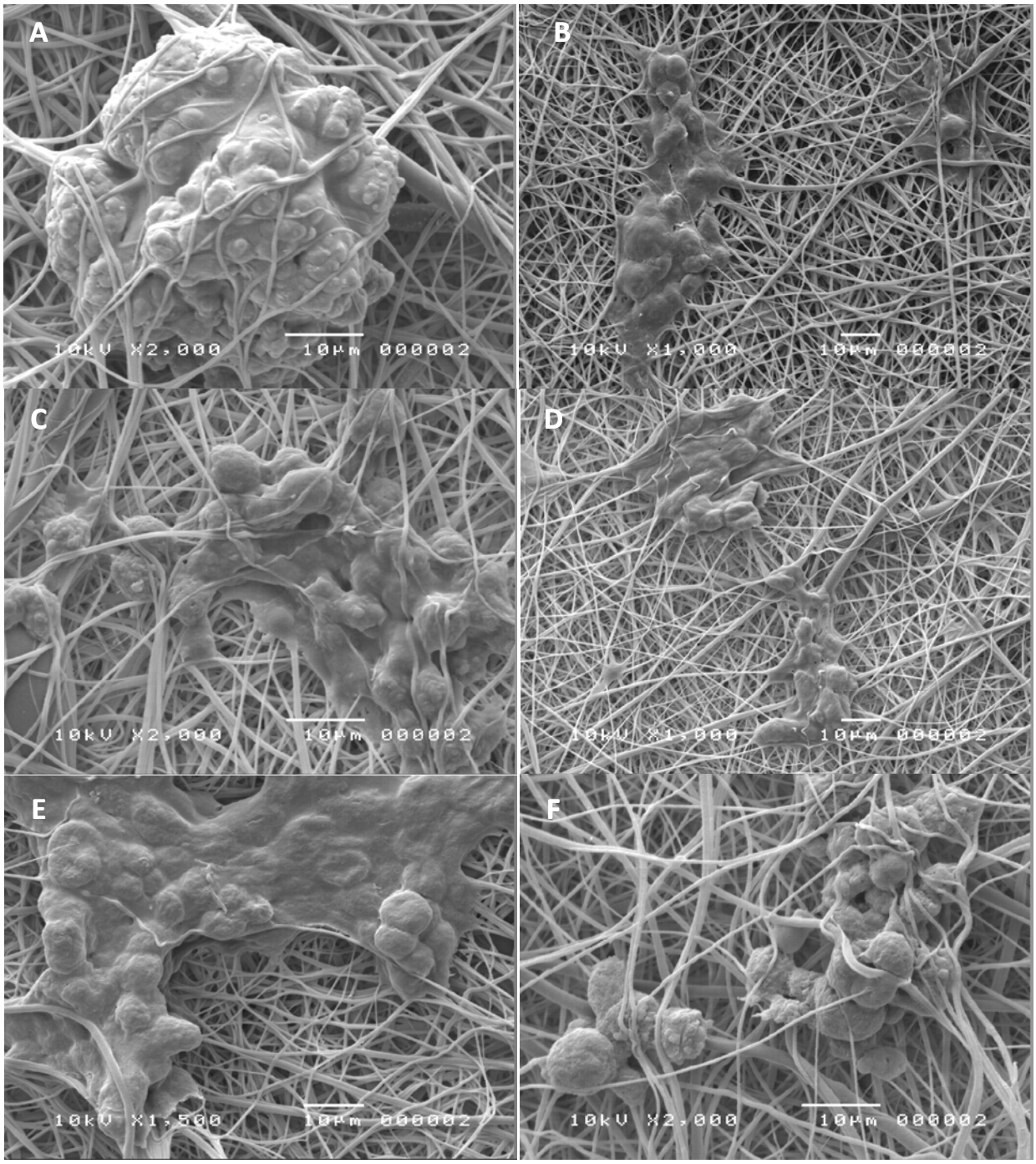

Figure 7. 5 SEM images of PC12 cells seeded on electrospun cellulose scaffolds during one day. A) Untreated cellulose fibers, B) Laminin treated cellulose fibers, C) XG-RGD modified fibers, D) XG-RGD and laminin treated fibers, E) THAMP modified cellulose fibers, and F) THAMP modified and laminin treated cellulose fibers.

Comparison of the cell morphology in Figures 7.4 A& E and 7.5 A& E suggests the THAMP treated surface produced clusters of cells well elongated over the surface relative to the untreated cellulose surface that shows aggregates of cells with more circular shape. The formation of poorly extended cells may suggest that the cells interact with themselves preferentially than with the untreated cellulose surface. This observation also suggests that the adhesion of cell was better on THAMP modified cellulose than non treated cellulose. In Fig 7.5 A to F it can be observed that the cells not only adhered to the surface but actually interacted with the cellulose fibers. In the majority of the images the cells were surrounded by the fibers (Fig. 7.5 A, B, C, E, and F). In order to obtain quantitative evidence in the effect of surface composition on cell proliferation and to establish a proper difference between treatment s a MTS assay was performed as well (Fig. 7.6). To quantify the proliferation of PC12 cells attached to the scaffolds, an MTS assay was performed at one day following cell seeding, Fig. 7.6. As illustrated by Fig 7.6 and supported by Figs 7.4 and 7.5 all cellulose surfaces supported the growth of PC12 cells. The cell growth of PC12 cells demonstrates that cellulose and surface modified cellulose scaffolds were not cytotoxic (in direct contact of cells with substrate).

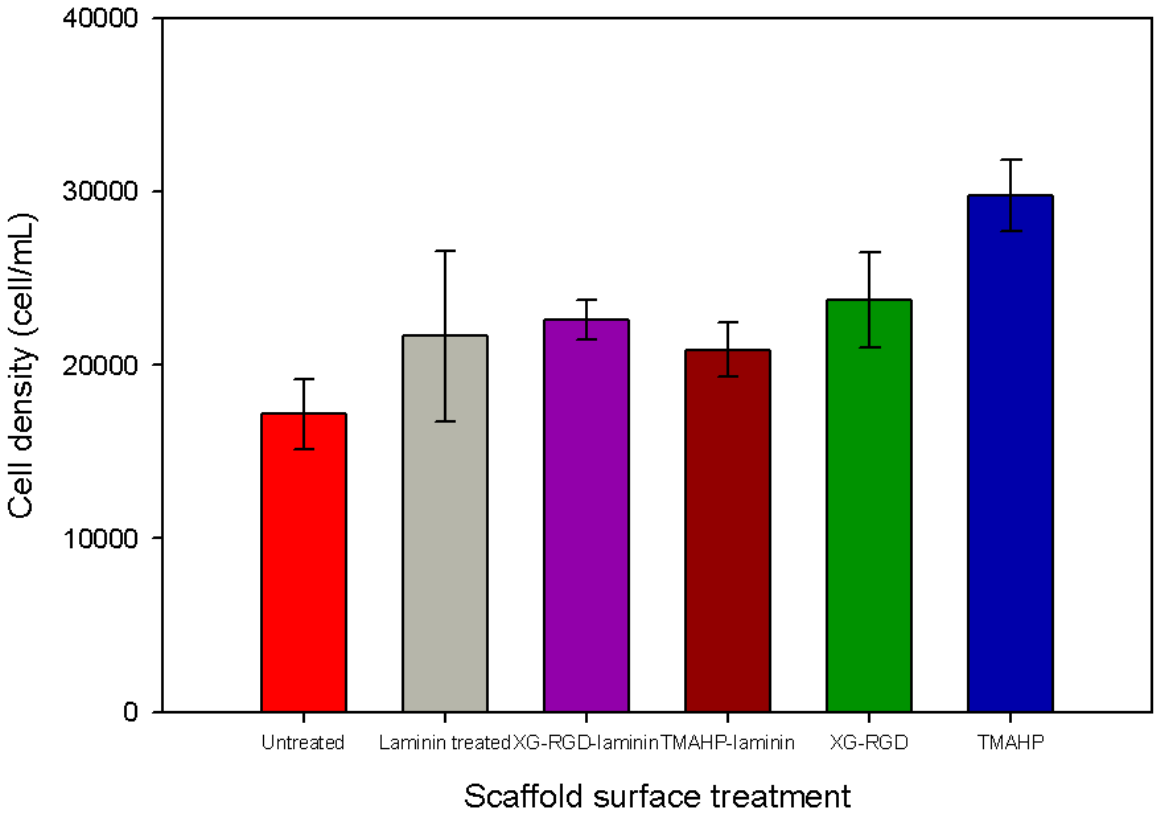

Figure 7. 6 Cell viability determined by MTS assay of PC12 cells cultured on electrospun cellulose scaffolds with different surface treatments after one day of culture.

It was found by using a Kruskal-Wallis rank sum test that there was a significant difference between the 5 treated groups and the untreated group. A nonparametric multiple comparison test demonstrated that the difference between the median of the untreated vs THAMP, untreated vs THAMP laminin, untreated vs XG-RGD, untreated vs XG-RGD laminin, and Laminin vs THAMP treatments are significantly different at 5% level. The standard deviations between Laminin and XG-RGD laminin treatments are significantly different at 2% level. Whereas the standard deviations between the Laminin and THAMP laminin, THAMP and XG-RGD laminin, and XG-RGD and XG-RGD and laminin are significantly different at 10% level; the standard deviations between the Laminin and THAMP, and the Laminin and XG-RGD treatments are significantly different at the 15% level. All other pairs were not significant different.

The lowest number of cells was found on untreated cellulose scaffolds. All surface modification treatments besides the sample that was only laminin modified, statistically, improved cell proliferation on electrospun cellulose scaffolds. The largest average increase in cell activity was observed for the scaffolds modified by the cationization reaction, THAMP cellulose. This result that THAMP modification supported the highest number of viable cells agrees with the SEM observations, as suggested by Fig. 7.4. The positive charged quaternary ammonium domains of THAMP modified cellulose were available to PC12 cells and consequently cell proliferation was better on that surface than slightly anionic cellulose. It is not surprising that THAMP cellulose has promoted cell proliferation given that it is well established that neural cells preferentially adhere-to and grow-on positively charged surfaces [91, 139-144]. The XG-RGD adsorption treatment improved the cell proliferation of cellulose fibrous scaffolds. RGD amino acid sequence is a fragment of the active site that binds to the integrin family of adhesion receptors. After laminin adsorption, for all treatments, the average cell density for the scaffolds was around 22000; this average value only varied slightly for the different laminin-coated surfaces (cellulose, THAMP-modified, and XG-RGD treated).

Although the laminin-only modified samples registered a higher average absorbance than untreated cellulose samples, the variability within the sample was large and was not statistical different from the cellulose scaffold surfaces. The large variability of absorbance found on laminin coated cellulose samples may signify that the treatment was effective just in some areas of the scaffold surface and therefore the laminin treatment was not homogeneous among the sample. The other laminin treated surfaces (THAMP and XG-RGD) did not differ much from the laminin treated cellulose values, besides reducing

some of the variability found in the laminin only treated surface. This observation suggests that the presence of laminin on the surface causes similar cell proliferation. In the case of THAMP, adding laminin reduces the overall cell density, while the XG-RGD treated samples with laminin, had very similar values to the XG-RGD only values. As previously discussed, the XG-RGD adsorption treatment improved the cell proliferation of cellulose fibrous scaffolds. However, the addition of laminin coating treatment to the XG-RGD modified scaffold did not further enhance cell proliferation since the average absorbance values were comparable (Fig 7.6) although the XPS results on Chapter 6 suggested an increase in protein content due to the laminin treatment (Table 6.6). As mentioned in chapter 6, in previous work by Bodin *et al* it was demonstrated by QCM measurements that XG-RGD modified cellulose surface did not increase the adsorption of ECM proteins but actually decreased in contrast to plain cellulose [27]. Hence, it is suggested that the either adsorption of laminin did not take place on XG-RGD modified scaffolds or it was present and caused similar cell proliferation to the other laminin treated samples.

In the case of the THAMP cellulose modification, the subsequent treatment with laminin did not enable enhanced cell response, the opposite was observed with a decrease in cell density. In contrast to the XG-RGD scaffolds, the post treatment with laminin of THAMP cellulose scaffolds decreased the proliferation of PC12 cells. Nonetheless, the THAMP laminin treated scaffold had better proliferation than plain cellulose scaffolds and less variability than laminin treated scaffolds. The difference in cell response to THAMP and THAMP laminin scaffolds suggests that there was a difference in surface composition detected by the cells. However, it was expected that zwitterionic laminin would adsorb onto the THAMP cellulose surface via electrostatic interactions with negative domains of the laminin and the positively charged ammonium groups on the THAMP. The result should yield positive domains, from the amino acid sequences YIGSR and IKVAV, of laminin to interact with neural cells (adhesion and growth promotion). In contrast, the positive domains of THAMP modified cellulose were available to PC12 cells and consequently cell proliferation was better on that surface than the laminin treated surface. It has been discussed in literature that PC12 cells attach to surfaces coated with laminin or collagen by an active mechanism[140]. That active attachment requires Mg^{+2} ions and is inhibited at low temperature or in the presence of sodium azide [140, 145].

On the other hand, adhesion of PC12 to positively charged surfaces takes place via a passive mechanism that does not require divalent cations to promote adhesion or is inhibited by any of the other factors (low temperature or in presence of azide) [140]. As observed in Table 6.6 in Chapter 6, Mg or Ca elements were not detected in the THAMP laminin treated scaffold or in any of the cell media treated scaffolds. The active attachment mechanism seems to agree with the result of cell proliferation decrease.

7.4 Myoblast Cells

The evaluation of murine myoblast cell (C2C12) behavior on electrospun cellulose scaffolds was carried out at several time periods of culturing: three hours: one, seven, and fourteen days. In this study the influence of scaffold architecture to guide C2C12 cells towards myotube formation was evaluated by using random and aligned cellulose fibers. Random and aligned cellulose fibers (untreated) and aligned and random cellulose fibers modified by THAMP followed by C2C12 culture media adsorption were used. In this way the effect of surface chemistry of electrospun cellulose scaffolds in C2C12 cell adhesion and proliferation was evaluated. The morphology of cells seeded onto cellulose scaffolds was analyzed by fluorescence microscopy (Figs 7.7 and 7.8).

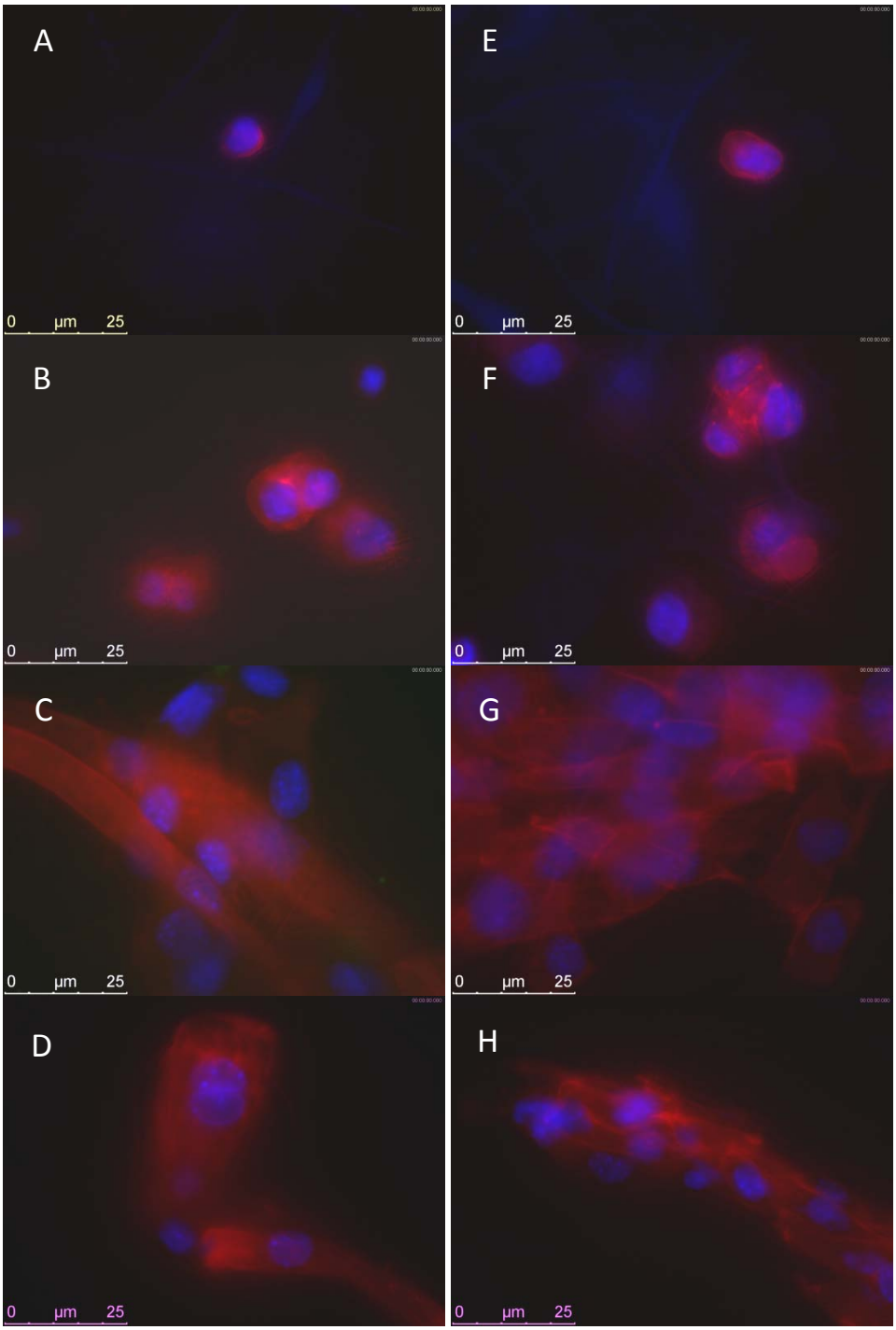

Figure 7. 7 C2C12 cells seeded on electrospun cellulose scaffolds, formed of random oriented fibers, with their nucleus dyed with DAPI, and F-actin stained with rhodamine phalloidin. Cells on untreated scaffold cultured for: A) 3 hours, B) 1 day, C) 7 days, and D) 14 days. Cells on THAMP modified and protein coated scaffolds cultured for: E) 3 hours, F) 1 day, G) 7 days, and H) 14 days.

After 3 hours of cell scaffold interaction only a small number of cells with round morphology were observed for all the scaffolds types Figs. 7.7 A&B and Figs. 7.8 A&B. This result indicated limited adhesion of C2C12 on cellulose scaffolds that was probably due to lack of incubation time since posterior point times showed better results in some of the scaffolds. The amount of cells observed on modified and untreated random oriented fibrous scaffolds was increased after 1 day of cell seeding (Figs. 7.7 B&F). Even though, cells on THAMP culture media treated random fibers were slightly larger than cells on untreated cellulose, the cells did not presented better adhesion on those scaffolds as suggested by the round morphology of the cytoskeleton highlighted with rhodamine (Figs. 7.7 B&F). As the incubation time increased to one and two weeks, cell adhesion and cell density were improved as evidenced by Figs. 7.7 C, D, G, and H. It can be seen in Figs. 7.7 C&D that the nuclei of the cells are elongated, which implicates the time of C2C12 adhesion on random cellulose scaffolds from 2 to 6 days. Since there are no images for that period of incubation, it is not possible to know if the THAMP modification improved cell attachment on random oriented fibrous scaffolds. Cell proliferation appeared to be enhanced on THAMP-modified scaffolds (Figs 7.7 G&H) than on untreated scaffolds (Figs 7.7 C&D). However, there were no drastic differences in cell behavior among modified and native random fibers. As a matter of fact, it can be observed the presence of an elongated, multinucleated myotube on untreated random fibers (Fig. 7.7D). In contrast to random fibrous scaffolds, the effect of THAMP modification had a larger impact on aligned fibrous scaffolds. THAMP and culture media treated aligned scaffolds performed better than untreated aligned scaffolds at 1, 7, and 14 days after cell culture (Figs 7.8 B, C, D, F, G, and H). The cytoskeleton of cells seeded on untreated aligned fibers did not elongate or fuse to create myotubes (Figs. 7.8 B, C, and D), but instead a pre-apoptosis process was observed. Apoptosis is a type of cell death that is accompanied by morphological changes [146]. After 14 days of cell seeding, nuclei and cytoskeleton of C2C12 cells displayed a morphology characteristic of blebbling stage of the apoptosis process (Fig. 7.8 D). This result implies that the adsorption of culture media proteins took place in some extent on native random fibers that did not occur to the same degree on untreated aligned fibers. The differentiation of myoblast to myotubes was enhanced on aligned modified fibers (Figs 7.8 G&H) than on random modified fibers (Figs 7.7 G&H). XPS analysis in Chapter 6 (Table 6.5), also demonstrated that THAMP aligned fibers were more efficient in the adsorption of culture media proteins than THAMP random fibers.

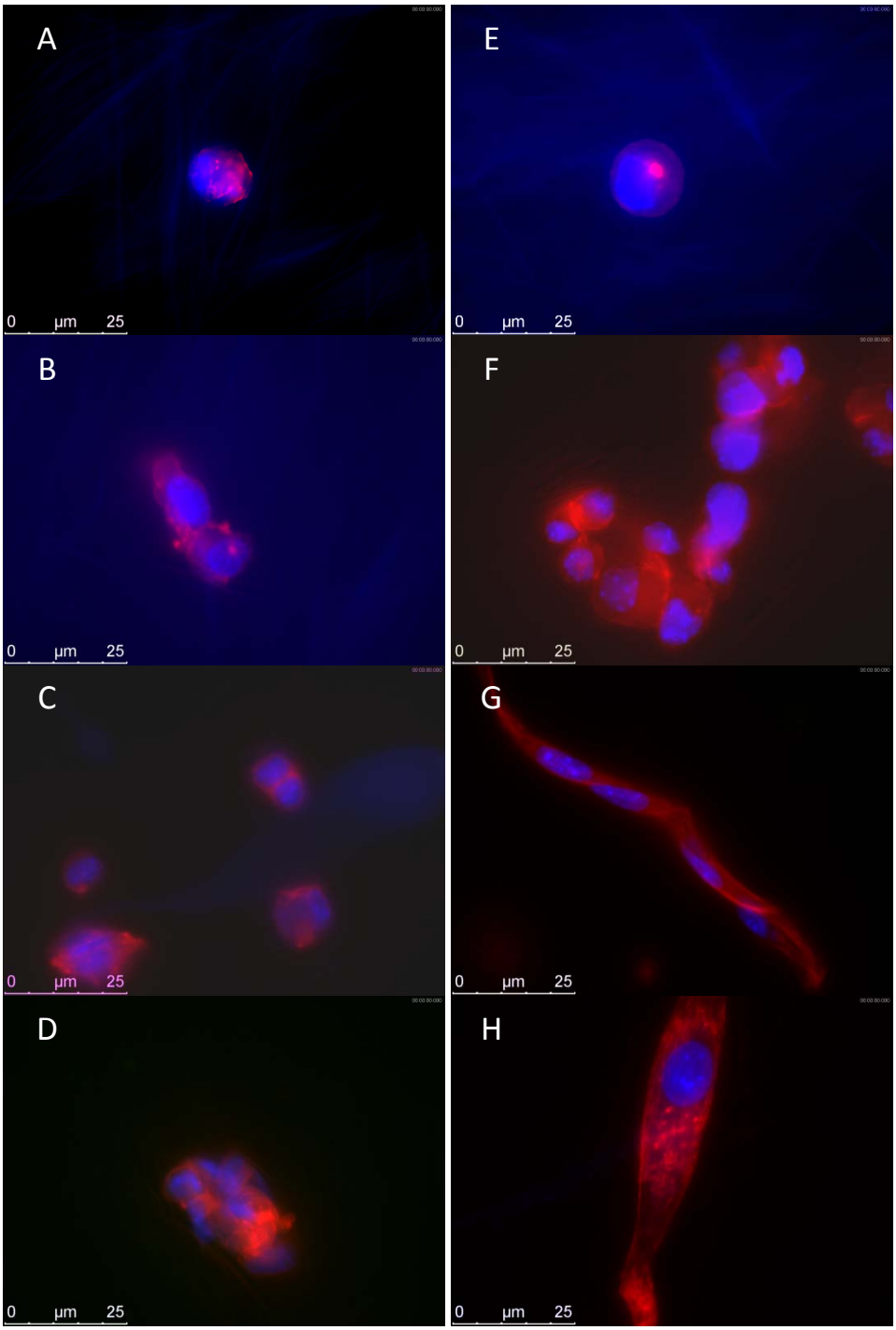

Figure 7. 8 C2C12 cells seeded on electrospun cellulose scaffolds, formed of aligned fibers, with their nucleus dyed with DAPI, and F-actin stained with rhodamine phalloidin. Cells on untreated scaffold cultured for: A) 3 hours, B) 1 day, C) 7 days, and D) 14days. Cells on THAMP modified and protein coated scaffolds cultured for: E) 3 hours, F) 1 day, G) 7 days, and H) 14 days.

This result is related to the larger surface area of aligned fibers (discussed on chapter 5). However, when the aligned fibers are not functionalized the adsorption of proteins is better on random native fibers, as suggested by C2C12 response. In chapter 4 this was envisaged that adsorption could be better on random fibers than aligned fibers although the surface area is greater on aligned fibers. The reason has to do with porosity of the scaffold; in the case of random fibers, porosity is greater. Porosity allows the infiltration of substances into the substrate and therefore creates a concentration gradient that overall increases the mass transport coefficient and finally enhances the adsorption process. Another aspect that may probably be involved on C2C12 scaffold interaction is the difference in mechanical properties among aligned and random fibers. It has been shown that myoblast differentiate optimally on substrates with tissue-like stiffness, Young's modulus of approximately 12 kPa [94]. Unmodified random cellulose fibers evaluated at physiological conditions presented elastic modulus value of 9.4 MPa and unmodified aligned fibers had a 32 fold increased stiffness, Chapter 5 Table 5.2. Nonetheless, the bulk mechanical properties are not what the cells experience on the microscopic and nano-scale levels, this information evidences that the stiffness of the scaffold was highly influenced by the arrangement of the fibers that agrees with the observed cell behavior towards fiber orientation. There was a significant difference in cell penetration between random and aligned fibrous scaffolds. By comparing images 7.7 B&F and 7.8 B&F, it can be observed that random oriented fibrous scaffolds exhibited cells at different depth of the scaffold (in different focal points), while aligned fibrous scaffolds only displayed cells on the surface. This change in penetration is also a consequence of reduced porosity in aligned fibrous scaffolds because of better packing of fibers. The infiltration of the cells can be improved by creation of porosity by laser ablation as suggested by different authors and proved to be a feasible technique for cellulose membranes in the present work (chapter 4). In contrast to the neural cell study, THAMP and cell culture media modification did not seem to be as homogeneous with the muscle cells. Since, cultures on these scaffolds presented good proliferation and formation of myotubes only in some areas. Nonetheless, untreated and modified random fibers and modified aligned fibers promoted the formation of myotubes. These results encourage more experiments to determine an optimal cell seeding density for electrospun cellulose scaffolds. An MTT or MTS assay to evaluate cell proliferation needs to be carried out to complement fluorescence microscope analysis for these muscle cells. Finally, microporosity of aligned fibrous scaffolds should be created to enhance cell infiltration.

Chapter 8. Summarized Results and Conclusions

The overall goal of this research project was to develop methods to produce electrospun cellulose nanofibers that can be used as substrate for cell growth and tissue regeneration. Towards this goal, five complementary tasks were performed: (1) fabrication of nanocellulose scaffolds by electrospinning technique (Chapter 3), (2) engineering scaffolding properties (Chapter 4), (3) evaluating physical, chemical, and mechanical properties (Chapter 5), (4) introducing bioactive molecules by means of surface modification to stimulate cell adhesion and proliferation (Chapter 6), and (5) evaluating the cytotoxicity, adhesion, and proliferation responses of mammalian cells to the designed materials (Chapter 7).

8.1 Summary

In the scaffold fabrication section (Chapters 3), it was determined that the electrospinning of cellulose acetate (CA) solution 17% (w/w) in acetone/DMAc (2:1, w/w) produced fibers with an average fiber size in the submicron range and the lowest size distribution among the solvents tested. The solution flow rate had a power law relationship of 0.26 with the CA fiber size. Solvent composition and flow rate also impacted the stability of the network structure of the electrospun fibers. Only acetone/DMAc at solution flow rates equal or higher than 1 mL/h produced fibrous membranes that were able to preserve their original network structure after deacetylation treatment. A range of scaffolding architectures were achieved in the electrospun cellulose membranes (Chapter 4). Uniaxial fiber orientation was produced by electrospinning CA solution on the edge of a wheel rotating a liner velocity of 21m/s. The aligned fibers produced in this fashion had 20% lower average fiber size and lower size distribution that the random oriented fibers. Pores with circular regular shape and 300 microns of diameter were fabricated in electrospun CA membranes by the laser ablation technique. FTIR analysis demonstrated that the porous membranes did not exhibit chemical degradation due to the laser irradiation. Hierarchical structures were produced by electrospinning nanoscale fibers onto lyocell microfibers. Aligned and random oriented nanofibers were also obtained in this architecture. The nano fiber coated lyocell microfiber constructs preserved their scale-integrated structure after deacetylation treatment.

The characterization of the electrospun membranes (Chapter 5) reveled that CA deacetylation can be carried out by NaOH ethanol solution with minimal degradation of the cellulose while retaining the original fiber structure of the electrospun mat. The morphology of the partially regenerated cellulose revealed only a broad diffraction peak for the scaffold material. The fully regenerated cellulose showed characteristic cellulose II diffraction pattern. Thermogravimetric analysis demonstrated that there was no detectable residual DMAc solvent after regeneration post treatment of the electrospun membranes, encouraging their use as biomaterial. Electrospun regenerated cellulose fibrous, aligned and random, membranes exhibited low water contact angles that classified them as hydrophilic surfaces. According to the nitrogen adsorption-desorption isotherms the electrospun membranes, of both random and aligned fibers, were considered macroporous adsorbents with pore size not less than 50 nm. The measurements shown higher surface area and reduced porosity in aligned in contrast to random oriented electrospun fibers. The tensile properties of aligned fibers were enhanced to those observed in the random oriented fibers, while random fibers were more ductile.

In the section concerning to bioactive surface modifications of the scaffolds (Chapter 6), a qualitative dye probe indicated that the fibers were readily modified with anionic groups through the physically adsorption of carboxymethylcellulose (CMC) in the presence of $CaCl_2$. Conductometric titration measurements confirmed the increase of carboxylic groups due to the CMC adsorption process. Hydroxyapatite (HA) like minerals were formed on the electrospun cellulose scaffolds for all the $CaCl_2$ treated samples. The samples were able to nucleate crystal growth by the process of pretreating the scaffolds by heating in aqueous alkali in the presence of $CaCl_2$. Biomimetic coating of Ca-P crystals on electrospun fibers was significantly enhanced by the carboxyl groups added by the modification process with CMC. CMC adsorption on the scaffolds created equal opportunity for mineralization on either the 45 min or 24 h regenerated scaffold. Since the surface is the only area of the material in contact with physiological environment, this finding implicates the process of controlling the CMC adsorption and calcium loading to the substrate material for the creation of mineralized scaffolds. This enhanced Ca-P mineralization on cellulose scaffolds can be accomplished by either increasing the negative charge (COO^-) or aqueous heating treatment in the presence of Ca ions. PBS treatment produced a more homogeneous Ca-P coating than SBF treatment. In the PBS treatment, Ca-P minerals coated the electrospun cellulose fibers exhibiting a flake-like structure in both porous (laser ablated) and non-porous membranes. In the porous membrane the Ca-P crystals were created on the fibers and also

within the pores wall. The Ca/P ratio in the inner pore surface was closer to the hydroxyapatite crystals value. For other surface modification treatments involving adsorption of a modified xyloglucan, XPS analysis was not sensitive enough to detect the presence of nitrogen due to the adsorption of xyloglucan modified with the RGD amino acid sequence (XG-RGD). However, XPS was useful to show chemical derivatization of the scaffolds to form a cationic cellulose surface; the presence of nitrogen and the relative increase in aliphatic carbons measured by XPS confirmed the formation of trimethyl ammonium betahydroxy propyl (THAMP) cellulose. Adsorption of culture media proteins after THAMP modification was verified by the increase in nitrogen content and the relative increase in aliphatic carbons registered by XPS. Those values suggested that the adsorption of proteins in THAMP modified samples was greater in aligned than in random oriented electrospun cellulose fibers. The presence of sulfur, attributed to the disulfide bonds of laminin, quantified by XPS suggested the adsorption of laminin on untreated and THAMP modified random electrospun cellulose fibers. CMC, XG-RGD, and THAMP modifications did not affect the fiber surface structure or cause any bulk modification as indicated by SEM analysis.

In the cell-material interaction task (Chapter 7) the *in vitro* cytotoxicity evaluation confirmed that there are no extractable or leachable substances presented in regenerated electrospun cellulose fibers at levels that can be harmful or pose any adverse effect on mammalian cells. A combination of porosity and surface chemistry, through Ca-P mineralization, enhanced osteoprogenitor cell adhesion within the electrospun cellulose scaffolds, as revealed by cell size and cell density measurements. SEM analysis and MTS assay confirmed that THAMP modification resulted in the most promising surface modification to enhance neural-like cell (PC12) attachment and proliferation. The PC12 cell study through the MTS assay confirmed the adsorption of RGD-XG onto electrospun random cellulose scaffolds. Differentiation of myoblast cells (C2C12) to myotubes on electrospun cellulose scaffolds was a function of surface chemistry, fiber orientation and mechanical properties.

8.2 Conclusions

Through the tasks performed in this research work, it was shown that it was advantageous to use cellulose acetate as a starting material because of the enhanced solubility over cellulose in typical electrospinning solvents. CA solubility in dimethylacetamide/acetone allowed for the controlled size of the fibers by electrospinning, while maintaining the scaffold integrity during regeneration. Moreover, the T_m of CA facilitated the fabrication of porosity by laser ablation. Computer assisted design (CAD) together with direct writing laser permitted controlled micro-ablation on the scaffolds with minimal melting of the bulk of the scaffold. The integration of electrospun fibers on microscale textile fibers through the electrospinning of CA fibers onto Lyocel, opened the possibility of creating hierarchical structures that resemble those of natural tissues, for instance muscle architecture. Control of size, orientation, and architecture of fibers together with size, shape, and quantity of pores in electrospun scaffolds will help to enable *in vitro* preparation with structure and function that mimics biological tissues. Within the cellulosic family, bacterial cellulose, microfribillated nanocellulose, regenerated cellulose sponges, and Lyocell do not offer all the possibilities of design architectures observed in electrospun nanocellulose.

The variation of the degree of deacetylation of electrospun CA fibers suggested changes in crystallinity, which can be used to influence its mechanical properties and *in vivo* degradation profile. The conversion of electrospun fibers from CA to cellulose increased the number of hydroxyl groups implying: hydrophilic behavior, water swelling capability, biocompatibility, and increased chemical reactivity. The high content of hydroxyl groups together with the surface roughness conferred to electrospun regenerated cellulose a hydrophilic nature. This result may imply good blood compatibility in electrospun cellulose and therefore good *in vivo* biocompatibility as observed in bacterial cellulose without dissolution. This hydrophilic behavior gives advantages to electrospun cellulose next to synthetic polymers such as polystyrene, polyethylene, and polypropylene.

Cellulose is a neutral polysaccharide with no charged groups for molecular recognition, which confers biocompatibility but limits cells adhesion and migration. In this work, it was shown several approaches to make of cellulose a biologically recognizable substrate.

8.3 Future Work

Degree of crystallinity of the regenerated cellulose scaffolds should be determined. Regarding the tensile measurements, advanced imaging mechanical testing frames, and also the use of a better clamping technique to reduce the initial strain from the adjustment of the sample height. Biaxial tensile testing of the samples, due to its relevance in scaffold performance, is also suggested for future work. The adsorption of XG-RGD on electrospun cellulose scaffolds should be quantified with a technique more sensitive to nitrogen quantification such a carbon, nitrogen, sulfur (CNS) elemental analyzer. Laminin adsorption can also be quantified by CNS analyzer. Laminin and XG-RGD distribution on the electrospun cellulose surface can be determined by immunochemistry. A study in the presence of magnesium or calcium ions should be performed in the laminin and THAMP laminin treated cellulose scaffolds to clarify the cause of laminin coating failure.

Experiments with longer incubation time towards PC12 cell differentiation need to be carried out. The use of the nano fiber coated lyocell microfiber constructs with aligned and random fibers is highly recommended for neural and myoblast cell grow. In the osteoprogenitor cell study, a cell proliferation assay is necessary to clarify the importance of addition of microporosity on osteoprogetinor cells adhesion and proliferation. Scaffolds with larger thickness and micropores are also suggested to evaluate cell infiltration. The thickness of the scaffolds can be increased by assembling several layers of electrospun CA membranes by polymer sintering or hot pressing. In the myoblast cell study, the results encouraged to carry out more experiments to determine an optimal cell seeding density for electrospun cellulose scaffolds. An MTT or MTS assay to evaluate myoblast cells proliferation needs to be carried out to complement fluorescence microscope analysis. Finally, microporosity of aligned fibrous scaffolds should be created to enhance cell infiltration. The *in vivo* biocompatibility evaluation of electrospun cellulose fibers is highly recommended together with a biodegradation study. Since cellulases are not naturally presented in the human body, it would be interesting to perform an animal study to evaluate cellulose migration.

References

1. Lannutti, J., et al., *Electrospinning for tissue engineering scaffolds.* Materials Science and Engineering: C, 2007. **27**(3): p. 504-509.
2. Lee, K.Y., et al., *Electrospinning of polysaccharides for regenerative medicine.* Advanced Drug Delivery Reviews, 2009. **61**(12): p. 1020-1032.
3. Sill, T.J. and H.A. von Recum, *Electrospinning: Applications in drug delivery and tissue engineering.* Biomaterials, 2008. **29**(13): p. 1989-2006.
4. Lutolf, M.P. and J.A. Hubbell, *Synthetic biomaterials as instructive extracellular microenvironments for morphogenesis in tissue engineering.* Nat Biotech, 2005. **23**(1): p. 47-55.
5. Seal, B.L., T.C. Otero, and A. Panitch, *Polymeric biomaterials for tissue and organ regeneration.* Materials Science and Engineering: R: Reports, 2001. **34**(4-5): p. 147-230.
6. Liu, H. and Y.-L. Hsieh, *Ultrafine fibrous cellulose membranes from electrospinning of cellulose acetate.* Journal of Polymer Science Part B: Polymer Physics, 2002. **40**(18): p. 2119-2129.
7. Tungprapa, S., et al., *Electrospun cellulose acetate fibers: effect of solvent system on morphology and fiber diameter.* Cellulose, 2007. **14**(6): p. 563-575.
8. Shukla, S., et al., *Electrospinning of hydroxypropyl cellulose fibers and their application in synthesis of nano and submicron tin oxide fibers.* Polymer, 2005. **46**(26): p. 12130-12145.
9. Entcheva, E., et al., *Functional cardiac cell constructs on cellulose-based scaffolding.* Biomaterials, 2004. **25**(26): p. 5753-5762.
10. Pajulo, O., et al., *Viscose cellulose sponge as an implantable matrix: Changes in the structure increase the production of granulation tissue.* Journal of Biomedical Materials Research, 1996. **32**(3): p. 439-446.
11. Märtson, M., et al., *Is cellulose sponge degradable or stable as implantation material? An in vivo subcutaneous study in the rat.* Biomaterials, 1999. **20**(21): p. 1989-1995.
12. Klemm, D., et al., *Bacterial synthesized cellulose -- artificial blood vessels for microsurgery.* Progress in Polymer Science, 2001. **26**(9): p. 1561-1603.
13. Zimmermann, K.A., et al., *Biomimetic design of a bacterial cellulose/hydroxyapatite nanocomposite for bone healing applications.* Materials Science and Engineering: C. **In Press, Corrected Proof**.
14. Svensson, A., et al., *Bacterial cellulose as a potential scaffold for tissue engineering of cartilage.* Biomaterials, 2005. **26**(4): p. 419-431.
15. Grande, C.J., et al., *Nanocomposites of bacterial cellulose/hydroxyapatite for biomedical applications.* Acta Biomaterialia, 2009. **5**(5): p. 1605-1615.
16. Wan, Y.Z., et al., *Biomimetic synthesis of hydroxyapatite/bacterial cellulose nanocomposites for biomedical applications.* Materials Science and Engineering: C, 2007. **27**(4): p. 855-864.
17. Bäckdahl, H., et al., *Mechanical properties of bacterial cellulose and interactions with smooth muscle cells.* Biomaterials, 2006. **27**(9): p. 2141-2149.
18. Andrade, F.k., et al., *Improving bacterial cellulose for blood vessel replacement: functionalization with a chimeric protein containing a cellulose-binding module and an adhesion peptide.* Acta Biomaterialia. **In Press, Accepted Manuscript**.
19. Rhee, S.-H. and J. Tanaka, *Hydroxyapatite formation on cellulose cloth induced by citric acid.* Journal of Materials Science: Materials in Medicine, 2000. **11**(7): p. 449-452.
20. Hofmann, I., et al., *Calcium phosphate nucleation on cellulose fabrics.* Surface and Coatings Technology, 2006. **201**(6): p. 2392-2398.

21. Ponader, S., et al., *In vitro response of hFOB cells to pamidronate modified sodium silicate coated cellulose scaffolds.* Colloids and Surfaces B: Biointerfaces, 2008. **64**(2): p. 275-283.
22. Liu, C., Z. Xia, and J.T. Czernuszka, *Design and Development of Three-Dimensional Scaffolds for Tissue Engineering.* Chemical Engineering Research and Design, 2007. **85**(7): p. 1051-1064.
23. Williams, D.F. and S.P. Zhong, *Biodeterioration/biodegradation of polymeric medical devices in situ.* International Biodeterioration & Biodegradation, 1994. **34**(2): p. 95-130.
24. Ramakrishna, S., et al., *Biomedical applications of polymer-composite materials: a review.* Composites Science and Technology, 2001. **61**(9): p. 1189-1224.
25. Temenoff, J.S. and A.G. Mikos, *Biomaterials : the Intersection of biology and materials science*. 2008, Upper Saddle River, N.J.: Pearson/Prentice Hall.
26. Ma, Z., Z. Mao, and C. Gao, *Surface modification and property analysis of biomedical polymers used for tissue engineering.* Colloids and Surfaces B: Biointerfaces, 2007. **60**(2): p. 137-157.
27. Bodin, A., et al., *Modification of Nanocellulose with a Xyloglucan–RGD Conjugate Enhances Adhesion and Proliferation of Endothelial Cells: Implications for Tissue Engineering.* Biomacromolecules, 2007. **8**(12): p. 3697-3704.
28. Gilbert, M., et al., *Chimeric Peptides of Statherin and Osteopontin That Bind Hydroxyapatite and Mediate Cell Adhesion.* Journal of Biological Chemistry, 2000. **275**(21): p. 16213-16218.
29. Cüneyt Tas, A., *Synthesis of biomimetic Ca-hydroxyapatite powders at 37°C in synthetic body fluids.* Biomaterials, 2000. **21**(14): p. 1429-1438.
30. Yang, F., et al., *Fabrication of nano-structured porous PLLA scaffold intended for nerve tissue engineering.* Biomaterials, 2004. **25**(10): p. 1891-1900.
31. Smith, I.O., et al., *Nanostructured polymer scaffolds for tissue engineering and regenerative medicine.* Wiley Interdisciplinary Reviews: Nanomedicine and Nanobiotechnology, 2009. **1**(2): p. 226-236.
32. Liang, D., B.S. Hsiao, and B. Chu, *Functional electrospun nanofibrous scaffolds for biomedical applications.* Advanced Drug Delivery Reviews, 2007. **59**(14): p. 1392-1412.
33. Riboldi, S.A., et al., *Electrospun degradable polyesterurethane membranes: potential scaffolds for skeletal muscle tissue engineering.* Biomaterials, 2005. **26**(22): p. 4606-4615.
34. Kim, C.-W., et al., *Structural studies of electrospun cellulose nanofibers.* Polymer, 2006. **47**(14): p. 5097-5107.
35. Thompson, C.J., et al., *Effects of parameters on nanofiber diameter determined from electrospinning model.* Polymer, 2007. **48**(23): p. 6913-6922.
36. Munir, M.M., et al., *Scaling law on particle-to-fiber formation during electrospinning.* Polymer, 2009. **50**(20): p. 4935-4943.
37. Li, D. and Y. Xia, *Electrospinning of Nanofibers: Reinventing the Wheel?* Advanced Materials, 2004. **16**(14): p. 1151-1170.
38. Li, D., Y. Wang, and Y. Xia, *Electrospinning of Polymeric and Ceramic Nanofibers as Uniaxially Aligned Arrays.* Nano Letters, 2003. **3**(8): p. 1167-1171.
39. Xu, C.Y., et al., *Aligned biodegradable nanofibrous structure: a potential scaffold for blood vessel engineering.* Biomaterials, 2004. **25**(5): p. 877-886.
40. Helenius, G., et al., *In vivo biocompatibility of bacterial cellulose.* Journal of Biomedical Materials Research Part A, 2006. **76A**(2): p. 431-438.
41. Klemm, D., et al., *Cellulose: Fascinating Biopolymer and Sustainable Raw Material.* Angewandte Chemie International Edition, 2005. **44**(22): p. 3358-3393.
42. Müller, F.A., et al., *Cellulose-based scaffold materials for cartilage tissue engineering.* Biomaterials, 2006. **27**(21): p. 3955-3963.

43. Ma, Z. and S. Ramakrishna, *Electrospun regenerated cellulose nanofiber affinity membrane functionalized with protein A/G for IgG purification.* Journal of Membrane Science, 2008. **319**(1-2): p. 23-28.
44. Laurence, S., et al., *Development of a resorbable macroporous cellulosic material used as hemostatic in an osseous environment.* Journal of Biomedical Materials Research Part A, 2005. **73A**(4): p. 422-429.
45. Fundueanu, G., et al., *Cellulose acetate butyrate microcapsules containing dextran ion-exchange resins as self-propelled drug release system.* Biomaterials, 2005. **26**(20): p. 4337-4347.
46. Fricain, J.C., et al., *Cellulose phosphates as biomaterials. In vivo biocompatibility studies.* Biomaterials, 2002. **23**(4): p. 971-980.
47. Kino, Y., et al., *Multiporous Cellulose Microcarrier for the Development of a Hybrid Artificial Liver Using Isolated Hepatocytes.* Journal of Surgical Research, 1998. **79**(1): p. 71-76.
48. *Hepatocyte culture on cellulose flat membranes.* Journal of Hepatology, 1988. **7**(Supplement 1): p. S135-S135.
49. Maneerung, T., S. Tokura, and R. Rujiravanit, *Impregnation of silver nanoparticles into bacterial cellulose for antimicrobial wound dressing.* Carbohydrate Polymers, 2008. **72**(1): p. 43-51.
50. Czaja, W., et al., *Microbial cellulose--the natural power to heal wounds.* Biomaterials, 2006. **27**(2): p. 145-151.
51. Märtson, M., et al., *Biocompatibility of Cellulose Sponge with Bone.* European Surgical Research, 1998. **30**(6): p. 426-432.
52. Miyamoto, T., et al., *Tissue biocompatibility of cellulose and its derivatives.* Journal of Biomedical Materials Research, 1989. **23**(1): p. 125-133.
53. Kim, J., Z. Cai, and Y. Chen, *Biocompatible Bacterial Cellulose Composites for Biomedical Application.* Journal of Nanotechnology in Engineering and Medicine, 2010. **1**(1): p. 011006.
54. Hoenich, N.A., et al., *Biocompatibility of membranes used in the treatment of renal failure.* Biomaterials, 1995. **16**(8): p. 587-592.
55. Singh, M., A.R. Ray, and P. Vasudevan, *Biodegradation studies on periodate oxidized cellulose.* Biomaterials, 1982. **3**(1): p. 16-20.
56. Dan Dimitrijevich, S., et al., *Biodegradation of oxidized regenerated cellulose.* Carbohydrate Research, 1990. **195**(2): p. 247-256.
57. Zaborowska, M., et al., *Microporous bacterial cellulose as a potential scaffold for bone regeneration.* Acta Biomaterialia, 2010. **6**(7): p. 2540-2547.
58. Watanabe, K., et al., *A new bacterial cellulose substrate for mammalian cell culture.* Cytotechnology, 1993. **13**(2): p. 107-114.
59. Zimmermann, K.A., et al., *Biomimetic design of a bacterial cellulose/hydroxyapatite nanocomposite for bone healing applications.* Materials Science and Engineering: C, 2011. **31**(1): p. 43-49.
60. Janne Laine, T.L., Gunborg Glad Nordmark and Gunnel Risinger, *Studies on topochemical modification of cellulosic fibres. Part 1. Chemical conditions for the attachment of carboxymethyl cellulose onto fibres.* Nordic Pulp and Paper research 2000. **15**(5): p. 520-526.
61. Fras-Zemljič, L., et al., *The effect of adsorbed carboxymethyl cellulose on the cotton fibre adsorption capacity for surfactant.* Cellulose, 2006. **13**(6): p. 655-663.
62. Thorvaldsson, A., et al., *Electrospinning of highly porous scaffolds for cartilage regeneration.* Biomacromolecules, 2008. **9**(3): p. 1044-9.
63. Katz, S., R.P. Beatson, and A.M. Scallan, *The determination of strong and week acidic groups in sulphite pulps.* Svensk Papperstidn, 1984. **87**: p. 48-53.
64. Andrady, A.L., *Factors Affecting Nanofiber Quality*, in *Science and Technology of Polymer Nanofibers*. 2007, John Wiley & Sons, Inc. p. 81-110.

65. Fong, H., I. Chun, and D.H. Reneker, *Beaded nanofibers formed during electrospinning.* Polymer, 1999. **40**(16): p. 4585-4592.
66. Huang, Z.-M., et al., *A review on polymer nanofibers by electrospinning and their applications in nanocomposites.* Composites Science and Technology, 2003. **63**(15): p. 2223-2253.
67. Veleirinho, B., M.F. Rei, and J.A. Lopes-Da-Silva, *Solvent and concentration effects on the properties of electrospun poly(ethylene terephthalate) nanofiber mats.* Journal of Polymer Science Part B: Polymer Physics, 2008. **46**(5): p. 460-471.
68. Han, S.O., et al., *Electrospinning of cellulose acetate nanofibers using a mixed solvent of acetic acid/water: Effects of solvent composition on the fiber diameter.* Materials Letters, 2008. **62**(4-5): p. 759-762.
69. Liu, H. and C. Tang, *Electrospinning of Cellulose Acetate in Solvent Mixture N,N-Dimethylacetamide (DMAc)/Acetone.* Polym. J, 2006. **39**(1): p. 65-72.
70. Son, W.K., et al., *Electrospinning of ultrafine cellulose acetate fibers: Studies of a new solvent system and deacetylation of ultrafine cellulose acetate fibers.* Journal of Polymer Science Part B: Polymer Physics, 2004. **42**(1): p. 5-11.
71. Han, D. and P.-I. Gouma, *Electrospun bioscaffolds that mimic the topology of extracellular matrix.* Nanomedicine: Nanotechnology, Biology and Medicine, 2006. **2**(1): p. 37-41.
72. Koombhongse, S., W. Liu, and D.H. Reneker, *Flat polymer ribbons and other shapes by electrospinning.* Journal of Polymer Science Part B: Polymer Physics, 2001. **39**(21): p. 2598-2606.
73. Han, S.O., et al., *Ultrafine porous fibers electrospun from cellulose triacetate.* Materials Letters, 2005. **59**(24-25): p. 2998-3001.
74. Baji, A., et al., *Electrospinning of polymer nanofibers: Effects on oriented morphology, structures and tensile properties.* Composites Science and Technology, 2010. **70**(5): p. 703-718.
75. Ma, Z., M. Kotaki, and S. Ramakrishna, *Electrospun cellulose nanofiber as affinity membrane.* Journal of Membrane Science, 2005. **265**(1-2): p. 115-123.
76. Li, W.-J., et al., *Electrospun nanofibrous structure: A novel scaffold for tissue engineering.* Journal of Biomedical Materials Research, 2002. **60**(4): p. 613-621.
77. Stevens, M.M. and J.H. George, *Exploring and Engineering the Cell Surface Interface.* Science, 2005. **310**(5751): p. 1135-1138.
78. McCullen, S.D., et al., *In Situ Collagen Polymerization of Layered Cell-Seeded Electrospun Scaffolds for Bone Tissue Engineering Applications.* Tissue Engineering Part C: Methods, 2010. **16**(5): p. 1095-1105.
79. Lim, Y.C., et al., *Micropatterning and characterization of electrospun poly(ε-caprolactone)/gelatin nanofiber tissue scaffolds by femtosecond laser ablation for tissue engineering applications.* Biotechnology and Bioengineering, 2011. **108**(1): p. 116-126.
80. Rebollar, E., et al., *Improvement of electrospun polymer fiber meshes pore size by femtosecond laser irradiation.* Applied Surface Science, 2011. **257**(9): p. 4091-4095.
81. Courtney, T., et al., *Design and analysis of tissue engineering scaffolds that mimic soft tissue mechanical anisotropy.* Biomaterials, 2006. **27**(19): p. 3631-3638.
82. Thorvaldsson, A., et al., *Controlling the Architecture of Nanofiber-Coated Microfibers Using Electrospinning.* Journal of Applied Polymer Science, 2010. **118**(1): p. 511-517.
83. Yao, L., et al., *Orienting neurite growth in electrospun fibrous neural conduits.* Journal of Biomedical Materials Research Part B: Applied Biomaterials, 2009. **90B**(2): p. 483-491.
84. Klumpp, D., et al., *Engineering skeletal muscle tissue – new perspectives in vitro and in vivo.* Journal of Cellular and Molecular Medicine, 2010. **14**(11): p. 2622-2629.
85. Karande, T.S., J.L. Ong, and C.M. Agrawal, *Diffusion in Musculoskeletal Tissue Engineering Scaffolds: Design Issues Related to Porosity, Permeability, Architecture, and Nutrient Mixing.* Annals of Biomedical Engineering, 2004. **32**(12): p. 1728-1743.

86. McCullen, S.D., C.M. Haslauer, and E.G. Loboa, *Fiber-reinforced scaffolds for tissue engineering and regenerative medicine: use of traditional textile substrates to nanofibrous arrays.* Journal of Materials Chemistry, 2010. **20**(40): p. 8776-8788.
87. Carrillo, F., et al., *Structural FTIR analysis and thermal characterisation of lyocell and viscose-type fibres.* European Polymer Journal, 2004. **40**(9): p. 2229-2234.
88. Pertile, R.A.N., et al., *Surface modification of bacterial cellulose by nitrogen-containing plasma for improved interaction with cells.* Carbohydrate Polymers, 2010. **82**(3): p. 692-698.
89. Wang, Y.-X., et al., *Effects of the Chemical Structure and the Surface Properties of Polymeric Biomaterials on Their Biocompatibility.* Pharmaceutical Research, 2004. **21**(8): p. 1362-1373.
90. De Bartolo, L., et al., *Evaluation of cell behaviour related to physico-chemical properties of polymeric membranes to be used in bioartificial organs.* Biomaterials, 2002. **23**(12): p. 2485-2497.
91. Parak, W.J., et al., *Effects of semiconductor substrate and glia-free culture on the development of voltage-dependent currents in rat striatal neurones.* European Biophysics Journal, 2001. **29**(8): p. 607-620.
92. Yasuda, T., T. Okuno, and H. Yasuda, *Contact Angle of Water on Polymer Surfaces.* Langmuir, 1994. **10**(7): p. 2435-2439.
93. Agrawal, C.M. and R.B. Ray, *Biodegradable polymeric scaffolds for musculoskeletal tissue engineering.* Journal of Biomedical Materials Research, 2001. **55**(2): p. 141-150.
94. Engler, A.J., et al., *Myotubes differentiate optimally on substrates with tissue-like stiffness.* The Journal of Cell Biology, 2004. **166**(6): p. 877-887.
95. Paszek, M.J., et al., *Tensional homeostasis and the malignant phenotype.* Cancer Cell, 2005. **8**(3): p. 241-254.
96. Wells, R.G., *The Role of Matrix Stiffness in Hepatic Stellate Cell Activation and Liver Fibrosis.* Journal of Clinical Gastroenterology, 2005. **39**(4): p. S158-S161.
97. Flanagan, L.A., et al., *Neurite branching on deformable substrates.* NeuroReport, 2002. **13**(18): p. 2411-2415.
98. Discher, D.E., P. Janmey, and Y.-l. Wang, *Tissue Cells Feel and Respond to the Stiffness of Their Substrate.* Science, 2005. **310**(5751): p. 1139-1143.
99. Knill, C.J. and J.F. Kennedy, *Degradation of cellulose under alkaline conditions.* Carbohydrate Polymers, 2003. **51**(3): p. 281-300.
100. Fras, L., et al., *Analysis of the oxidation of cellulose fibres by titration and XPS.* Colloids and Surfaces A: Physicochemical and Engineering Aspects, 2005. **260**(1-3): p. 101-108.
101. Johansson, L.-S., et al., *Evaluation of surface lignin on cellulose fibers with XPS.* Applied Surface Science, 1999. **144-145**: p. 92-95.
102. Fink, H.P., D. Hofmann, and B. Philipp, *Some aspects of lateral chain order in cellulosics from X-ray scattering.* Cellulose, 1995. **2**(1): p. 51-70.
103. Morgado, D.L. and E. Frollini, *Thermal decomposition of mercerized linter cellulose and its acetates obtained from a homogeneous reaction.* Polímeros, 2011. **21**: p. 111-117.
104. Huang, M.-R. and X.-G. Li, *Thermal degradation of cellulose and cellulose esters.* Journal of Applied Polymer Science, 1998. **68**(2): p. 293-304.
105. Flaqué, C. and S. Montserrat, *Thermal degradation of celluloses and their vinylic copolymers by thermogravimetric analysis.* Journal of Applied Polymer Science, 1999. **74**(1): p. 201-209.
106. Bhushan, B., M. Nosonovsky, and Y. Chae Jung, *Towards optimization of patterned superhydrophobic surfaces.* Journal of The Royal Society Interface, 2007. **4**(15): p. 643-648.
107. Wenzel, R.N., *RESISTANCE OF SOLID SURFACES TO WETTING BY WATER.* Industrial & Engineering Chemistry, 1936. **28**(8): p. 988-994.

108. Białopiotrowicz, T. and B. Jańczuk, *The wettability of a cellulose acetate membrane in the presence of bovine serum albumin.* Applied Surface Science, 2002. **201**(1-4): p. 146-153.
109. Zhu, X., et al., *Electrospun Fibrous Mats with High Porosity as Potential Scaffolds for Skin Tissue Engineering.* Biomacromolecules, 2008. **9**(7): p. 1795-1801.
110. Charles A, B., *8 - Substrates and Surface Quality*, in *Vacuum Deposition onto Webs, Films and Foils (Second Edition)*. 2011, William Andrew Publishing: Oxford. p. 135-175.
111. Liukkonen, A., *Contact angle of water on paper components: Sessile drops versus environmental scanning electron microscope measurements.* Scanning, 1997. **19**(6): p. 411-415.
112. Maretschek, S., A. Greiner, and T. Kissel, *Electrospun biodegradable nanofiber nonwovens for controlled release of proteins.* Journal of Controlled Release, 2008. **127**(2): p. 180-187.
113. Lu, P. and Y.-L. Hsieh, *Multiwalled Carbon Nanotube (MWCNT) Reinforced Cellulose Fibers by Electrospinning.* ACS Applied Materials & Interfaces, 2010. **2**(8): p. 2413-2420.
114. Rouquerol, J., et al., *Recommendations for the Characterization of Porous Solids.* Pure & Appl. Chem., 1994. **66**(8): p. 1739-1758.
115. Stylianopoulos, T., et al., *Computational predictions of the tensile properties of electrospun fibre meshes: Effect of fibre diameter and fibre orientation.* Journal of the Mechanical Behavior of Biomedical Materials, 2008. **1**(4): p. 326-335.
116. Lee, C.H., et al., *Nanofiber alignment and direction of mechanical strain affect the ECM production of human ACL fibroblast.* Biomaterials, 2005. **26**(11): p. 1261-1270.
117. Zong, X., et al., *Control of structure, morphology and property in electrospun poly(glycolide-co-lactide) non-woven membranes via post-draw treatments.* Polymer, 2003. **44**(17): p. 4959-4967.
118. Zong, X., et al., *Structure and Morphology Changes during in Vitro Degradation of Electrospun Poly(glycolide-co-lactide) Nanofiber Membrane.* Biomacromolecules, 2003. **4**(2): p. 416-423.
119. Greene, L.A. and A.S. Tischler, *Establishment of a noradrenergic clonal line of rat adrenal pheochromocytoma cells which respond to nerve growth factor.* Proceedings of the National Academy of Sciences, 1976. **73**(7): p. 2424-2428.
120. Bechara, S.L., A. Judson, and K.C. Popat, *Template synthesized poly([var epsilon]-caprolactone) nanowire surfaces for neural tissue engineering.* Biomaterials, 2010. **31**(13): p. 3492-3501.
121. Slaughter, G.E., et al., *Improving Neuron-to-Electrode Surface Attachment via Alkanethiol Self-Assembly: An Alternating Current Impedance Study.* Langmuir, 2004. **20**(17): p. 7189-7200.
122. Roach, P., et al., *Surface strategies for control of neuronal cell adhesion: A review.* Surface Science Reports, 2010. **65**(6): p. 145-173.
123. Badylak, S., T. Gilbert, and J. Myers-Irvin, *The extracellular matrix as a biologic scaffold for tissue engineering*, in *Tissue Engineering*, B. Clemens van, et al., Editors. 2008, Academic Press: Burlington. p. 121-143.
124. Zhou, Q., et al., *Xyloglucan in cellulose modification.* Cellulose, 2007. **14**(6): p. 625-641.
125. Koh, H.S., et al., *Enhancement of neurite outgrowth using nano-structured scaffolds coupled with laminin.* Biomaterials, 2008. **29**(26): p. 3574-3582.
126. Zamora, P.O., et al., *Biological distribution of 99mTc-labeled YIGSR and IKVAV laminin peptides in rodents: 99mTc-IKVAV peptide localizes to the lung.* Biochimica et Biophysica Acta (BBA) - Molecular Basis of Disease, 1993. **1182**(2): p. 197-204.
127. Masuda, T., et al., *Laminin peptide YIGSR and its receptor regulate sensory axonal response to the chemoattractive guidance cue in the chick embryo.* Journal of Neuroscience Research, 2009. **87**(2): p. 353-359.
128. Nurcombe, V., *Laminin in neural development.* Pharmacology & Therapeutics, 1992. **56**(2): p. 247-264.

129. Biosciences, B., *BD Extracellular Matrix Proteins. Available from.* http://www.bdbiosciences.com/cellculture/ecm/features/matrigel.jsp.
130. Boonen, K.J.M., et al., *Interaction between electrical stimulation, protein coating and matrix elasticity: a complex effect on muscle fibre maturation.* Journal of Tissue Engineering and Regenerative Medicine, 2011. **5**(1): p. 60-68.
131. Hutchens, S.A., et al., *Biomimetic synthesis of calcium-deficient hydroxyapatite in a natural hydrogel.* Biomaterials, 2006. **27**(26): p. 4661-4670.
132. Mahamid, J., et al., *Mapping amorphous calcium phosphate transformation into crystalline mineral from the cell to the bone in zebrafish fin rays.* Proceedings of the National Academy of Sciences, 2010.
133. Glimcher, M.J., *Bone: Nature of the Calcium Phosphate Crystals and Cellular, Structural, and Physical Chemical Mechanisms in Their Formation.* Reviews in Mineralogy and Geochemistry, 2006. **64**(1): p. 223-282.
134. Posner, A.S. and F. Betts, *Synthetic amorphous calcium phosphate and its relation to bone mineral structure.* Accounts of Chemical Research, 1975. **8**(8): p. 273-281.
135. Okada, S., et al., *Adhesion of osteoblast-like cells on nanostructured hydroxyapatite.* Acta Biomaterialia, 2010. **6**(2): p. 591-597.
136. Supaphol, P., et al., *Effect of Degree of Acetylation on In Vitro Biocompatibility of Electrospun Cellulose Acetate-Based Fibrous Matrices.* Journal of the Science Faculty of Chiang Mai University. **Under review**
137. Phachamud, T. and M. Phiriyawirut, *In Vitro Cytotoxicity and Degradability Tests of Gallic Acid-loaded Cellulose Acetate Electrospun Fiber.* Research Journal of Pharmaceutical, Biological and Chemical Sciences, 2011. **2**(3): p. 85-98.
138. Suwantong, O., U. Ruktanonchai, and P. Supaphol, *In vitro biological evaluation of electrospun cellulose acetate fiber mats containing asiaticoside or curcumin.* Journal of Biomedical Materials Research Part A, 2010. **94A**(4): p. 1216-1225.
139. Torimitsu, K. and A. Kawana, *Selective growth of sensory nerve fibers on metal oxide pattern in culture.* Developmental Brain Research, 1990. **51**(1): p. 128-131.
140. Turner, D., L. Flier, and S. Carbonetto, *Identification of a cell-surface protein involved in PC12 cell- substratum adhesion and neurite outgrowth on laminin and collagen.* The Journal of Neuroscience, 1989. **9**(9): p. 3287-3296.
141. Soekarno, A., B. Lom, and P.E. Hockberger, *Pathfinding by Neuroblastoma Cells in Culture Is Directed by Preferential Adhesion to Positively Charged Surfaces.* NeuroImage, 1993. **1**(2): p. 129-144.
142. Healy, K.E., B. Lom, and P.E. Hockberger, *Spatial distribution of mammalian cells dictated by material surface chemistry.* Biotechnology and Bioengineering, 1994. **43**(8): p. 792-800.
143. Rajnicek, A.M., K.R. Robinson, and C.D. McCaig, *The Direction of Neurite Growth in a Weak DC Electric Field Depends on the Substratum: Contributions of Adhesivity and Net Surface Charge.* Developmental Biology, 1998. **203**(2): p. 412-423.
144. Schöttelndreier, H., G.W. Mayr, and A.H. Guse, *[beta]1-Integrins Mediate Ca2+-Signalling and T Cell Spreading via Divergent Pathways.* Cellular Signalling, 1999. **11**(8): p. 611-619.
145. Turner, D.C., L.A. Flier, and S. Carbonetto, *Magnesium-dependent attachment and neurite outgrowth by PC12 cells on collagen and laminin substrata.* Developmental Biology, 1987. **121**(2): p. 510-525.
146. Okamoto, K., et al., *Process of apoptosis induced by TNF-α in murine fibroblast Ltk-cells: Continuous observation with video enhanced contrast microscopy.* Apoptosis, 2002. **7**(1): p. 77-86.

Appendix A: Tensile Properties

In this section is presented the tensile properties of aligned and random oriented electrospun cellulose of: 1) samples dry at room temperature inside a hood, with 3.3% humidity as established by TGA (Chapter 5 section 5.3), and evaluated at 22 °C and 45 % RH, 2) samples wet in a water bath at 22 °C, and 3) samples evaluated at physiological conditions in a phosphate buffer saline (PBS) solution bath at 37 °C. This data is presented as obtained from the software of the tensile tester instrument and shows the values of all the samples that were tested. This information complements the results shown in Chapter 5, section 5.6.

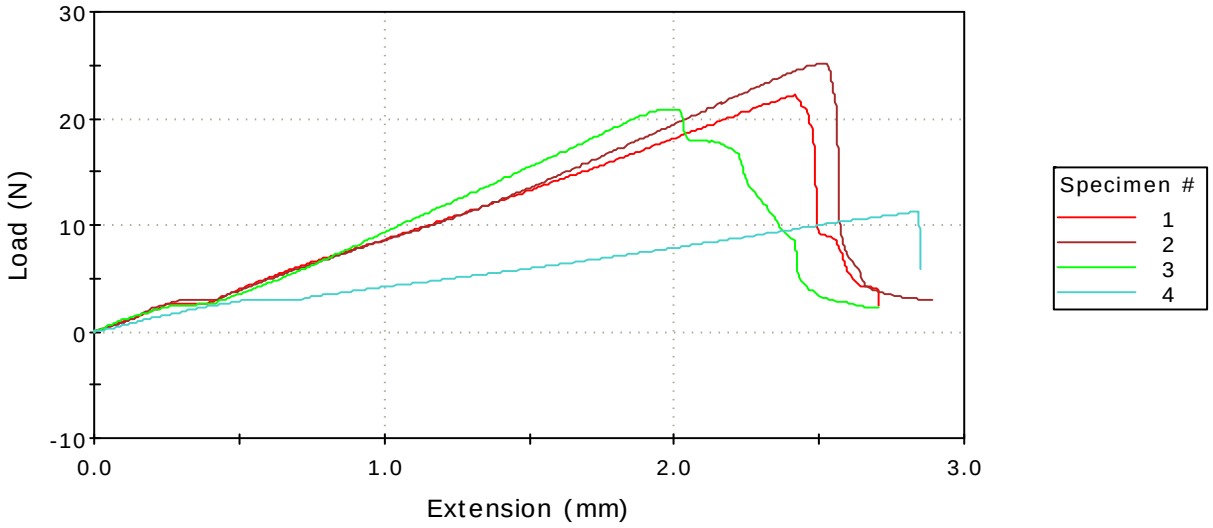

Figure A. 1 Load-extension curves of aligned electrospun fibrous mats at dry conditions.

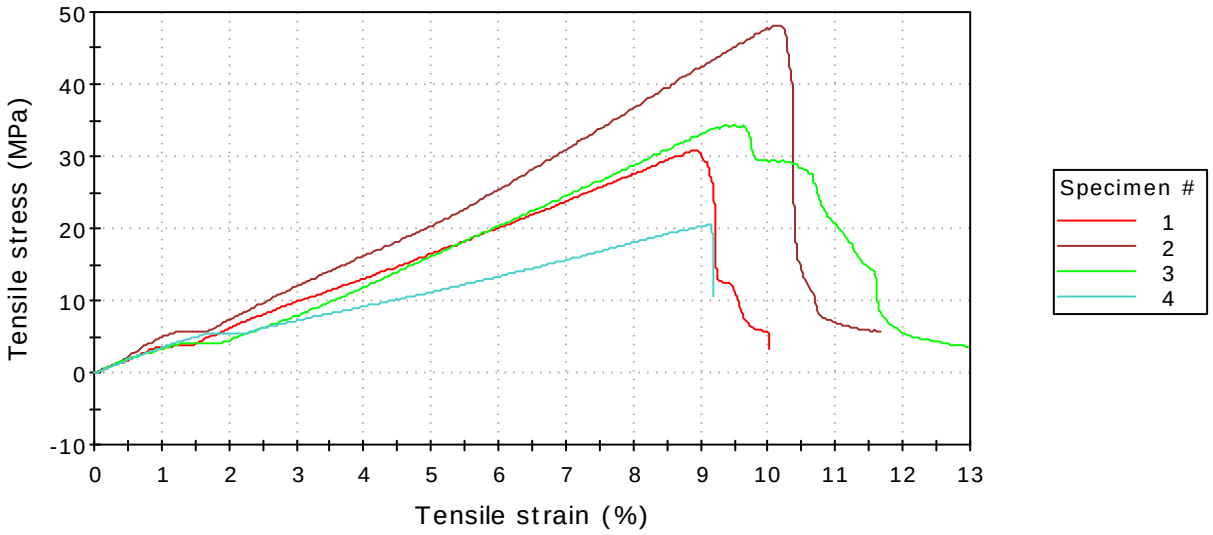

Figure A. 2 Stress-strain curves of aligned electrospun fibrous mats at dry conditions.

Table A.1 Dimensions of aligned electrospun fibrous meshes before evaluation at dry conditions.

	Length (mm)	Thickness (mm)	Width (mm)
1	27,00000	0,03630	19,76000
2	24,72000	0,02600	20,14000
3	20,85000	0,03070	19,85000
4	31,00000	0,03770	14,53000
Mean	25,89250	0,03267	18,57000
Standard Deviation	4,24714	0,00538	2,69821

Table A.2 Tensile properties of aligned electrospun fibrous meshes at dry conditions.

	Extension at Maximum Load (mm)	Maximum Load (N)	Tensile strain at Maximum Load (mm/mm)	Tensile stress at Maximum Load (MPa)	Modulus (Young's Tensile stress - Cursor) (MPa)
1	2,41730	22,17507	0,08953	30,91516	355,59562
2	2,51716	25,20455	0,10183	48,13336	571,44678
3	2,00862	20,89134	0,09634	34,28211	434,69354
4	2,83379	11,25736	0,09141	20,55083	200,45789
Mean	2,44422	19,88208	0,09478	33,47037	390,54846
Standard Deviation	0,34037	6,02746	0,00551	11,38867	154,95066

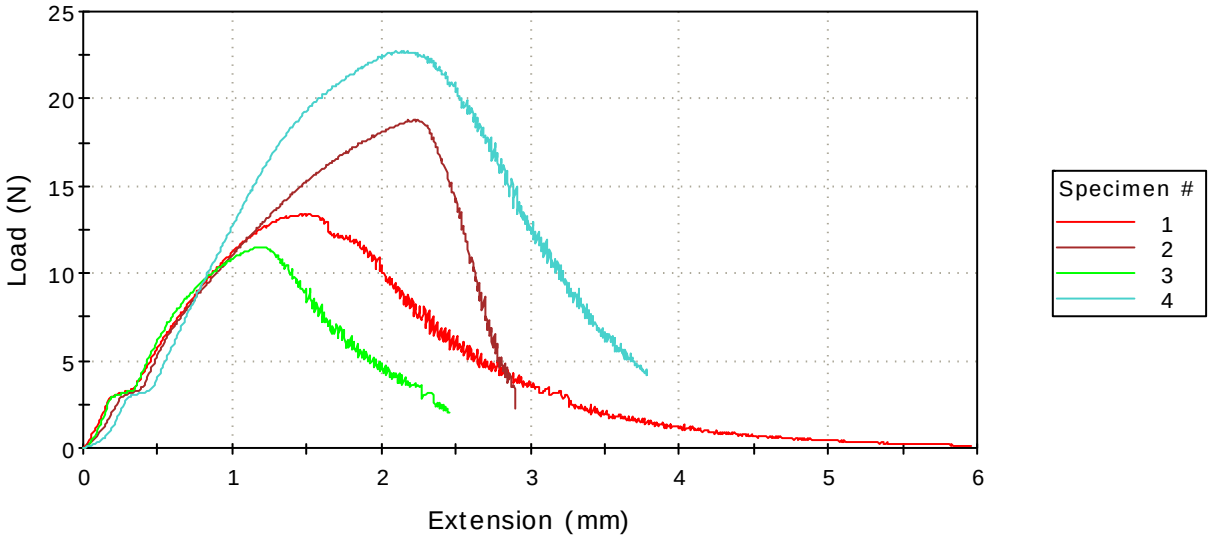

Figure A. 3 Load-extension curves of random electrospun fibrous mats at dry conditions.

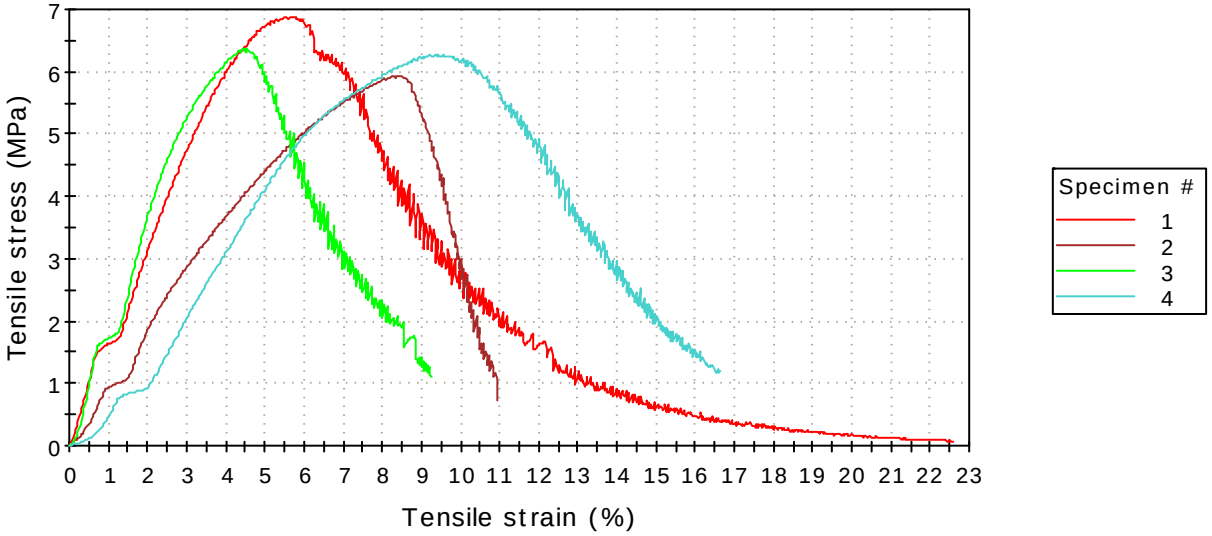

Figure A. 4 Stress-strain curves of random electrospun fibrous mats at dry conditions.

Table A.3 Dimensions of aligned electrospun fibrous meshes before evaluation at dry conditions.

	Length (mm)	Thickness (mm)	Width (mm)
1	26,35000	0,13700	14,20000
2	26,53000	0,16550	19,12000
3	26,55000	0,09700	18,69000
4	22,78000	0,21700	16,72000
Mean	25,55250	0,15412	17,18250
Standard Deviation	1,85052	0,05046	2,24616

Table A.4 Tensile properties of random electrospun fibrous meshes at dry conditions.

	Extension at Maximum Load (mm)	Maximum Load (N)	Tensile strain at Maximum Load (mm/mm)	Tensile stress at Maximum Load (MPa)	Modulus (Young's Tensile stress - Cursor) (MPa)
1	1,48382	13,40295	0,05631	6,88956	211,06540
2	2,21743	18,80097	0,08358	5,94148	174,13532
3	1,17548	11,52823	0,04427	6,35889	337,84656
4	2,17547	22,77521	0,09550	6,27721	119,23184
Mean	1,76305	16,62684	0,06992	6,36678	210,56978
Standard Deviation	0,51632	5,12896	0,02369	0,39254	92,86139

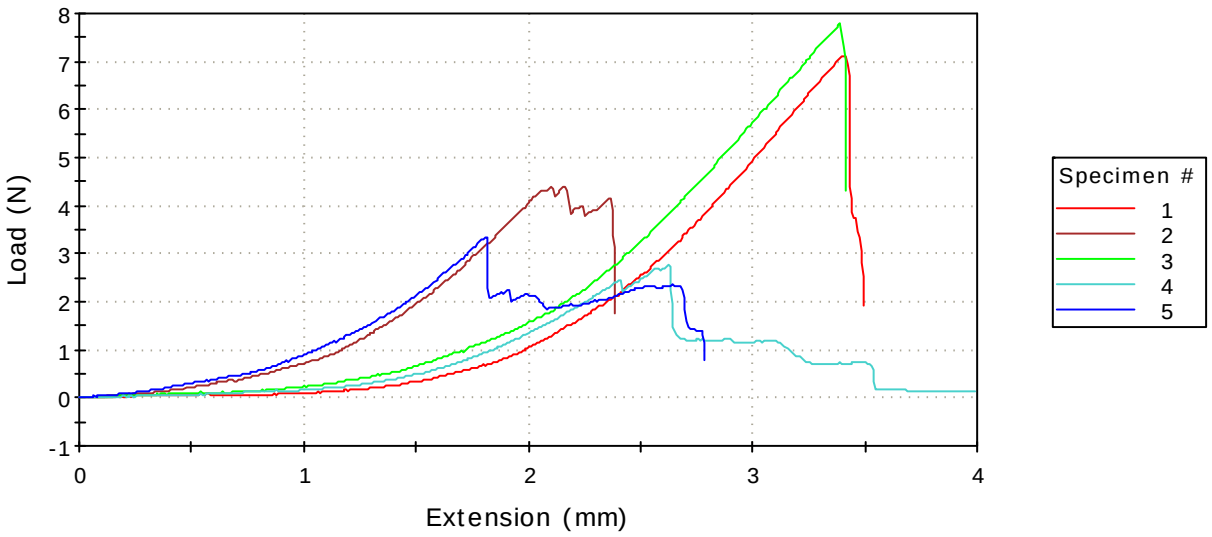

Figure A. 5 Load-extension curves of aligned electrospun fibrous mats at water wet conditions.

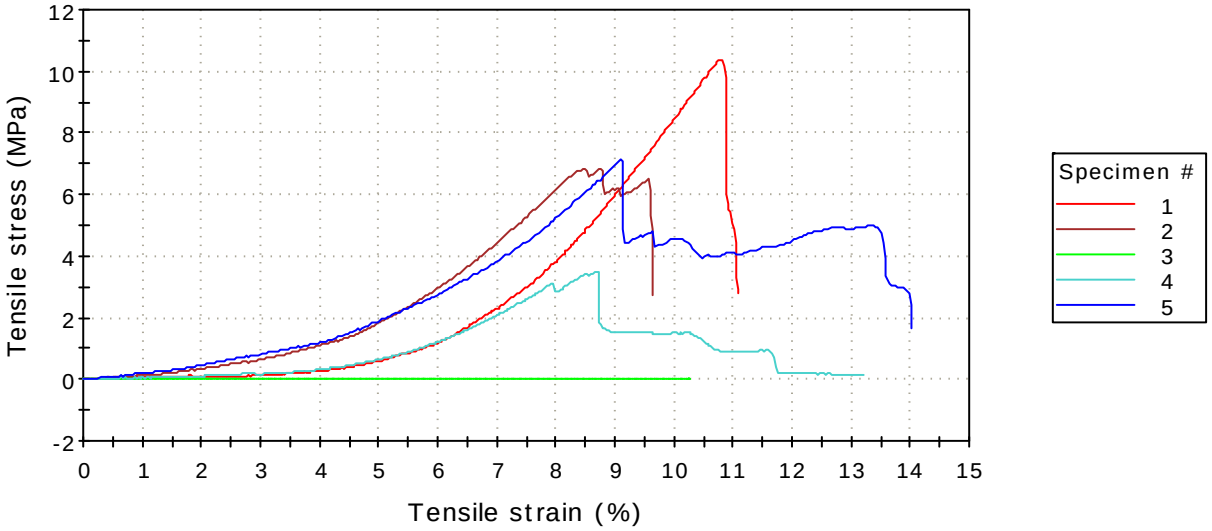

Figure A. 6 Stress-strain curves of aligned electrospun fibrous mats at water wet conditions.

Table A.5 Dimensions of aligned electrospun fibrous meshes before evaluation at water wet conditions.

	Length (mm)	Thickness (mm)	Width (mm)
1	31,53000	0,03400	20,15000
2	24,74000	0,03200	20,00000
3	33,34000	32,00000	20,00000
4	30,23000	0,03860	20,30000
5	19,90000	0,02570	18,28000
Mean	27,94800	6,42606	19,74600
Standard Deviation	5,52661	14,29627	0,82890

Table A.6 Dimensions of aligned electrospun fibrous meshes before evaluation at water wet conditions.

	Extension at Maximum Load (mm)	Maximum Load (N)	Tensile strain at Maximum Load (mm/mm)	Tensile stress at Maximum Load (MPa)	Modulus (Young's Tensile stress - Cursor) (MPa)
1	3,40023	7,11263	0,10784	10,38188	246,42325
2	2,10002	4,38910	0,08488	6,85797	189,50564
3	3,39096	7,80920	0,10171	0,01220	0,27904
4	2,62547	2,75335	0,08685	3,51381	108,45412
5	1,80875	3,35339	0,09089	7,13798	181,10651
Mean	2,66508	5,08353	0,09443	5,58077	145,15371
Standard Deviation	0,72827	2,26119	0,00992	3,94931	94,67147

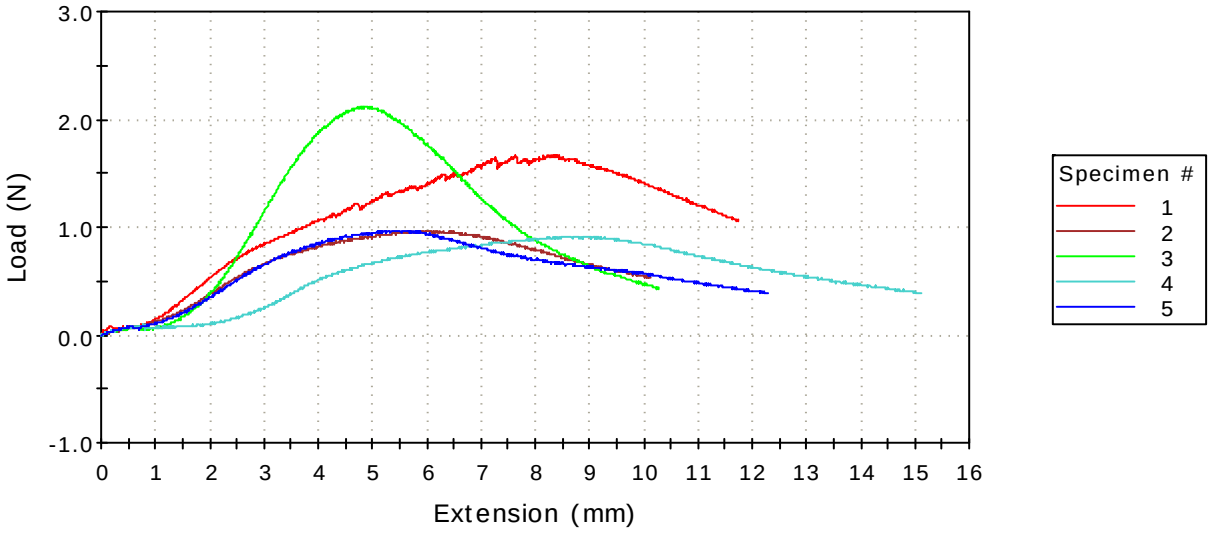

Figure A. 7 Load-extension curves of random electrospun fibrous mats at water wet conditions.

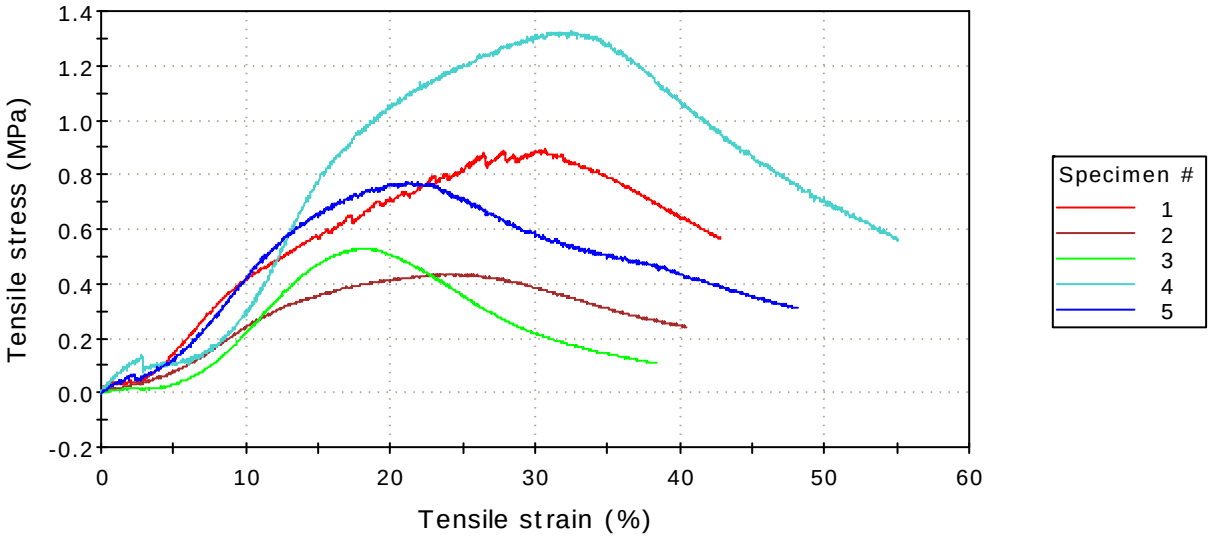

Figure A. 8 Stress-strain curves of random electrospun fibrous mats at water wet conditions.

Table A.7 Dimensions of random electrospun fibrous meshes before evaluation at water wet conditions.

	Length (mm)	Thickness (mm)	Width (mm)
1	27,43000	0,11200	16,75000
X 2	25,05000	0,13100	16,90000
3	26,81000	0,20600	19,40000
4	27,46000	0,04300	16,00000
5	25,57000	0,08100	15,51000
Mean	26,81750	0,11050	16,91500
Standard Deviation	0,88398	0,06964	1,73337

Table A. 8 Tensile properties of random electrospun fibrous meshes at water wet conditions.

	Extension at Maximum Load (mm)	Maximum Load (N)	Tensile strain at Maximum Load (mm/mm)	Tensile stress at Maximum Load (MPa)	Modulus (Young's Tensile stress - Cursor) (MPa)
1	8,43389	1,67346	0,30747	0,89203	6,12033
X 2	5,89201	0,96262	0,23521	0,43481	4,44851
3	4,86697	2,12013	0,18154	0,53051	5,69222
4	8,93397	0,91123	0,32534	1,32446	12,40051
5	5,43421	0,97273	0,21252	0,77428	7,11595
Mean	6,91726	1,41939	0,25672	0,88032	7,83225
Standard Deviation	2,06320	0,58118	0,07045	0,33217	3,10336

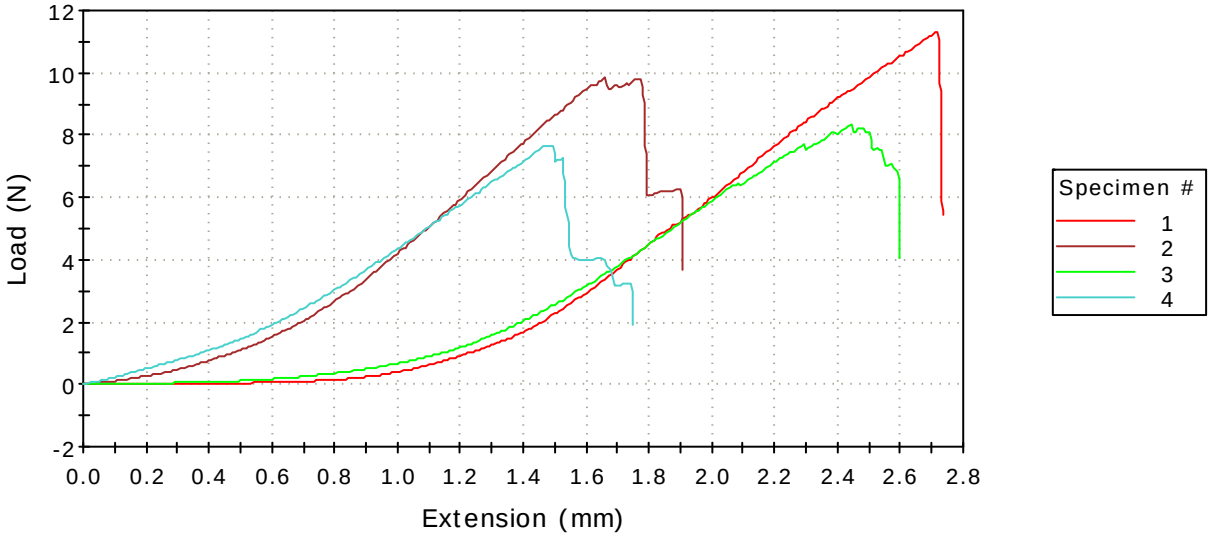

Figure A. 9 Load-extension curves of aligned electrospun fibrous mats at physiological conditions.

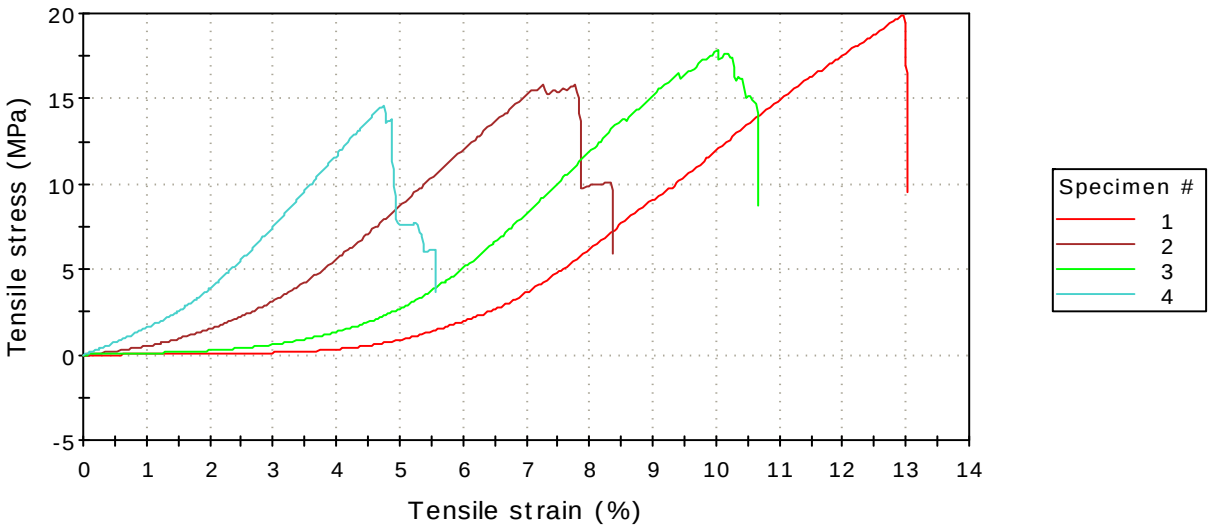

Figure A. 10 Stress-strain curves of aligned electrospun fibrous mats at physiological conditions.

Table A.9 Dimensions of aligned electrospun fibrous meshes before evaluation at physiological conditions.

	Length (mm)	Thickness (mm)	Width (mm)
1	20,97000	0,02170	26,20000
2	22,78000	0,02630	23,60000
3	24,37000	0,01870	24,91000
4	31,35000	0,02400	21,94000
Mean	24,86750	0,02268	24,16250
Standard Deviation	4,53940	0,00325	1,82264

Table A.10 Tensile properties of aligned electrospun fibrous meshes at physiological conditions.

	Extension at Maximum Load (mm)	Maximum Load (N)	Tensile strain at Maximum Load (mm/mm)	Tensile stress at Maximum Load (MPa)	Modulus (Young's Tensile stress - Cursor) (MPa)
1	2,71751	11,33261	0,12959	19,93282	302,91870
2	1,65897	9,83933	0,07283	15,85250	325,30684
3	2,44251	8,31989	0,10023	17,86085	348,42180
4	1,49260	7,67433	0,04761	14,57447	407,98968
Mean	2,07790	9,29154	0,08756	17,05516	346,15925
Standard Deviation	0,59445	1,63559	0,03531	2,34736	45,21316

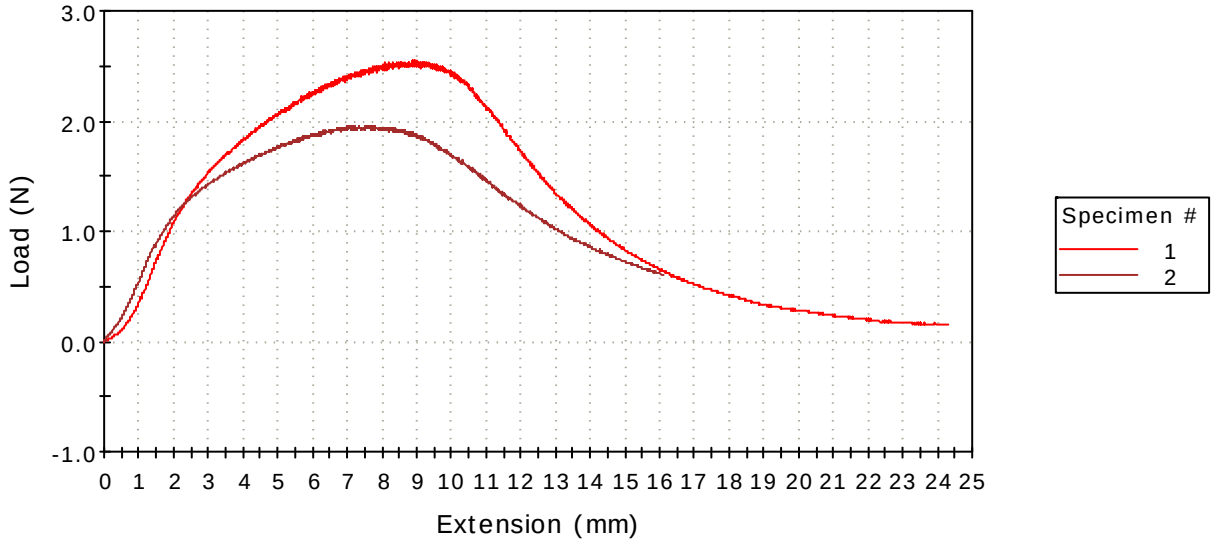

Figure A. 11 Load-extension curves of random electrospun fibrous mats at physiological conditions.

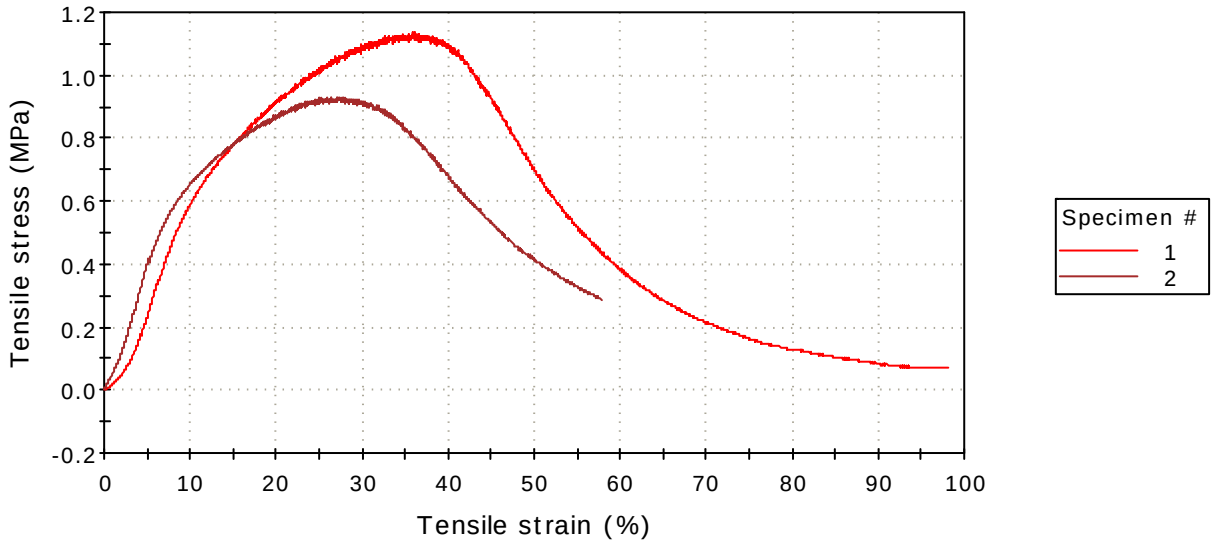

Figure A. 12 Stress-strain curves of aligned electrospun fibrous mats at physiological conditions.

Table A.11 Dimensions of random electrospun fibrous meshes before evaluation at physiological conditions.

	Length (mm)	Thickness (mm)	Width (mm)
1	24,76000	0,08870	25,32000
2	27,81000	0,08270	25,45000
Mean	26,28500	0,08570	25,38500
Standard Deviation	2,15668	0,00424	0,09192

Table A.12 Tensile properties of random electrospun fibrous meshes at physiological conditions.

	Extension at Maximum Load (mm)	Maximum Load (N)	Tensile strain at Maximum Load (mm/mm)	Tensile stress at Maximum Load (MPa)	Modulus (Young's Tensile stress - Cursor) (MPa)
1	8,93251	2,54753	0,36076	1,13431	9,44147
2	7,50772	1,95770	0,26996	0,93015	10,63523
Mean	8,22011	2,25262	0,31536	1,03223	10,03835
Standard Deviation	1,00747	0,41707	0,06420	0,14436	0,84411

Appendix B: XPS Data

In this section the C1s peaks of the XPS data for the different surface modification, Chapter 6 in Tables 6.5 and 6.6, are presented. The spectra analysis was performed using peak fitting with Gaussian-Lorentzain peak shape. Figure B.1 and B.2 correspond to data in Tables 6.5 and 6.6, respectively. Fig. B.1A shows the peak assignation of the different C1s carbons.

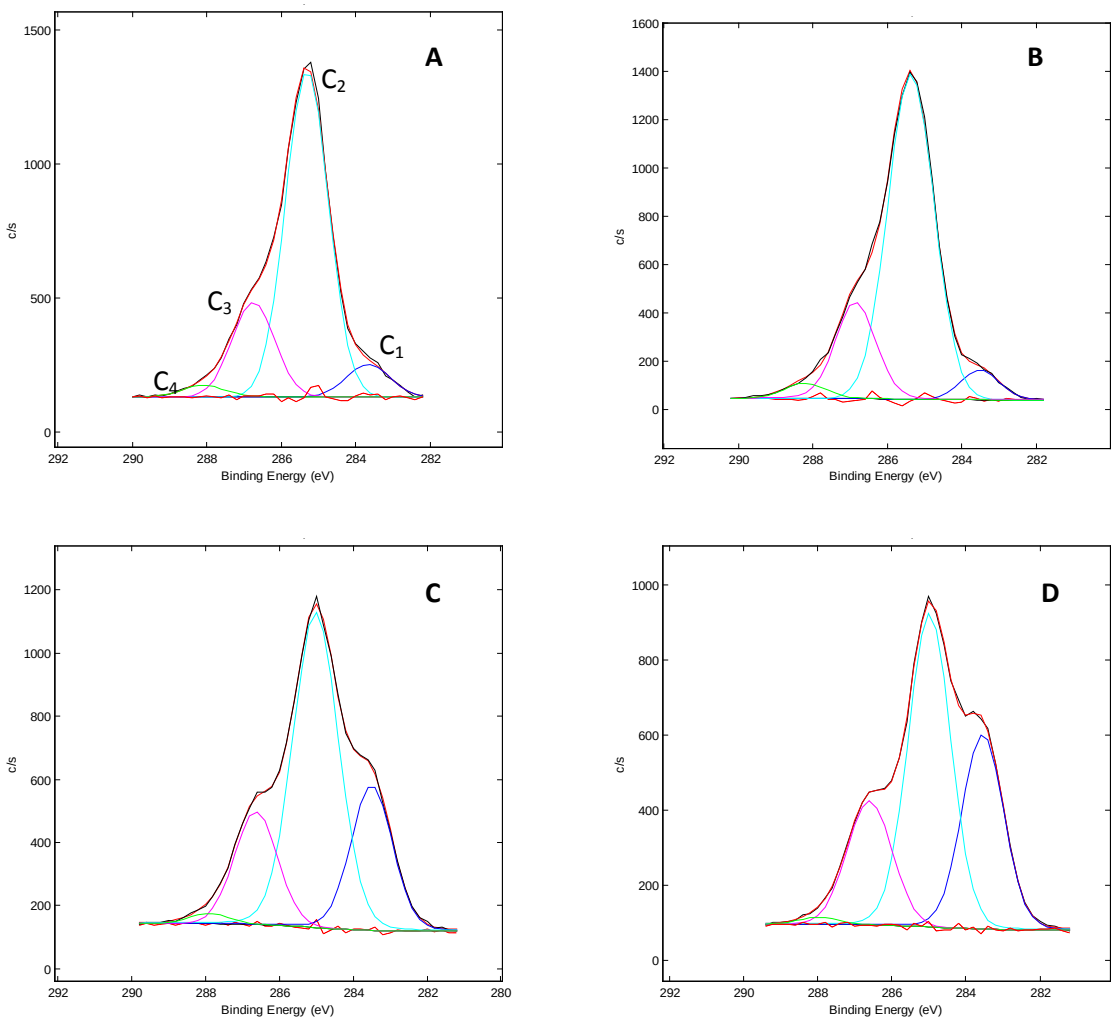

Figure B. 1 Deconvolution of the carbon peak for: A) Random cellulose fibers untreated, B) Aligned cellulose fibers untreated, C) THAMP C2C12 culture media modified random cellulose, and D) THAMP C2C12 culture media aligned cellulose.

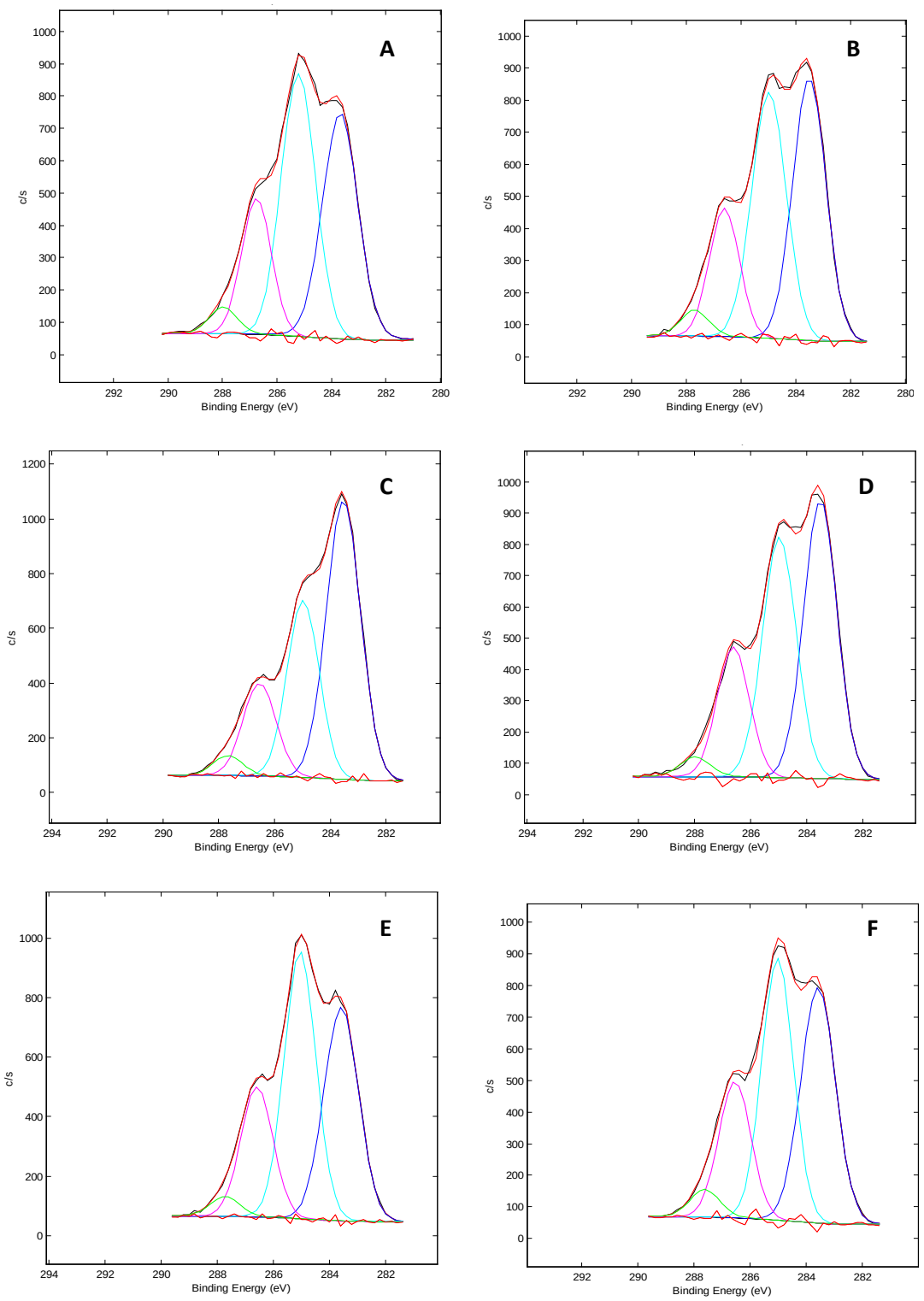

Figure B. 2 Deconvolution of the carbon peak for: A) Random cellulose with PC12 culture media, B) Random cellulose laminin and PC12 culture media modified, C) THAMP and PC12 media modified random cellulose, D) THAMP laminin and PC12 media modified random cellulose, E) RGD-xylogucan and PC12 media modified random cellulose, F) RGD-xylogucan, laminin and PC12 media modified random cellulose.

Appendix C: *In Vitro* Cytotoxcity Evaluation

The cytotoxicity evaluation of electrospun cellulose fibers by indirect contact was carried out by Nelson laboratories in conformity with procedures established by United States Pharmacopeia and National Formulary (USP 87) and the ANSI/AAMI/ISO 10993-5 standards. Nelson laboratories are located in Salt Lake City, UT, USA. The cytotoxicity evaluation as reported by Nelson laboratories is presented in this section. This information complements the results shown in Chapter 7, section 7.1.